

Utilisation of RPAS in oil and chemicals detection

Jukka Sassi | Sami Siikanen | Marko Höyhtyä



Utilisation of RPAS in oil and chemicals detection

Jukka Sassi, Sami Siikanen & Marko Höyhtyä



ISBN 978-951-38-8640-0 (Soft back ed.)

ISBN 978-951-38-8639-4 (URL: <http://www.vttresearch.com/impact/publications>)

VTT Technology 328

ISSN-L 2242-1211

ISSN 2242-1211 (Print)

ISSN 2242-122X (Online)

<http://urn.fi/URN:ISBN:978-951-38-8639-4>

Copyright © VTT 2018

JULKAISIJA – UTGIVARE – PUBLISHER

Teknologian tutkimuskeskus VTT Oy

PL 1000 (Tekniikantie 4 A, Espoo)

02044 VTT

Puh. 020 722 111, faksi 020 722 7001

Teknologiska forskningscentralen VTT Ab

PB 1000 (Teknikvägen 4 A, Esbo)

FI-02044 VTT

Tfn +358 20 722 111, telefax +358 20 722 7001

VTT Technical Research Centre of Finland Ltd

P.O. Box 1000 (Tekniikantie 4 A, Espoo)

FI-02044 VTT, Finland

Tel. +358 20 722 111, fax +358 20 722 7001

Cover image: <https://www.shutterstock.com>

Juvenes Print, Tampere 2018

Preface

An elementary part of successful oil and chemical countermeasures is the proper ability to carry out surveillance actions in demanding environmental conditions. In the case of a marine oil or chemical spill, the most important information is usually valid data on the spill size and location and oil movement. When oil flows out of a broken tank, it has the tendency to start drifting away from the broken vessel due to various environmental forces, mainly winds and currents. The oil outflow dynamics may also vary considerably depending on the accident type and scenario, position and form of the tank rupture, in addition to local conditions. As a consequence of oil outflow dynamics, the risk of coastline pollution increases without implementation of effective countermeasures.

The Finnish Environment Institute (SYKE) is the responsible oil combating authority using a diverse set of tools for carrying out marine surveillance. The tools selected are also commonly used in other countries, and many of these tools and systems have been developed during the past years through actual experiences of oil spills. Standard surveillance tools are based on satellite technology, aerial surveillance concepts, a set of different sensor systems mounted on board vessels and visual means supported by special cameras and video systems. Almost all of these systems will be used in accident situations in an integrated way to form a valid situational awareness view.

The rapid development of Remotely Piloted Aircraft Systems (RPAS) technology has introduced new possibilities for the oil combating authorities to design a new-generation of tools for local surveillance, for both oil and chemical spill response tasks. In order to gain a better understanding of RPAS development, SYKE has joined other agencies in following developments, studying test reports and performing their own tests and demos.

This report provides an overview of various sensor technologies and deployment platform options utilised in the remote sensing of oil and chemicals in field conditions. The publication is based on the joint efforts by VTT and SYKE to define the state of the art level of sensor and RPAS technology development to design new RPAS-based tools for pollution prevention tasks.

Jorma Rytkönen

Head of Pollution Response Unit, Finnish Environment Institute (SYKE)

Contents

Preface	3
List of abbreviations	6
1. Introduction	10
2. Surface remote sensing options for oil and chemical detection in field conditions	13
2.1 Background.....	13
2.2 Optical sensors.....	16
2.2.1 Visual observations with cameras.....	16
2.2.2 Ultraviolet (UV) sensors	20
2.2.3 Multispectral (MS) and Hyperspectral (HS) sensors.....	21
2.3 Infrared sensors and radiometers.....	29
2.3.1 Thermal Infrared (TIR) sensors.....	29
2.3.2 Microwave radiometers (MWRs).....	32
2.4 Radar sensors	33
2.4.1 Side-Looking Airborne Radar (SLAR) and Synthetic Aperture Radar (SAR).....	33
2.4.2 Marine radar.....	36
2.4.3 Ground Penetrating Radar (GPR).....	38
2.5 Lasers and fluorosensors.....	40
2.5.1 Fluorosensors.....	40
2.5.2 Tunable Diode Laser Spectroscopy (TDLS)	42
2.5.3 Laser-Ultrasonic Remote Sensing of Oil Thickness (LURSOT) ...	42
2.5.4 Light Detection and Ranging (LiDAR)	43
2.6 Experimental sensors	46
2.6.1 Acoustic sensors.....	46
2.6.2 Nuclear Magnetic Resonance (NMR).....	47
2.6.3 Trained dogs.....	48
2.6.4 Visual observations.....	49
2.7 Multi-sensor data integration	50
2.7.1 Operational multi-sensor systems.....	50
2.7.2 Conceptual systems.....	53
2.8 Application in ice-affected water	54
2.9 Mode of operation.....	56
2.10 Summary of sensor technologies for oil detection	58
2.11 Options for chemical detection	67
3. Deployment platforms	71
3.1 Surface vessels	71
3.2 Manned aircraft systems	73
3.3 Satellite systems.....	75
3.4 Unmanned Aerial System (UAS)	78

3.5 Autonomous Underwater Vehicle (AUV) and Remote Operated Vehicle (ROV).....	82
3.6 Aerostats.....	86
4. HSE issues in field operations.....	90
5. Wireless data transmission.....	91
6. Recent field experiments in Finland	95
6.1 Oil detection field trials in Kalajoki (2016).....	95
6.1.1 Description and objectives.....	95
6.1.2 Test arrangements.....	95
6.1.3 Platforms	104
6.1.4 Sensors	106
6.1.5 Results	113
6.1.6 Conclusions.....	129
6.2 Chemical detection field trials and demonstrations in Kuopio (2016)....	131
6.2.1 Description and objectives.....	131
6.2.2 Platforms	131
6.2.3 Target chemicals.....	133
6.2.4 Sensors	134
6.2.5 Results	146
6.2.6 Demonstrations.....	149
6.2.7 Conclusions.....	155
7. Discussion.....	156
Acknowledgements	160
References.....	161

Appendices

Appendix A: Properties of the test oil HFO180 in the Kalajoki trials

Abstract

List of abbreviations

AIS	Automatic Identification System
AEGL	acute exposure guideline levels
AIF	Air Intelligence Finland Ltd
AMOP	Arctic and Marine Oilspill Program
AUV	autonomous underwater vehicle
AVIRIS	Airborne Visible Infrared Imaging Spectrometer
BAOAC	Bonn Agreement Oil Appearance Code
BOOS	Baltic Operational Oceanographic System
BVLOS	beyond visual line-of-sight
CC	cross correlation
CDOM	coloured dissolved organic matter
CIS	Canadian Ice Service
CRISP	Centre for Remote Imaging, Sensing and Processing
CWA	chemical warfare agent
DoD	US Department of Defence
DWH	DeepWater Horizon
EASA	European Aviation Safety Agency
EGO	European Gliding Observatories
EM	Electromagnetic
EMSA	European Maritime Safety Agency
ESC	Emergency Services College
FAA	Federal Aviation Administration
FAME	fatty acid methyl esters
FIOH	Finnish Institute of Occupational Health
FLIR	Forward Looking Infrared

FMI	Finnish Meteorological Institute
FPA	focal plane array
FPI	Fabry-Pérot interferometer
FWHM	full width of half maximum
GC/MS	gas chromatography/ mass spectrometry
GIS	Geographic Information System
GMDSS	Global Maritime Distress and Safety System
GNSS	Global Navigation Satellite System
GOOS	Global Ocean Observing System
GPR	Ground Penetrating Radar
GPS	Global Positioning System
GSD	geometric standard deviation
GSM	global system for mobile communication
HF	high frequency
HFO	heavy fuel oil
HLIF	hyperspectral laser induced fluorescence
HNS	hazardous and noxious substances
HS	hyperspectral
HSE	Health, Safety, Environment
HSI	hyperspectral imaging
ICAO	International Civil Aviation Organization
IEEE	Institute of Electrical and Electronics Engineers
IFR	instrument flight rules
IMS	ion mobility spectrometry
IR	infrared
ISTOP	Integrated Surveillance and Tracking of Pollution
ITOPF	International Tanker Owners Pollution Federation
JIP	Joint Industrial Programme
LED	light-emitting diode
LFS	laser fluorosensor
LIF	laser induced fluorosensor
LiDAR	light detection and ranging
LOS	Line-of-Sight

LTE	long term evolution
LURSOT	laser-ultrasonic remote sensing of oil thickness
MIR	mid-infrared
MS	multispectral
MTMF	mixture tuned match filtering
MWR	microwave radiometer
NASA	National Aeronautics and Space Administration
NCOC	North Caspian Operating Company
NIR	near-infrared
NLS	National Land Survey of Finland
NMR	Nuclear Magnetic Resonance
NOAA	National Oceanic and Atmospheric Administration
NOFO	Norsk Oljevernforening for Operatørselskap
NRT	Near Real-Time
ODC	oil detection canine
OGP	International Association of Oil and Gas Producers
OSR	oil spill response
OSSAS	Oil Spill Scene Analysis System
PAH	polycyclic aromatic hydrocarbon
PID	photo-ionisation detector
PMR	passive microwave radiometers
ppb	parts per billion
ppm	part per million
PPR	pre-set pulse repetitio
QoS	quality of service
RMS	root mean square
ROV	Remote Operated Vehicle
RPAS	Remotely Piloted Aircraft Systems
RPM	revolutions per minute
SAM	spectral angle mapper
SAR	search and rescue
SAR	synthetic aperture radar
SCAT	shoreline clean-up assessment technique

SCC	shore control centre
SIGIS	scanning infrared gas imaging system
SIFT-MS	selective-ion flow-tube mass spectrometry
SLAR	side-looking airborne radar
SNR	signal-to-noise ratio
SOP	standard operating procedures
SWIR	short-wave infrared
SYKE	Finnish Environment Institute
TIC	toxic industrial compounds
TD-GC-MS	thermal desorption-gas chromatography-mass spectrometry
TDLS	tunable diode laser spectroscopy
TIR	thermal infrared
UAV	Unmanned Aerial Vehicle
UAS	Unmanned Aerial System
UV	ultraviolet
VFR	visual flight rules
VHF	very high frequency
VLOS	visual line-of-sight
VIS	visible
VOC	volatile organic compound

1. Introduction

In ice-covered sea areas, the behaviour of oil differs substantially from that in open water conditions. Ice prevents oil from spreading around freely, since oil mainly spreads via cracks, and with drifting ice field and sea currents. In cold climates, evaporation is slow and oil remains quite fresh for longer times than in warmer waters, especially if oil enters under the ice cover (Figure 1).

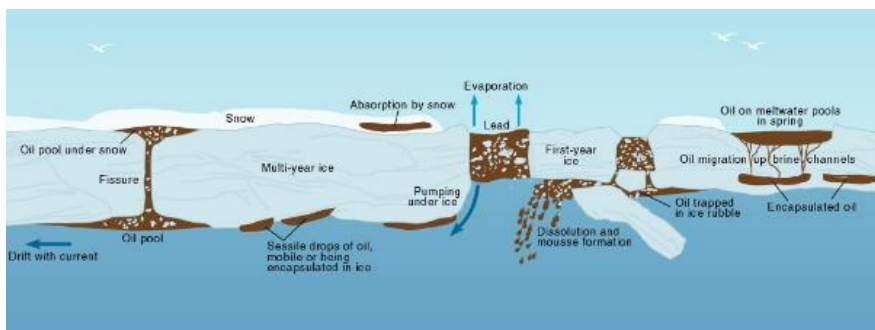


Figure 1. Oil-Ice interaction. (AMAP, 1998)

Depending on wind and current conditions, long-term ice can move hundreds or thousands of kilometres from the spill site before the ice starts to melt. Then oil fills up the open water areas between the ice floes and causes trouble for birds and other animals. It is therefore important to collect the oil from the ice already during winter. Natural cleaning takes decades in arctic conditions, compared to a few years in temperate climates.

Figure 1 above illustrates well that the spilled oil can have several locations depending on the ice scenario (e.g. packed ice, first year ice, multiyear ice). It can be located visibly on the ice and between ice floes or cracks, hidden under the snow, trapped inside the ice and/or capsuled between the ice cracks. Oil distribution can also change during the OSR (Oil Spill Response) operation due to variations in temperature and wind conditions. These dynamic conditions challenge standard oil detection technologies. Therefore, it is essential that the leaked oil can be detected

rapidly and reliably, and that the selected combating methods and operations can be executed as soon as possible.

The detection of oil in dynamic ice conditions presents numerous challenges. Ice is always a heterogeneous material and contains air, sediment, salt and water, many of which may present false oil-in-ice signals to the detectors. Additionally, snow on the top of the ice or even incorporated into the ice adds complications. During freeze-up in autumn and thaw in spring, distinct layers of water and ice may not occur. There are also many different types of ice and different ice crystalline orientations. Snow is also heterogeneous and may consist of several layers with different densities. Furthermore, oil may penetrate snow easily and thus move to the subsurface of the snow, which may be ice or soil. Figure 2 illustrates a situation in which oil is in a lead between ice floes showing several different types of ice and snow. Oil derived from a single spill is distributed to several locations in the lead.



Figure 2. Oil in different ice and snow conditions. (Fingas and Brown, 2013)

The reference (Fingas, 2015) concludes that oil spills in ice-infested waters undergo complex behaviour and fate processes. There is some understanding of the processes involved in oil interaction with ice. Modelling of this behaviour can be carried out at present but there are gaps and uncertainties in some of the algorithms. Especially quantitative research is needed before full capacity to predict oil behaviour and its fate in ice-infested water can be achieved.

Comprehensive studies regarding oil behaviour in arctic conditions have been published by e.g. Arctic Monitoring and Assessment Programme (1998), Nuka Research (2007) and SINTEF (2008 and 2010).

Before the oil recovery actions can be executed, the leaked oil needs to be found. This report presents various sensor options for oil and chemical detection in field conditions and suitable platforms for the sensors. Additionally, the latest field experiments with oil and chemical detection performed by VTT Technical Research Centre of Finland, Finnish Environmental Institute (SYKE) and their partners are presented.

2. Surface remote sensing options for oil and chemical detection in field conditions

2.1 Background

Sensors used for traditional remote sensing are classified as passive or active. Passive sensors receive naturally transmitted radiation, whereas active sensors transmit and receive radiation by the objects being observed. The ability to sample both naturally occurring radiation and specially configured man-made radiation from across the electromagnetic (EM) spectrum is a key strength of remote sensing technology (Figure 3).

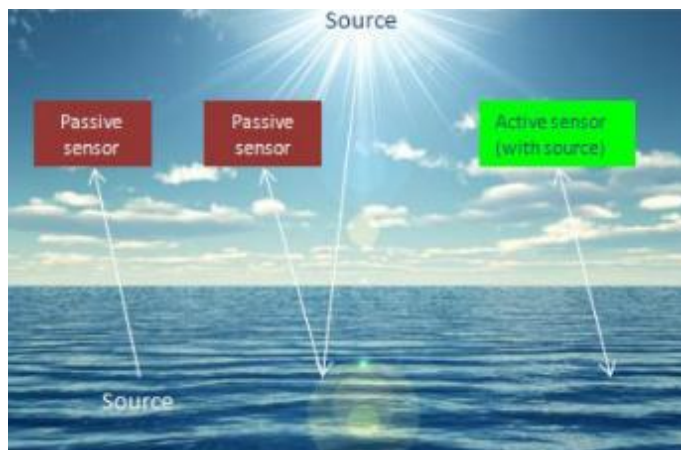


Figure 3. Schematic illustration of passive and active remote sensing. (Partington, 2014)

Reflected sunlight and thermal emissions are the most common sources of EM energy measured by passive sensors. These remote sensing systems utilize a variety of detectors that are sensitive to wavelengths spanning from the optical (i.e. visible) to the thermal infrared (TIR) range of the EM spectrum. These passive imaging sensors rely on external sources of energy that are reflected or emitted from objects on the ground to a detector sensitive to specific wavelengths. The human eye can detect only the visible portion of this spectrum, which represents a very small part (Figure 4).

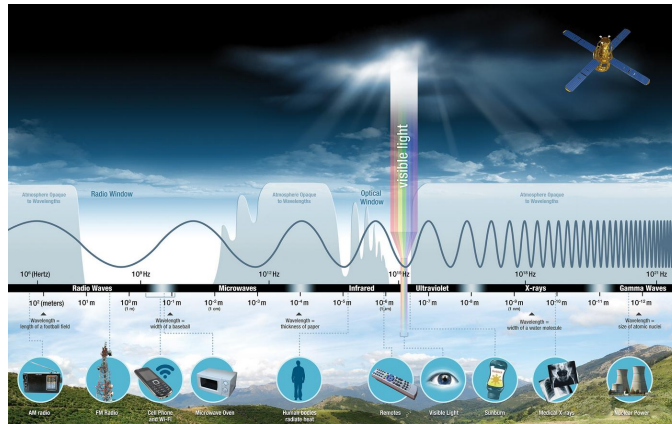


Figure 4. The electromagnetic spectrum. (NASA, 2017)

Although only data in the visible part of the spectrum is interpretable to the human eye, other parts of the spectrum offer great advantages, notably in terms of being able to penetrate through clouds (microwave) and being sensitive to absorption or refraction by oil (IR, UV). (API, 2013; Partington, 2014).

Passive sensors can collect electromagnetic radiation from across the spectrum, but because they depend on natural processes there are limitations in terms of diurnal sampling (some need daylight), sensitivity to weather (primarily cloud cover, fog or mist, which can absorb or distort the radiation) and effective spatial resolution (because the radiation cannot be configured to enable high resolution to be achieved through signal processing and other techniques).

Visible (VIS) imaging involves the use of colour in detecting and characterising oil spills. Airborne observation has historically involved trained observers, but nowadays also involves a range of sensors that can support more data intensive and analytical assessment.

Infrared (IR) extends from near IR (NIR) to short wave IR (SWIR). In this part of the spectrum, outside the range of detection of the human eye, there are absorption wavelengths associated with hydrocarbons which can be useful for detection, and potentially other characterisation, including ~ 1.20 , ~ 1.72 , ~ 1.75 , 2.37 and $3.3 \mu\text{m}$. SWIR can be used through thin cloud, haze and fog.

Thermal infrared (TIR) is part of the spectrum responding to both the temperature and emissivity of the target. The emissivity is the efficiency with which incoming radiation is emitted by an object, the reference being the idealised case of a black body in which all incoming radiation is emitted and none absorbed by the surface or object. TIR sensors are useful for detection of oil during day and night and for classifying oil thickness $>10 \mu\text{m}$. The ability of thermal sensors to detect oil depends on its thickness, type, degree of emulsification and time of day, and they are not effective during rough weather.

Passive microwave radiometers (PMR) detect naturally occurring microwave radiation and are also sensitive to the emissivity properties of the surface. Passive

microwave radiometers can also be used during day or night, as in the case of TIR sensors. In the case of microwave sensors there is less sensitivity to weather conditions. (Partington, 2014)

Active sensors (i.e. radar and laser) are able to perform observations during day or night, since they have their own source of energy for illumination. The energy source can be configured to optimise sampling of the surface, focusing the energy to achieve e.g. high spatial resolution or to minimise atmospheric absorption. These sensors come with their own challenges in terms of data processing and interpretation due to complex technology. For example, coherent imaging sensors have speckle, which is a form of radiometric noise present when the data are analysed at their full spatial resolution.

Laser is coherently transmitted optical radiation. The coherence refers to the control over the radiation wavelength and phase. Although laser can be used during day or night, it is impacted by atmospheric attenuation of the signal, for example in conditions of fog or cloud. Laser can be used in a variety of ways to interpret conditions on the target surface, e.g. by:

- Measuring distance to the target (via time of flight of the signal), which may be used to estimate surface elevation, known as “LiDAR” in this configuration. Over land LiDAR may be used to assess vegetation canopy height. Over the ocean it may be used to penetrate below the surface, depending on specific wavelength.
- Stimulating a fluorescent response in the target from UV radiation (excitation of the target producing a unique spectral response distinct from the transmitted signal, laser fluorescence) which is then detected and analysed to identify the target;
- Stimulating an acoustic response in the target that can then be used to infer properties of the target (laser acoustics); and
- Detecting absorption from compounds emitted from the surface that can then be used to identify the target (laser spectroscopy).

Radar also involves the transmission of coherent radiation but at microwave frequencies, and is sensitive to the roughness and dielectric properties of the surface being imaged, the latter being strongly influenced, for example, by moisture content. Radar can be used to measure distance to the surface, in vertically configured form, or can be used to generate images of the surface. Radars measure radiation at a range of wavelengths which are sensitive to different scales of surface roughness (typically from mm to dm scale), and some of the longer wavelengths are able to penetrate vegetation or even dry ground.

Although radar sensors are useful because they can observe the surface during almost all atmospheric conditions, radars are particularly complex to interpret because they are sensitive to very different surface conditions to those of optical sensors and the human eye, and so are far from intuitively understandable. (Partington, 2014)

2.2 Optical sensors

Optical sensors are passive devices sensitive in the ultraviolet (UV), visible (VIS) and near-infrared (NIR) spectral regions. They exploit differences in reflectance as the primary mechanism for detecting oil on water. Optical sensors include hyperspectral sensors, multispectral imaging systems, still and video cameras, UV and NIR sensors. (Puestow *et al*, 2013)

2.2.1 Visual observations with cameras

Aerial visual observation uses the human eye as the primary sensor. As it is one of the simplest sensing techniques, visual observation often serves as the backbone of a surveillance program during an oil spill response actions. Trained observers can provide interpretation of visual oil signatures as well as spatial patterns related to appearance and relative thickness. Aerial visual observation can be used both in a preventive (prior to an environmental event) and a reactive mode (during a response), and is typically one of the first types of surveillance data received. Thus the visual interpretation of oil spills by trained operators remains an important method for detecting oil on water (API, 2013; Puestow *et al*, 2013)

The primary sensors mounted on aircraft, surface vessels or rigs include digital still or video cameras sensitive to reflected visible light (i.e. corresponding to wavelengths ranging from 400 to 700 nm) as well as the near-infrared range (i.e. from 700 to ~1000 nm). An aerial photograph in which oiled and clean water are visible is presented in Figure 5. (Puestow *et al*, 2013; Jha *et al*, 2008)



Figure 5. Aerial Image of an oil sheen and slick observed during the DWH blowout. (Puestow *et al*, 2013)

Since the amount of oil is a critical parameter to guide response actions, it is important for operators to relate the visual appearance of oil to layer thickness and

volume. An example of the appearance of oil on different types of water is presented in Figure 6.

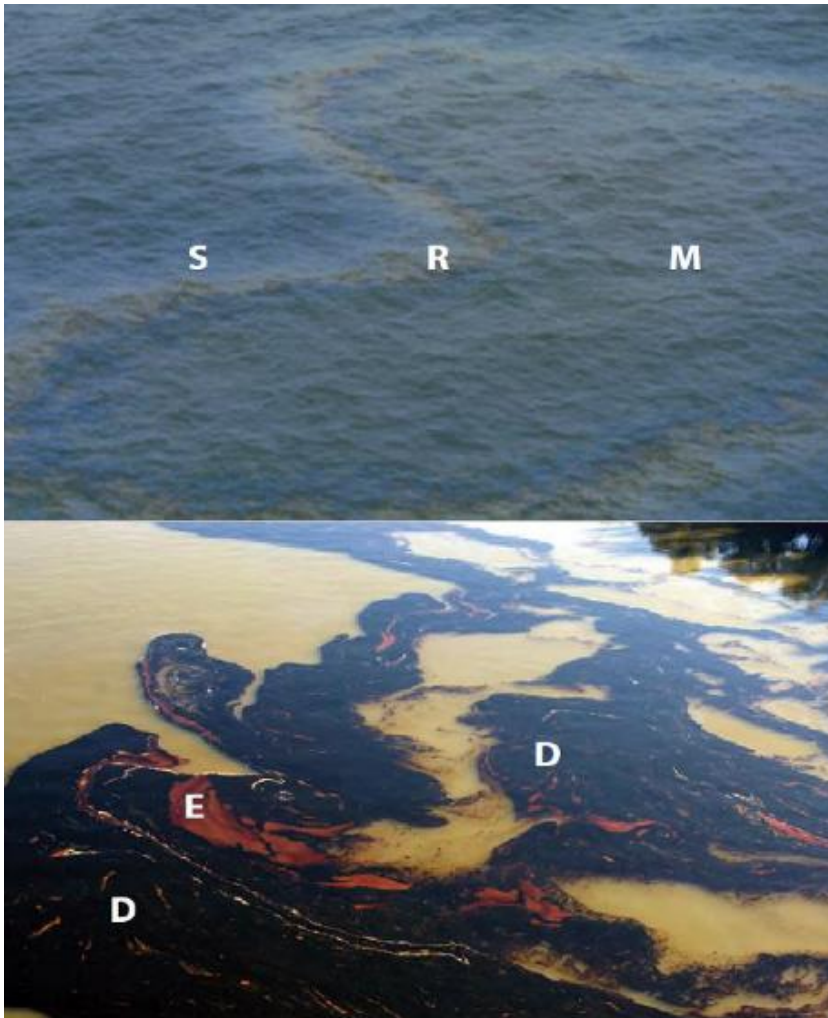


Figure 6. Aerial digital photography of oil spilled on (top) the ocean and (bottom) the Mississippi River. S: silver/grey; R: rainbow; M: metallic; D: dark or true colour; E: emulsified. (Puestow et al, 2013)

The letters in Figure 6 were assigned according to the modified Bonn Agreement Oil Appearance Code (BAOAC), represented in Table 1 as an interpretation key to relate the brightness and colour of oil on water to layer thickness and oil volume per km².

Table 1. Relationships between appearance, layer thickness and volumes of oil according to the Bonn Agreement Oil Thickness guide. (Partington, 2014)

Code	Appearance	Layer thickness [μm]	Litres/ km^2
1	Silvery/grey sheen	0.04–0.30	40–300
2	Rainbow	0.30–5.0	300–5 000
3	Metallic	5.0–50	5 000–50 000
4	Discontinuous true oil colour	50–200	50 000–200 000
5	Continuous true oil colour	200 → 200	200 000 → 200 000

Silvery/grey and rainbow sheens are caused by optical interference effects over the thin oil film, whereas the metallic appearance is caused by the reflection of skylight. For thick layers, the true colour of the oil dominates. In addition to colour, shape, size, contrast and context are used to interpret oil thickness on open water.

Since oil does not have specific absorption bands in the visible and NIR spectral ranges, detecting oil on water relies on differences in contrast between the oil and the surrounding oil-free water. The difference in reflectance between oil and water increases for shorter wavelengths and the contrast may be enhanced by filtering out any response above 450 nm and by using cameras positioned at the Brewster angle¹ of water (i.e. at an incidence angle of 53°) in conjunction with a horizontal polarising filter (Figure 7).

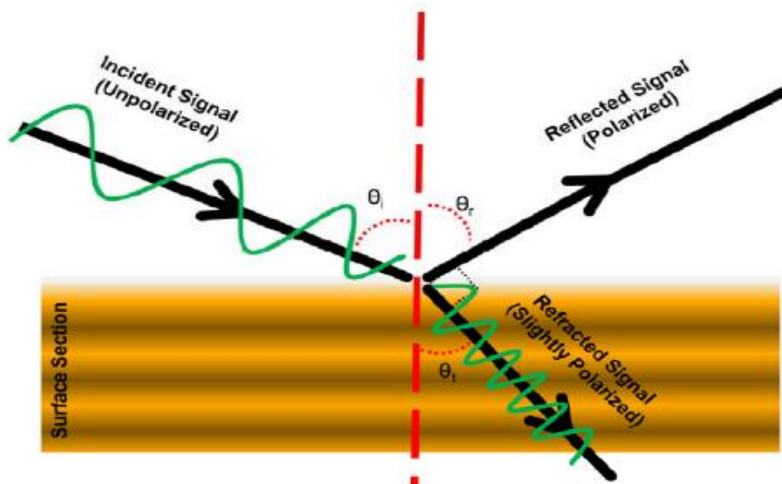


Figure 7. Incident, reflected, refracted, Brewster angle and polarization of signal that occurs on an interface of a surface section at Brewster's angle (not to scale). (Najibi and Jin, 2013)

¹ Brewster's angle (also known as the polarization angle) is an angle of incidence at which light with a particular polarization is perfectly transmitted through a transparent dielectric surface, with no reflection. When unpolarised light is incident at this angle, the light that is reflected from the surface is therefore perfectly polarized.

Visible sensors, such as still and video cameras, are widely used for aerial investigation of open water spills since they are readily available, inexpensive and easy to use. However, visible imaging of oiled water is affected by false alarms due to sun sparkle and wind sheens, and biogenic materials such as seaweed, sunken kelp beds and fish sperm can be confused with thicker oil slicks. Algal blooms, wind shadows and biogenic oil may also cause false alarms, which emphasises the importance of the expertise of the observers.

Typical camera systems are limited to use during sunlight hours, but visible-range detection of spills may be extended into dark and low light conditions using night-vision technology. However, the capabilities of the current low-light systems for detecting oil on water have not been thoroughly documented.

Optical satellite imaging has also been used to monitor and map oil slicks on water. However, the dependence on cloud cover, infrequent revisiting and low spatial resolution make optical satellite imagery an ancillary rather than a primary data source. Interpretation of satellite data requires specialized expertise and may take too long in tactical situations (see section 3.3).

Despite its limitations, optical satellite surveillance has been used successfully in conjunction with radar-based oil spill monitoring to identify areas of algal blooms and remove them as sources of false alarms from SAR (Synthetic Aperture Radar) images. The need for specially-trained, experienced personnel is essential. Due to the relatively long imaging and data processing time required for both aerial and satellite-based sensors, observations by trained personnel will probably remain more time- and cost effective for rapid surveys of large spills.

When ice is present, the utilisation of optical methods is hindered. Optical signals are attenuated in ice and snow, making passive optical sensors ineffective for characterising oil encapsulated in ice and under snow or ice. Dark melt pools as well as sediment and dirt on ice during the break-up season can be confused with oil on the ice. Even with oil on snow or bare ice, visible detection may be difficult due to synoptic conditions in Arctic regions, including the presence of fog, marine layer, low cloud ceiling and long periods of darkness. Newly formed ice may also be misinterpreted as oil. In relatively high ice concentrations the oil is contained within the ice and remains fairly localized. Under these conditions, the equilibrium thickness of the oil can be quite thick (i.e. of the order of millimetres) and the oil has a true colour appearance (Table 1).

In the case of open ice (<3/10 concentration), the oil spreads more freely and the oil sheen may appear similar to that expected in open water conditions.

Visible (VIS 0.4–0.74 μm), and Near Infrared (NIR 0.74–1.4 μm) sensors are effective during daylight hours. Short-Wave Infrared sensors (SWIR 1.4–3.0 μm) are effective from daylight hours to dusk. VIS, NIR and SWIR sensors are effective on sea states between calm and rough (calm = flat seas and no wind; rough = waves approximately 2 m and winds approximately 35 km/h or 9.72 m/s). VIS and SWIR are effective in clear skies with limited cloud cover, and SWIR is also effective in hazy or foggy conditions.

These techniques are not effective during night time, on very rough seas and in significant cloud and fog conditions. Seaweed, wind and cloud shadows, and

sunlight can cause false positive (oil-look alike) observations. (Puestow *et al*, 2013; API, 2013; Partington, 2014)

2.2.2 Ultraviolet (UV) sensors

The ultraviolet (300–400 nm) reflectance of oil is greater than that of water. Aerial passive UV scanners have been engineered to collect and analyse UV sunlight reflected from the water surface and to separate oiled water from oil-free water through observed variations in the electromagnetic intensity. UV sensors have detected sheens as thin 0.1 μm but they are insensitive to oil thicker than 10 μm .

The required level of expertise to operate a UV detector is similar to that of a Thermal Infrared (TIR) system, although TIR and visible-range sensors are more developed. Oil spill detection in open water with UV requires clear atmospheric conditions due to the high reduction of UV light by fog and clouds (Jha *et al*, 2008). Sun glints, wind slicks and biogenic material cause false alarms in UV-based oil spill detection. (Fingas and Brown, 2013; Partington, 2014)

UV and TIR are frequently used together to assess thinner and thicker parts of an oil slick (Jha *et al*, 2008) (Figure 8). Additionally, the false positive observations of TIR images are often different from those of UV images, and thus the results obtained from both offset individual limitations.

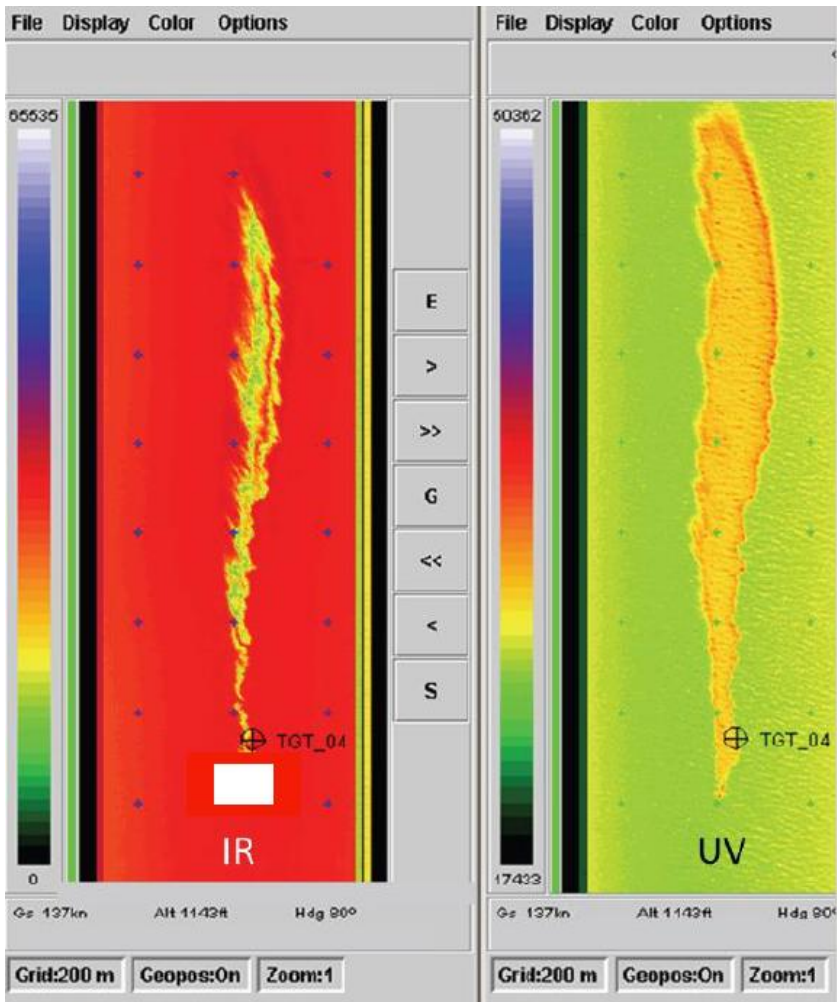


Figure 8. Concurrent TIR and UV images from oil slick. (Puestow et al, 2013)

In ice-affected waters the effectiveness of airborne UV sensors is not well understood and assumptions concerning their performance in such situations are based on how they perform in open water spills. UV imaging could be useful for detecting thin oil layers on melt ponds as well as between floes. The performance of UV sensors in slush and brash ice is unknown. (Puestow *et al*, 2013)

2.2.3 Multispectral (MS) and Hyperspectral (HS) sensors

All materials leave unique fingerprints across the EM spectrum, known as spectral signatures. A material's spectral signature is determined by how much energy is

absorbed or reflected at a certain wavelength. Whereas the human eye sees the colour of visible light in mostly three bands (red, green, and blue), spectral imaging divides the spectrum into many more bands. MS sensors are able to “view” objects within a wide range of the EM spectrum at discrete bandwidths, while HS sensors are able to “view” objects within a vast portion of the EM spectrum and at very small bandwidths. An example of an HS image is presented in Figure 9.

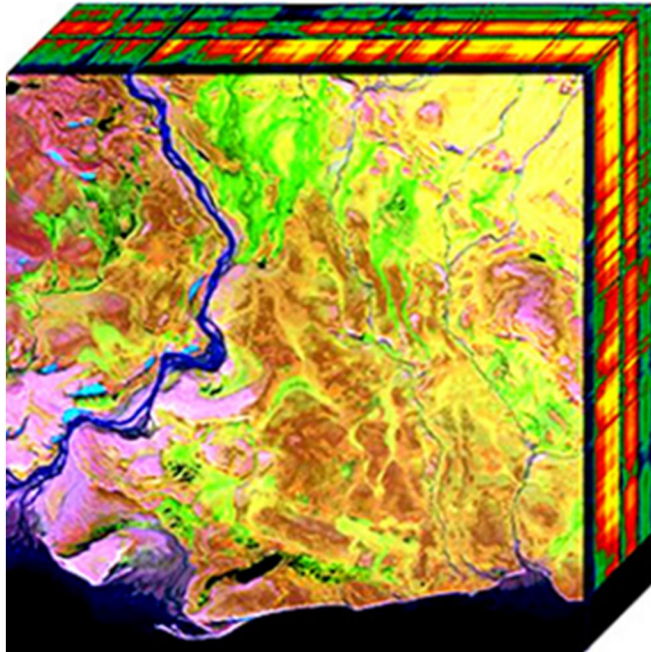


Figure 9. Two-dimensional projection of a hyperspectral cube. Every pixel of spatial map of an object contains spectrum information. (Wikipedia, 2017)

The goal of hyperspectral imaging is to obtain the spectrum for each pixel in the image of a scene, with the purpose of finding objects, identifying materials, or detecting processes. The hyperspectral sensors and processing systems are built for applications in astronomy, agriculture, biomedical imaging, geosciences, physics and surveillance. Because hydrocarbons have a distinct spectral signature, MS and HS imaging can be utilized in determining the extent of oil, affected shorelines and actionable areas of surface oiling with less occurrence of false detections. (API, 2013; Hagen and Kudenov, 2013; Chein-I, 2003)

MS refers to passive sensors that measure reflected and/or emitted radiation in the UV, VIS, and IR wavelengths in a relatively small number of discrete spectral bands (4–50 spectral bands). Whereas human vision is limited to visible light, multispectral sensors, or imagers, can collect data over a wider range of the EM spectrum and record the energy of a discrete number of spectral bands. MS sensors usually cover the VIS portion of the EM spectrum in addition to the NIR and SWIR.

Frequently, an MS platform will have a variety of different sensors onboard and therefore can collect data across the EM spectrum from the VIS to the TIR range. (API, 2013)

HS imaging differs from MS imaging in that it divides the image spectrum into much narrower spectral wave bands. HS sensors are passive sensors that collect data across the EM spectrum. Whereas human vision is limited to visible light, HS imagers can collect data over a wider range of the EM spectrum and divide the energy into many more bands (>100 spectral bands). Although most HS sensors operate between the VIS and SWIR wavelengths, several sensors also collect data in the TIR range. (API, 2013)

Most HS imaging systems operate in the visible through NIR wavelengths and rely on solar illumination, which may limit their use in arctic conditions. This limitation can be addressed by active illumination of the area in question. Laboratory and outdoor tests have shown that using an active illumination source can improve target detection performance while reducing false alarms for both multispectral and hyperspectral imagers. The improved performance is important for applying the system in automated or semi-automated mode and for oil monitoring in darkness.

In open water conditions the higher spectral resolution of HS imagers allows them to assess spectral signatures specific to oil. For example, the NIR portion of the spectrum is sensitive to oil thickness and the water-to-oil ratio in an emulsion. An example of laboratory spectra of oil emulsions sampled during the Deepwater Horizon (DWH) spill is presented in Figure 10.

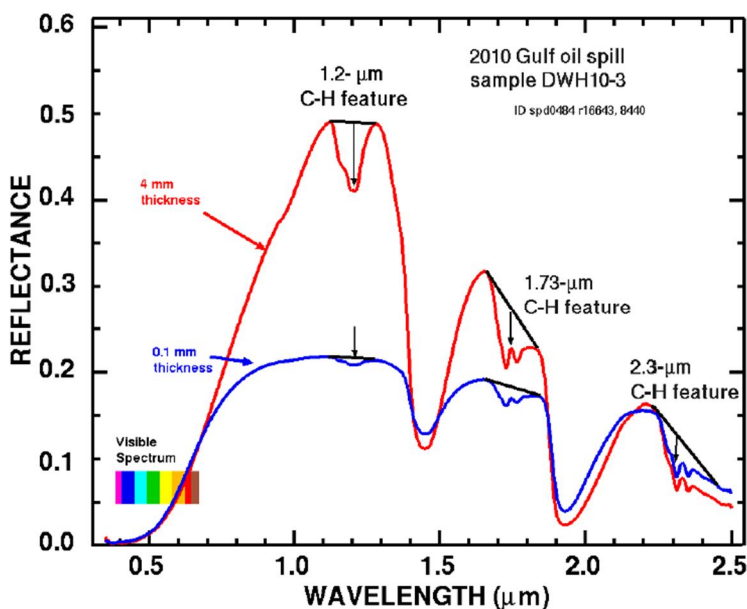


Figure 10. Laboratory spectra collected from a sample of oil emulsion. (Puestow et al, 2013)

At visible wavelengths ($\sim 0.4\text{--}0.7\ \mu\text{m}$), the oil is very absorbing and does not change colour significantly with depth. At infrared wavelengths ($\sim 0.74\text{--}1.4\ \mu\text{m}$), both reflectance levels and absorptions due to organic compounds vary in strength with thickness. The emulsion exhibits clearly defined spectral features in the NIR. The shape of the spectrum depends on emulsion thickness. The black lines and arrows highlight spectral regions corresponding to the absorption bands in the oil. (Puestow *et al*, 2013; Partington, 2014)

Analysis of field data collected over the DWH spill using the Airborne Visible Infrared Imaging Spectrometer (AVIRIS) provided quantitative values for oil thickness and oil-water ratio. Maps of oil thickness and emulsion ratio (Figure 11) were generated using emulsion ratios of oil absorption bands. This information was subsequently used to estimate oil volume.

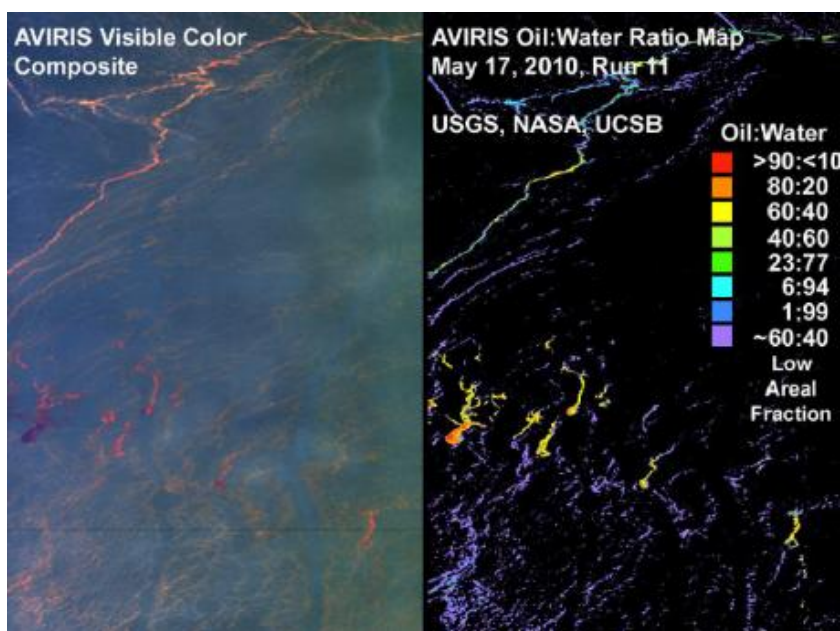


Figure 11. Colour composite and corresponding oil-water ratio map generated with AVIRIS. (Puestow *et al*, 2013)

The results from HS measurements can be generated relatively quickly but the analysis can be quite complex. Classifying the surface material (oil on water) requires a priori knowledge of the spectral response of the material being probed. This means that in-situ field measurements must be taken before classification can be carried out. Operators require a higher level of expertise to use and interpret hyperspectral measurements. Additionally, these detectors can be quite large and are not readily deployed.

In ice-affected waters the application of hyperspectral imaging has not been field tested. Given the high spectral resolution and approximately 1 m spatial resolution, it is expected that this sensor would be at least as effective as a low spatial resolution, multispectral visible range camera for detecting oil around ice. However, the analysis of hyperspectral data can be complicated. In the future, operational applications need to consider automated products that can be easily interpreted in near real-time (NRT) for tactical oil spill response (OSR).

There is a potential to use hyperspectral measurements to quantify oil spill characteristics (e.g. thickness, oil-to-water ratio). In order to be a viable method in oil-in-ice detection, spectral libraries corresponding to the applicable surface conditions need to be developed. The necessary reflectance spectra depend on the oil, the ice conditions (e.g. is the oil mixed with brash ice), visibility and atmospheric state.

Up-coming hyperspectral satellite missions may provide useful information for OSR. Planned missions to be launched within the next few years are presented in Table 2.

Table 2. Future hyperspectral satellite missions. (Puestow et al, 2013)

Instrument	Spectral range [nm]	Number of bands	Spatial resolution [m]
ENMAP	420–2 450	155	30
HYSPIRI	380–2 500	213	60
PRISMA	400–2 500	211	20–30

Based on the information presented in the references (Puestow *et al*, 2013; API, 2013; and Fingas and Brown, 2013), the following conclusions can be made regarding the advantages and disadvantages of multispectral and hyperspectral sensors.

The advantages of MS and HS sensors are that the data collection across multiple spectral ranges may reduce false positives. A potential also exists for combining bands together into one image that can quantitatively measure oil thickness or provide other specialty data sets.

The disadvantages of MS and HS sensors are that more complex sensor systems may require longer turn-around times for producing usable data and images. MS and HS sensor operators typically need greater technical specialization and training to operate the equipment. Furthermore, an extensive volume of data is generated, and post-processing data can be time consuming. Additionally, final image products cannot be provided in near real-time (NRT) based on the large size of files and the status of the current technology. Hyperspectral Sensors can be deployed on aircraft and satellite systems. (API, 2013)

The reference (API, 2013) noted that the MS sensors typically flown on satellites have variable spatial, spectral, and temporal resolutions, which probably require a combination of different sensors for the most effective result. Several long-term series and high spatial resolution satellites are equipped with MS sensors and several off-the-shelf aerial sensors are available for rapid deployment.

Most hyperspectral imaging systems operate in the visible through NIR wavelengths and rely on solar illumination, which may limit their use in an arctic environment. Actively illuminating the scene of interest offers a way to address these limitations while providing additional ad-vantages (Figure 12).

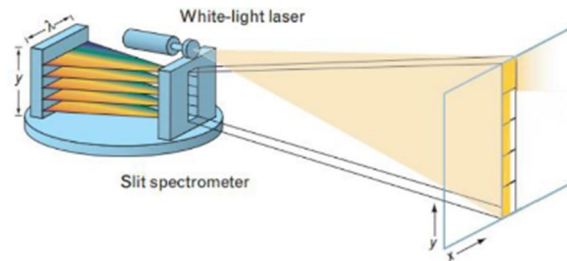


Figure 12. Visible and NIR hyperspectral push-broom imager for acquisition of a spectral signature for every pixel in y (vertical slit field of view of the imager) and wavelength. (Puestow et al, 2013)

Passive hyperspectral imaging during night time is only possible in the infrared portion of the spectrum. Experimental research results show that it is difficult to find stable spectrum characters in the long-wave infrared spectrum. However, the broadband images in the long-wave infrared spectrum band could provide a high contrast ratio between oil and water. A reliable oil detection model using a passive hyperspectral imaging system is under development by Yu Hui's group in China. (Hui et al, 2017)

Limitations of hyperspectral imaging in oil spill detection are summarised in the following sections:

- In the region 720–1000 nm, oil reflectance is higher than that of water (1%–2%) for all thicknesses apart from very thin slicks (sheens) of crude oils (some micrometres) and thin slicks of light oils (less than 300 μm). (Karathanassi, 2014)
- It is not possible to estimate oil thickness on shallow water based on oil spectral signatures due to environmental effects. (Karathanassi, 2014)
- The visible and infrared bands, from 468 nm to 933 nm, are suitable to identify crude or diesel oil. In addition, when the background is pack ice, the infrared region from 1134 nm to 1326 nm is another potentially useful zone. Through the visible-to-infrared bands, sensitivity to the presence of diesel is inferior to that of crude oil. Relatively, the bands greater than 1134 nm have the potential to separate diesel from water or sea ice. (Liu et al, 2016)
- Present passive hyperspectral sensors require sunlight to operate. Active optical hyperspectral systems with e.g. white light laser illumination can be used in darkness (Puestow et al, 2013). Nevertheless, passive hyperspectral imaging is possible in the thermal infrared portion of the spectrum. (Hui et al, 2017)

- Detecting oil under ice or snow or encapsulated in ice, or detecting oil in blowing snow, fog or rain is not recommended (Puestow *et al*, 2013). Nevertheless, identifying diesel beneath compact ice is possible. (Liu *et al*, 2016)
- Natural phenomena such as oil appearance changing because of the sun's angle may result in incorrect outcomes. (Keshavarz *et al*, 2016)
- From experiments implemented in marine environment, oil density, oil quantity in association to wind intensity, and the depth of the sea bottom have been found to be the main factors that affect the spectral signatures. (Karathanassi, 2014)
- It is not possible to distinguish the oil or petroleum product type using unmixing-based methods. An extended spectral library of oil types and petroleum products, based on spectral measurements in marine environments, could enable labelling of the various oil types and thicknesses and lead to oil type detection. (Karathanassi, 2014)

The following recommendations related to hyperspectral and multispectral imaging in oil spill detection are presented:

- Hyperspectral imaging can overcome most if not all of the drawbacks of the conventional application of oil detection using multispectral satellite or microwave imagery. (Salem, 2002)
- Hyperspectral sensors offer potential for detecting oil present on the surface of sea ice or on melt ponds, and on all pack ice concentrations. (Puestow *et al*, 2013)
- For operational monitoring of the environment in detection of oil spill, hyperspectral imagery is a more accurate technique than multi-spectral systems. By using the airborne hyperspectral temporal image, it can predict how an oil spill will spread on water bodies and which sensitive places can be affected in the existing ecological environments. (Keshavarz *et al*, 2016)
- When spectral signature-based target detection algorithms and one anomaly detection-based algorithm were tested for oil spill detection using AVIRIS hyperspectral image datasets, the Spectral Fringe-adjusted Joint Transformation Correlator SFJTC and the Constrained Energy Minimization CEM partial detected the test target regions. (Alam and Sidike, 2012)
- Hyperspectral imaging can utilize methods beyond the standard statistical-based image classification used in multispectral remote sensing. One approach is Mixture Tuned Match Filtering (MTMF). (Salem, 2002)
- Labelling can be accomplished using an existing reference spectral library. An example of such a labelling procedure is that for every extracted endmember and for each one of the spectral signatures which are included in the reference spectral library, two spectral similarity measures, the

Spectral Angle Mapper (SAM) and Cross Correlation (CC) values, can be used for the labelling (Karathanassi, 2014). An example of spectral angle mapper oil spill detection is seen in Figure 13.

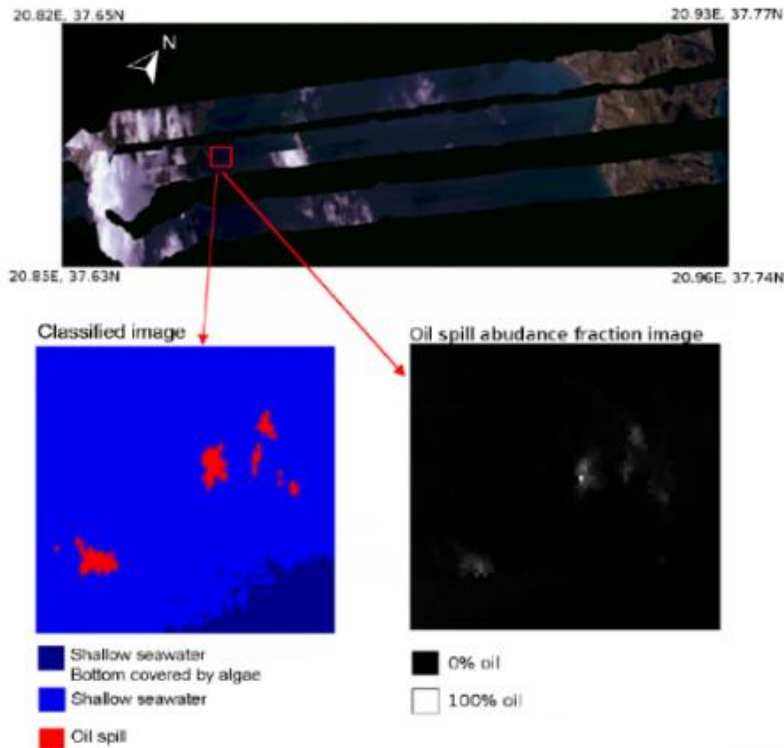


Figure 13. SAM algorithm classification results (product of the proposed hyperspectral oil-spill detection methodology) and map of the relative thickness of the oil spill (oil abundance fraction image) for the CASI hyperspectral camera image (thin oil spill event). (Karathanassi, 2014)

- There is little research available to describe the performance of remote sensing technologies for detecting and monitoring oil in ice-affected marine environments. It is therefore recommended to investigate the performance in ice conditions for technologies currently used to monitor oil in open water. Hyperspectral sensors, which include UV, visible, and IR wave ranges, have great potential and should be explored further. (Puestow et al, 2013)

There are two general branches of spectral imagers. Push-broom scanners and the related whisk broom scanners read images over time, whereas snapshot hyperspectral imaging uses a staring array to generate an image in an instant (Grahn and Geladi, 2007). The Finnish company Specim Oy is marketing several

push-broom hyperspectral cameras with decades of experience and various spectral regions (Specim, 2017).

VTT has developed and is currently developing its own hyperspectral camera technology, which is based on the staring array Tunable Fabry Perot Interferometer method. Wavelength ranges cover VIS, NIR and SWIR spectral regions. The Finnish company Senop Oy markets the Rikola VIS hyperspectral camera, which is based on VTT Fabry Perot Interferometer technology. (Senop, 2017)

2.3 Infrared sensors and radiometers

2.3.1 Thermal Infrared (TIR) sensors

The nature of energy radiated from an object is dependent on its temperature. Passive Thermal Infrared (TIR) sensors are sensitive to the radiant energy emitted by objects according to their kinetic temperature. Absorption in the atmosphere affects most of the TIR spectrum except for atmospheric windows from 3 to 5 μm (mid-wave infrared (MWIR), some heat sensitivity) and 8–14 μm (long-wave infrared (LWIR), good heat sensitivity), where most TIR sensors are designed to operate. (API, 2013; Puestow *et al*, 2013)

Oil and water have different emissivities, causing a thermal contrast that can be identified using TIR sensors. During daylight thick spills appear warmer than the surrounding water since they absorb solar radiation faster. By contrast, thin films tend to appear cooler than oil-free water. The apparent decreased temperature of a thin slick is not well understood but it may be due to electromagnetic interference effects over the oil film. For night-time TIR imagery this pattern is reversed, with thin slicks appearing warmer than the water background and thicker oil acting as a thermal insulator and thus appearing cooler. Although TIR imagery does not rely on solar illumination, the contrast between oil and water tends to be higher during daylight hours.

Many TIR sensors used in maritime oil spill detection operate in the 8–14 μm spectrum. TIR sensors are available as cooled (cryogenic) or more recently, uncooled systems. Older cooled systems required liquid nitrogen, which limited the period of operation to several hours. Newer systems use cooling based on gas expansion. More recently, uncooled systems have become available that are smaller and more easily operated and maintained. However, cooled systems have a lower noise floor and greater sensitivity to detect thermal contrast, resulting in longer operating ranges and higher spatial resolution compared to uncooled systems. (Puestow *et al*, 2103; Svejksky *et al*, 2012)

TIR sensors are relatively inexpensive, easy to deploy and commercially available as handheld or airborne units. TIR sensors are used widely for oil spill detection and response, as they can operate day or night and provide information on relative slick thickness. TIR sensors can be paired with UV sensors to capture slicks thicker than 20 μm , while UV scanners are used to map thinner accumulations of oil.

Although TIR sensors do not rely on solar illumination, they are adversely affected by fog, poor weather and rough water. TIR imagery may also generate false positive observations from aquatic vegetation, shoreline and oceanographic phenomena (e.g. fronts). Emulsions with 60% water content were successfully mapped by Svejkovsky *et al* (2012) using an uncooled Jenoptik IR-TCM640 microbolometer. Figure 14 presents emulsified oil of different thicknesses and textures as imaged by the thermal IR (top) and visible multispectral sensors (bottom) using 450, 551 and 600 nm bands for the blue, green and red image components. The bottom graph shows digital number and temperature profiles along the yellow line in the imagery.

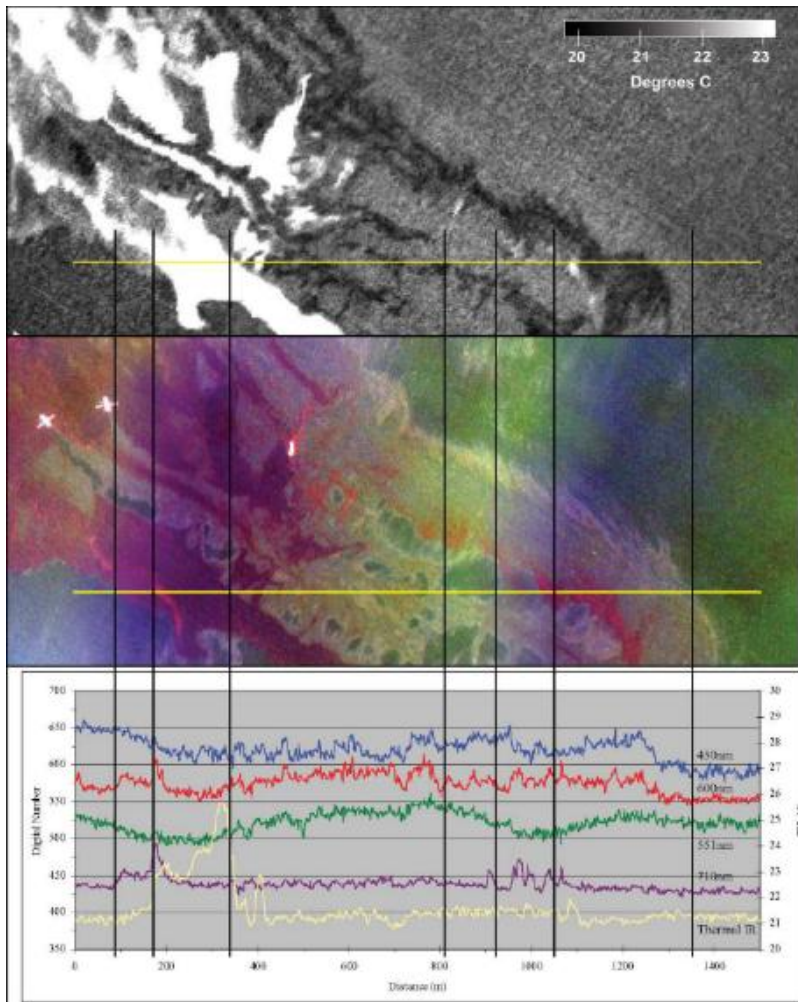


Figure 14. Emulsified DWH oil of different thicknesses and textures captured by thermal (top) and multispectral (bottom) sensors. (Svejkovsky *et al*, 2012)

In addition to nadir-viewing line scanners, Forward Looking Infrared (FLIR) is frequently used in aerial oil spill surveillance. FLIR sensors perform similarly to TIR scanners, although varying viewing angles make area and distance measurements less feasible. FLIR systems are also routinely used in other maritime surveillance applications, such as vessel detection and search and rescue missions. An example of a FLIR image is presented in Figure 15.



Figure 15. Example of FLIR image of an oil spill. (Puestow et al, 2013)

Since the emissivities of ice and water are similar over much of the TIR spectrum, it is expected that TIR will be suitable for detecting oil in ice-affected waters. Puestow et al (2013) concluded that TIR sensors are promising tools for detecting oil on water between ice floes, but will probably not be effective in detecting oil in ice or under snow, since the radiation emitted by the oil is absorbed during its passage through the overlaying ice and snow (Figure 16).

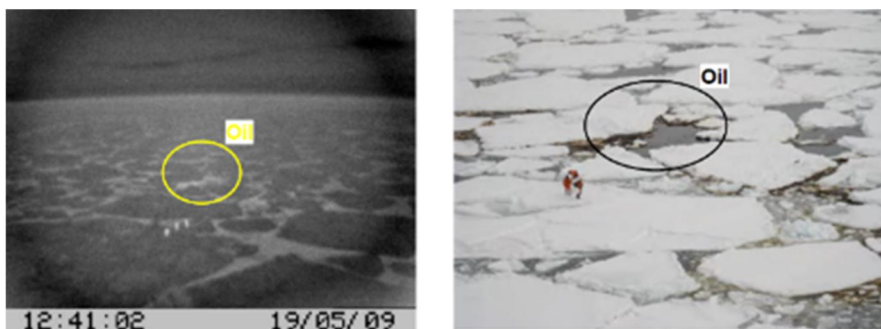


Figure 16. Oil between ice floes imaged with TIR sensor (left) and with an optical camera (right). (Puestow et al, 2013)

Additional research is required to fully test and validate the performance of TIR imaging systems in different ice conditions. The detection of oil on ice as well as on surface melt ponds should also be investigated. These investigations may include sensors mounted on vessels or platforms, as well as airborne TIR scanners and FLIR systems. Satellite-based TIR sensors are unlikely to provide valuable tactical information for detecting oil in ice environments due to their limited spatial resolution. (Puestow *et al*, 2013)

2.3.2 Microwave radiometers (MWRs)

Microwave radiometers (MWRs) measure emitted radiation with wavelengths in the range of millimetres. As with TIR detection, observed differences in the surface microwave emissivity enable discrimination between different surface materials. Passive MWRs detect the presence of an oil film on water by measuring the reflection of the surface as excited by the radiation from space. The apparent emissivity factor of water is 0.4 compared to 0.8 for oil (Fingas and Brown, 2014), and can appear brighter than oil-free water in MWR. Microwave emission from oil slicks can be influenced by interference over the oil layer and is greatest when the round-trip electromagnetic phase difference over the oil layer is equal to a multiple of π . (Jha *et al*, 2008)

The brightness measured by the MWR sensor can theoretically be related to estimates of oil slick thickness. In practice, signal uncertainties have been reported as a result of the cyclic nature of the constructive interference condition and the resulting thickness estimation. Attempts to resolve this issue include the use of multi-frequency scanning radiometers, and relating oil thickness to variations in polarization of the microwave signal.

Although not widely used, multi-frequency MWR sensors are deployed for operational pollution surveillance in Germany in open water conditions. Optimare's MWR is capable of detecting, measuring, and mapping oil layers with thicknesses in the range from 0.05 to 3 mm. MWR instruments enable oil film thickness measurement in the range of 0.05 to 2.5 mm when flying at an altitude of 300 m. MWR systems operating at 18, 36 and 89 GHz provide complementary information at varying spatial resolutions as follows:

- 18 GHz: sensitive to thicker films, spatial resolution is 22 m;
- 36 GHz: compromise regarding spatial resolution (11 m) and all-weather capability and
- 89 GHz: sensitive to thin films, spatial resolution is 5 m.

MWRs can operate in conditions of low visibility (e.g. fog, rain and night), although false positives can be generated by waters of different temperatures, seaweed and biogenic material. MWR systems can be costly and require a dedicated aircraft to accommodate a special antenna. (Jha *et al*, 2008)

MWR systems have not been tested or validated in ice conditions and their potential for characterising oil in ice-affected water is unknown. Research on

utilisation of MWR sensors in ice conditions, especially in low ice concentrations (< 3/10), could be useful in the evaluation of this technology for operational application. (Puestow *et al*, 2013)

2.4 Radar sensors

Radar sensors are active systems and include Side-Looking Airborne Radar (SLAR), Synthetic Aperture Radar (SAR), X-Band (Marine Navigation) Radar and Ground Penetrating Radar (GPR).

2.4.1 Side-Looking Airborne Radar (SLAR) and Synthetic Aperture Radar (SAR)

SLAR and SAR are active sensors that provide their own microwave energy source and record how much of an emitted signal is returned to the sensor. Therefore they do not require sunlight and are not affected by cloud cover. Radar backscatter signal depends on the parameters of the imaged surface, such as target material and conductivity, and on system characteristics such as wavelength, incidence angle and polarisation. Current systems operate in frequencies that provide capabilities for both terrestrial and marine event response.

Radars use an antenna to emit and collect the microwave signal, and spatial resolution improves as the length of the antenna increases. Due to the large antenna size, SLAR is restricted to aerial platforms, typically fixed-wing planes. By contrast, SAR uses the forward motion of the sensor platform while taking into account the Doppler shift of the collected signal to synthetically increase antenna aperture. Imaging satellite radars rely on SAR, although airborne SAR sensors are also used. SAR satellites are emerging as the predominant means of ice surveillance over large areas and are widely used by national ice centres around the world.

The presence of oil is detected by textural discrimination, as natural sea roughness is greater than that in surface areas with oil. Oil slicks on water are detectable by radar imagery because of the dampened capillary waves which correspondingly reduce backscatter compared with the surrounding oil-free water (Figure 17).

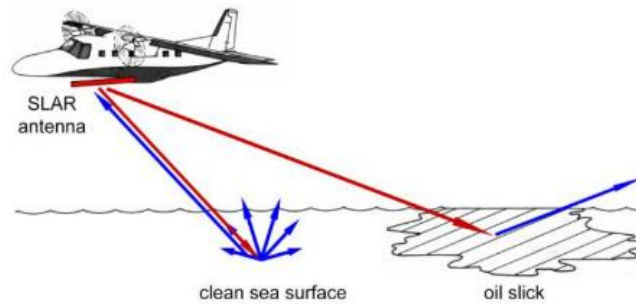


Figure 17. Principle of radar scattering from an oil spill vs. open water. (Partington, 2014)

Oil on water appears as dark patches on radar images (Figure 18). Capillary waves are also reduced by other phenomena and verification by other means is therefore required to identify oil unambiguously.

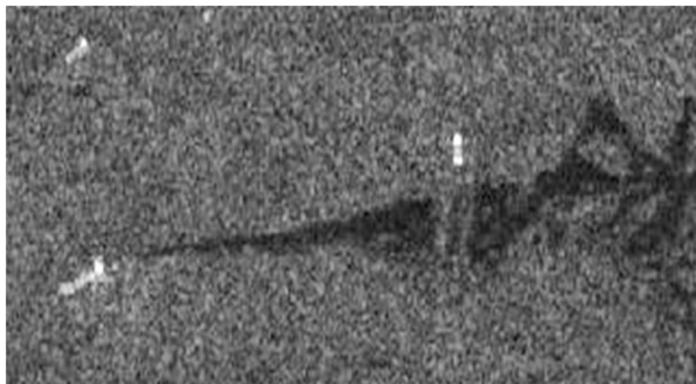


Figure 18. SAR image of a ship (bright target near the bottom left corner) discharging oil into the sea. (Centre for Remote Imaging, Sensing and Processing (CRISP), 2015)

Wind speed is a major factor in the detection of oil with radar. At low wind speeds there is relatively little wave activity and almost no scattering from the ocean surface, which minimises the contrast between oil-affected and oil-free areas. At very high wind speeds, the larger waves are substantial enough to overcome damping effects caused by the oil. Under these conditions the brightness contrast between the oil and surrounding water is diminished and the presence of oil cannot be detected. In general, wind conditions between approximately 3–10 m/s are favourable for detecting oil on open water using SLAR or SAR sensors.

False alarms can also be caused by biogenic slicks, presence of fresh water, grease ice, shear zones and internal waves. These all may have a radar signature similar to oil on water. Discriminating oil from the water background typically relies

on analysis of a local image contrast as well as the shape and distribution of observed dark patches.

Satellite-based oil spill monitoring has become an integral part of national pollution control in Europa and Canada. In Europe, the European Maritime Safety Agency (EMSA) administers satellite-based monitoring through a network of service providers, while in Canada the Integrated Surveillance and Tracking of Pollution (ISTOP) program is executed through the Canadian Ice Service (CIS).

The presence of oil slick look-alikes remains a constant issue, with false alarm rates ranging from 15 to 85%. However, recent research indicates that automated algorithms are increasingly able to differentiate between oil slicks and look-alikes, with classification accuracies ranging from 73% to 92%. Present operational oil spill monitoring using satellite SAR is based on manual or semi-automatic interpretation with significant input from operators, suggesting that automated algorithms may not yet be able to fully take account of environmental conditions, look-alikes and slick characteristics encountered in the routine surveillance of large areas. (Puestow *et al*, 2013; API, 2013)

An overview of current and future SAR satellites is presented in Table 3.

Table 3. Current and future SAR satellites. (Puestow *et al*, 2013)

Sensor	Band	Polarisations ²	Spatial resolution [m]	Swath width [km]	Revisit frequency	Status
RADARSAT-1	C	HH	10–100	50–500	2–3 days	Safe mode*
RADARSAT-2	C	HH, VV, HV, VH	1–100	50–500	2–3 days	Operational
COSMOSKYMED	X	HH, VV, HV, VH	1–100	10–200	2 days	Operational
TERRASAR-X	X	HH, VV, HH/VV, HV, VV, VH	1–18	10–150	3–4 days	Operational
SENTINEL-1	C	HH, VV, HH/VV, HV, VV, VH	20	250	1–3 days	Operational
RCM	C	HH, VV, HV, VH	1–100	50–500	Daily	Launch in 2018

* RADARSAT-1 stopped accepting new tasking requests in April 2013 but may become operational again.

Concerning the application of SLAR and SAR in ice-affected waters, the reduced wave activity limits the utility of radar for detecting oil spills. Recent studies have indicated that SLAR and SAR were not able to detect oil contained between close-packed ice. It was suggested that radar may be useful for imaging spills in open pack ice, where the ocean wave behaviour is closer to that of open water conditions, but this assertion has not been field-validated. Furthermore, new ice may dampen ocean waves like oil, which may result in false oil observations.

The reference (API, 2013) concludes that SLAR and SAR are effective in sea states between 0.2–1 m, daylight hours and night-time and in cloud, rain or fog conditions. They are not effective in very calm seas with wind speeds less than 5.5

² HH =horizontal transmit and receive, HV = horizontal transmit, vertical receive, VV = vertical transmit and receive, VH = vertical transmit, horizontal receive.

km/h (approximately 3 knots or 1.53 m/s) and in very rough seas with wind speeds greater than 22.5 km/h (approximately 12 knots or 6.25 m/s).

Additionally, the reference (API, 2013) summarises the advantages and disadvantages of SLAR and SAR sensors as follows. Advantages of SLAR are that little data processing time is required, it performs day or night and under clear or cloudy conditions, the technology has been successfully used during oil spills for decades, and SLAR is readily available.

Disadvantages of SLAR are that the range resolution is altitude dependent, because at higher altitudes the sensor sees a larger area but at a lower resolution, interpretation of true oil is complex, it does not discriminate between thin or thick oil, the imagery is prone to false positives due to other sea-dampening phenomena (e.g. seaweed and wind shadow) and the technology is difficult to use in areas cluttered with wind shadows (e.g. an area with a high concentration of small islands).

Advantages of SAR are that it works day or night under clear or extreme weather conditions, little data processing time is required, the technology has been successfully used during oil spills for decades, it is readily available as both airborne and satellite systems from both private and government sources and SAR imagery provides spatial resolution superior to SLAR imagery by simulating a longer antenna length through signal processing. (API, 2013)

SAR cannot penetrate thick ice cover due to the high attenuation of saline ice. The ice thickness is particularly critical when operating at high SAR frequencies (e.g. X-band 8–12 GHz), as the attenuation coefficient increases with frequency. Although attempts to detect oil within high ice concentration during the SINTEF Joint Industrial Programme (JIP) project were unsuccessful, it was suggested that there was no technical reason why such sensors could not detect oil in open ice (1/10–3/10). Further work is required to determine the full capabilities of SAR and SLAR systems in ice. (Puestow *et al*, 2013)

Disadvantages of SAR are that the interpretation to discern oil is complex and requires a skilled expert, the imagery is prone to false positives due to other sea-dampening phenomena (e.g. seaweed, wind shadows and rain), it does not distinguish between thin or thick oil and it is difficult to use in areas cluttered with wind shadows (e.g. an area with a high concentration of small islands). (API, 2013)

2.4.2 Marine radar

The frequency range for X-band (marine) radar is specified by the Institute of Electrical and Electronics Engineers (IEEE) at 8.0 to 12.0 GHz with a wavelength range of 3.75–2.50 cm.

Marine radar is used primarily for navigation purposes, but the systems can be reconfigured to maximize sea clutter in order to observe the reduction of return signals associated with calmer areas. Like all radar systems they are active sensors that provide their own energy source. Therefore no sunlight is required for operation, and X-band radar is not affected by cloud cover.

Ship-based radars have been developed in such a way that they could be utilised to detect oil in the presence of ice in order to supplement aerial and satellite sensors. SLAR and SAR typically operate at steep incidence angles that are more favourable to ocean backscatter, but the relatively low elevation of the marine radar on a ship's superstructure means that it must operate at much shallower angles of incidence. Therefore there is less backscatter, making discrimination between individual objects in the scene more challenging. To compensate for this, commercially available marine radars integrate successive radar images to produce stable images of potential targets.

The integration is possible since marine radar is able to dwell on an area of interest for many revolutions of the antenna and improve the ability to discriminate between different objects in the scene. Current commercially available radars integrate up to 128 images. For typical marine radar scanners that operate in the range of 20–30 RPM, this necessitates a dwell time of the order of four to six minutes to create a stable image. (Puestow *et al*, 2013)

Several commercially available scan averaging radar systems exist, including e.g. SeaDarq, Rutter Sigma S6, Miros OSD and Consilium, and are offered as an add-on to standard marine X-Band radars. An example of vessel-based Furuno Oil radar FOIL-200 radar output is provided in Figure 19. FOIL-200 is connected to Furuno navigation radar without affecting any of its properties or performance. (Furuno, 2017)

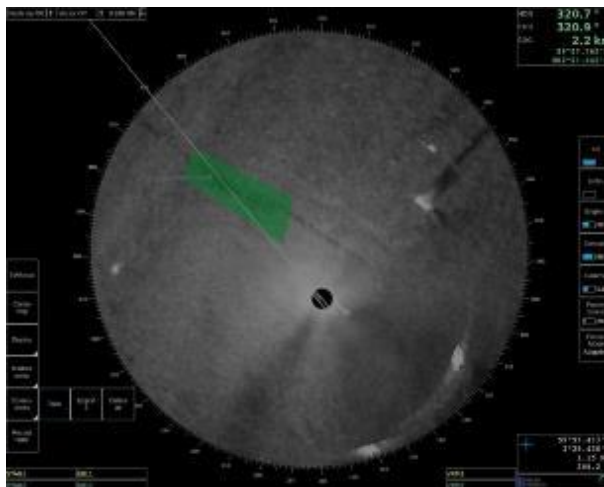


Figure 19. Screenshot of Furuno Oil radar: oil detection marked with green. (Furuno, 2015)

The range of ship-borne radar is limited to approximately 8–30 km, largely by the height of the antenna. Ship radars can be adjusted to reduce the effect of sea clutter.

During trials in the Baltic Sea, ship-borne radar successfully detected a surface slick at a distance of 8 km, and during a trial off the coast of Canada slicks were

detected at a maximum range of 17 km. During the Prestige spill a Netherlands vessel successfully used this technique to guide a recovery vessel into slicks. However, sea state limits the use of the technique and ship radars will provide little legal evidence in cases where the presence and location of the slick were already known or suspected.

The ability of marine radars to detect oil in the presence of ice has not been validated yet but it is expected that the ability to detect oil reliably will decline with increasing ice concentration. Further validation is required to identify the window of opportunity within which oil can be detected in sea ice. (Puestow *et al*, 2013)

The reference (API, 2013) summarises the marine radar characteristics in oil detection as follows. Marine radar is effective in sea states between 0.2–1 m, in daylight hours and night-time and in cloud, rain or fog conditions. It is not effective in very calm seas with wind speeds less than 5.5 km/h (approximately 3 knots or 1.53 m/s) or in very rough seas, with wind speeds greater than 22.5 km/h (approximately 12 knots or 6.25 m/s).

Advantages of marine radar are that it provides real-time processing on the scene and the technology works day or night under clear or cloudy conditions.

Disadvantages of marine radar are that most navigation radars are not configured for oil slick detection, the low altitude of the sensor limits the observable range of the field of view, it does not discriminate between thin or thick oil, the imagery is prone to false positives due to other sea-damping phenomena (e.g. seaweed, wind shadows, and biogenic oils), the interpretation to distinguish the presence of oil is complex and requires a skilled expert, and marine radar cannot provide an estimate of slick thickness. (API, 2013)

2.4.3 Ground Penetrating Radar (GPR)

GPR uses electromagnetic waves in the microwave region (typically 250 MHz–1 GHz) to probe the surface of the area. An electromagnetic pulse is produced and directed into material below the GPR. Through analysis of the resulting backscattered signal, information about the composition of the underlying material structure is obtained. The collected data consist of a collection of returned pulses corresponding to reflections at interfaces where the dielectric permittivity or electrical conductivity change. (Puestow *et al*, 2013)

GPR reflections will be seen if the targets have different electromagnetic properties, i.e. dielectric permittivity and conductivity (Table 4).

Table 4. Dielectric constant and conductivity. (Fingas and Brown, 2013)

	Dielectric constant	Conductivity [S/m]
Snow	1.4–2.5	10^{-7}
Oil	2–4	10^{-5}
Fresh water ice	3	
Sea ice	4–7	$>10^{-2}$
Frozen soil	4–5	
Water	80	

Sea ice is a heterogeneous media since it often contains salt water intrusions with a dielectric constant of 80, which complicates the detection of oil under ice or snow. The processing of GPR is complex, but can sometimes be used to define targets.

GPR propagates easily through snow and the dielectric permittivity is also relatively favourable (Table 4). On the other hand, sea ice has low conductivity and can possess structure and therefore heterogeneity. Snow being more consistent, it is an easier media to penetrate. Oil and snow have rather similar electromagnetic properties and thus are more difficult to distinguish. Oil may be more easily distinguished from snow when oil displaces air in the snow, thus creating a higher dielectric target. This anomaly from air-filled snow may be easier to detect using GPR.

The depth of an oil layer can be distinguished when it is at least one quarter of the radar wavelength. Since most commercial GPRs have upper frequency limits of 1–1.5 GHz, one quarter wavelength in snow is about 4–8 cm. This is actually quite a thick oil layer and would be achieved only in special circumstances. Oil spills could constitute a very complex environment if they drain through a snow pack rather than form on ice in one consistent layer. The penetration of GPR through snow depends on the density of snow and the presence of ice. A mature snow pack with ice and other heterogeneities would constitute a difficult situation for the GPR to discriminate between substituents. (Fingas and Brown, 2013)

GPR technique has been used to characterize ice and snow structures in the Arctic. GPR can detect oil spills under snow and ice. The dielectric permittivity ratio between sea ice and sea water is much greater than the corresponding ratio between sea ice and oil. Therefore GPR has potential for imaging an oil layer within ice and snow. The large difference of permittivity at the ice/water interface compared to that of an oil/ice interface, however, poses problems both in signal strength and in sensitivity range and requires that the GPR receiver has a large dynamic area. (Puestow *et al*, 2013)

Although GPR has potential for detecting oil under ice snow, obtaining quantitatively meaningful values for properties such as oil type is a difficult problem. The scattering process can be quite complex, and analysis of the collected reflection signals can be plagued by ambiguities. Variations in snow and ice structure, such as stratification in snow as well as deformations at the ice interfaces, can lead to observable changes in amplitude. Hence, the GPR response to an oil spill is not unique and is similar to the response from ice layers and channels in snow.

Therefore, an important task is to develop semi-automated classification algorithms and software to help analyse the GPR signal. (Puestow *et al*, 2013)

The reference (Fingas and Brown, 2013) concluded that GPR interpretations cannot provide absolute information about the location of a spill, nor will GPR provide a unique indicator of oil.

In the tank tests and field experiments reported in (Dickins, 2010), GPR could clearly detect and map the presence of oil films as thin as 1–3 cm underneath the ice and trapped as layers within the ice. Based on the numeric modelling GPR system, operating at low altitude from a helicopter should be able to detect thin oil layers under cold ice in mid-winter, as well as oil on the ice surface buried under snow.

The results indicated that readily available, commercial GPR systems can be used effectively to detect crude oil spills within or under snow in arctic environments. (Dickins, 2010)

2.5 Lasers and fluorosensors

Airborne laser remote systems for oil pollution monitoring can be divided into several groups: multispectral, hyperspectral and laser-ultrasound (LURSOT). Active lasers and fluorosensor technologies have been widely tested for oil spill monitoring. (Puestow *et al*, 2013)

2.5.1 Fluorosensors

Certain hydrocarbons have fluorescent properties. For these materials when UV light (typically 300–400 nm) is incident on an oil sample, visible light within the range of 500–600 nm is produced through a sequence of energy transition in the hydrocarbon molecules. This fluorescence signal is unique to oil and can be used to differentiate a probed sample from materials such as chlorophyll, kelp, water, ice and snow. The fluorescence peak is unique for each oil sample and can be used to classify oil. For thin slicks on water (approximately 1 μm), information on the oil thickness can be deduced through intensity analysis of Raman spectral peaks observed from the water beneath the oil. As the oil thickness increases, the intensity of the Raman peak (stemming from inelastic light scattering in the water) decreases.

Fluorosensors can be deployed from aircraft or the surface. In case of aircraft, a UV laser pulse is emitted from the bottom of the plane or other aerial platform. The laser is scanned across the flight track to cover a horizontal swath of land. The visible-range spectral response is monitored and a spectral peak between 400–600 nm clearly indicates the presence of oil. This spectral analysis may be performed in real-time on the aircraft. A typical laser footprint of FLS-LiDAR is shown in Figure 20.

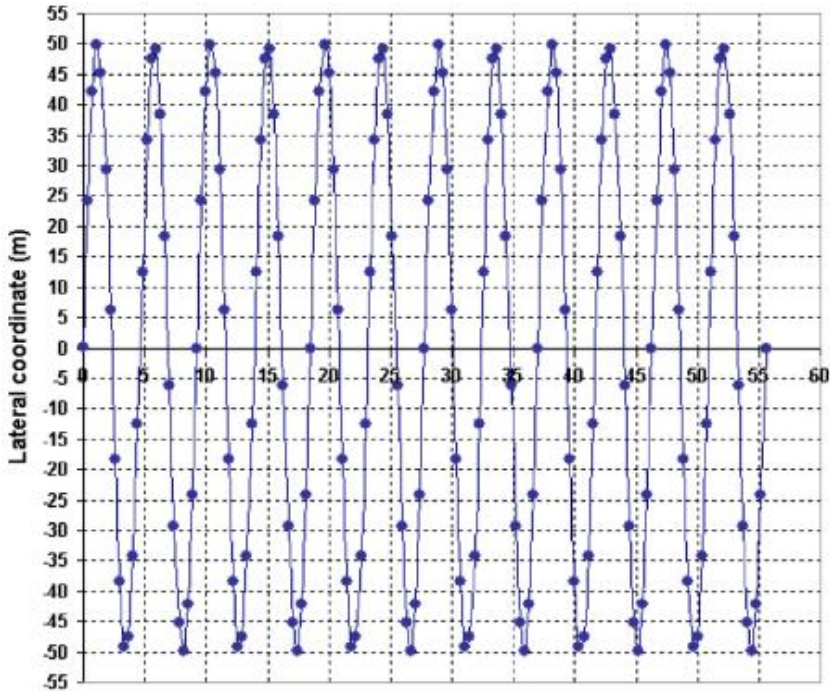


Figure 20. Laser footprints on the ground of FLS-LiDAR. (Babichenko et al, 2006)

Whereas fluorosensors can be used to detect oil on a variety of backgrounds, the relatively high attenuation of UV light in water renders the system ineffective in fog, low cloud-ceiling and rough weather. The system requires a dedicated aircraft with an open belly hatch and depressurized cabin.

Only a limited number of airborne laser fluorosensors are in routine operation, due to difficulty of operation and the relatively high maintenance costs. Systems are operated in Germany and Estonia, whereas Environment Canada has discontinued their laser fluorosensor (LFS) programme.

Fluorosensors operating in the UV spectrum are not suitable for oil detection under snow, because light in the UV to visible range is highly attenuated in snow. The attenuation in ice is not as high over this spectral range, suggesting that fluorosensors may be able to penetrate snow-free ice up to about 1 m thick.

LFS is capable of detecting oil on different surface types, whereas it is ineffective for detecting oil under ice and/or snow. LFS has future potential for discriminating between oil and uniled surfaces. (Puestow *et al*, 2013)

LFSs are effective in daylight hours and night-time. LFSs are not effective when fog and weather conditions limit the transmission of laser and returning fluorescent light. The extent of limitation by weather is determined by the power of the laser system. Altitude also affects the performance of LFFs, and current systems may not

be effective above 500 m. Because water surface roughness may backscatter returning light, surface dynamics can affect the image quality. (API, 2013)

Advantages of LFSs include that they enable real-time analysis and the technology discriminates oil from non-oil false positives, and LFSs may be able to provide slick measurements in both daylight and darkness.

Disadvantages of LFSs are that the current technology is a large system and typically requires a dedicated aircraft, aircraft mission altitude is determined by the power of the laser, oil weathering produces additional complexities in analysis of the data and LFSs cannot provide wide aerial coverage due to their narrow beam width. (API, 2013)

2.5.2 Tunable Diode Laser Spectroscopy (TDLS)

Ethane/methane gas sensors based on the principle of TDLS have been used to measure hydrocarbon mass flux rates generated by oil under ice in the laboratory and in the field. The atmospheric concentration of the gas can be deduced using a tunable diode laser to scan the absorption bands specific to methane and ethane. Concentrations less than 1 ppb are detectable. Since there are several sources that result in methane gas, ethane is a more unique marker for oil. Ethane detection should have a lower false alarm rate for oil than methane detection.

Concerning the application of TDLS systems in ice-affected water, the reference (Puestow *et al*, 2013) noted that practical application of TDLS sensors for detecting oil spills of unknown location is limited. Furthermore, preparing TDLS-based sensors for detecting and mapping ethane and methane from oil under ice and snow is challenging due to the cold weather and the relatively long collection times, with measurements taking several minutes to complete. Furthermore, data interpretation can be challenging, as the observed signal and system performance is sensitive to changes in wind direction and the release of fumes from nearby machinery.

The test results from initial field tests with a TDLS sensor suggested that the emission of light hydrocarbons during a large spill would be sufficient to be detected by Shell's LightTouch system at distances of several kilometres. However, these findings were contested by stating that the ethane and methane would be released from the oil within 10 minutes after the spill occurrence, rendering the TDLS sensor ineffective for detecting an actual spill due to the short window of opportunity.

TDLS sensors are most appropriate during blowouts where a continuous supply of oils occur. Apparently in that case the position of the leakage would be known. Since oil trapped under ice weathers much more slowly, TDLS may be useful for detecting oil concealed in ice. (Puestow *et al*, 2013)

2.5.3 Laser-Ultrasonic Remote Sensing of Oil Thickness (LURSOT)

LURSOT is an aerially-deployed three laser airborne system for determining absolute thickness of an oil spill. Measurements are based on the excitation and

detection of an acoustic pulse in the oil. Since the acoustic wave velocity of oil is known, oil thickness can be deduced from the acoustic wave time-of-flight.

In open water conditions, oil thickness has been successfully determined in both laboratory and small-scale field tests with this sensor. Due to the high attenuation of lasers in ice and snow, LURSOT would be impractical for characterizing oil under ice cover. The performance of this technique in an ice environment is unknown, since the system has never been applied to ice conditions. LURSOT may have potential to determine oil thickness for spills in broken ice when oil is contained between floes. According to Puestow *et al* (2013), LURSOT is not considered a priority for research and evaluation in ice conditions in the near term.

2.5.4 Light Detection and Ranging (LiDAR)

LiDAR systems are based on laser technology similar to fluorescence sensors. A number of airborne and ship-based LiDAR systems which operate in visible (i.e. non-UV) and IR ranges using CO₂ lasers were developed and tested in the USSR. (Puestow *et al*, 2013)

According to Puestow *et al* (2013), it is possible to detect oil on water in open water conditions by analysing the backscattered LiDAR signal (Figure 21).

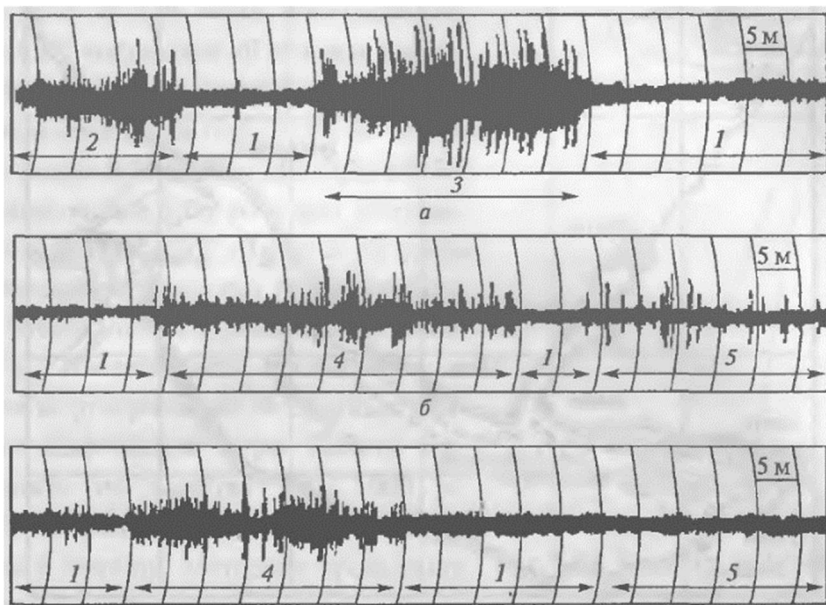


Figure 21. Recorded signal of optical LiDAR: river (top) and lake (middle, bottom). Section of the signal: 1: clear water, 2 and 4: oil film with thickness of 0.2–0.5 micron, 3: oil slick 3 microns, 5: biological film. (Puestow *et al*, 2013)

Oil is easily detected on lakes and rivers, provided that wave heights are low, which suggests that the system may function in ice-covered water where there are no waves. Experiments in the Baltic Sea in high winds (up to 14 m/s) have demonstrated that ship-based LiDAR systems using a CO₂ laser are effective.

Figure 22 presents signal scatter from a diesel fuel spill and sea water with winds of about 1–5 km/h (0.28–1.39 m/s).

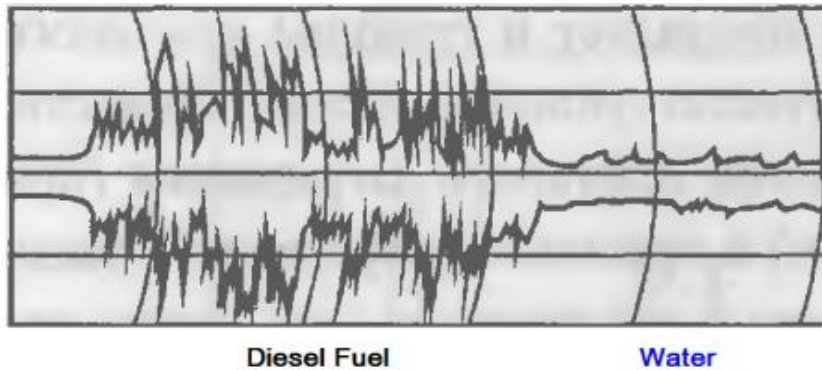


Figure 22. Backscatter from CO₂ LiDAR from the Baltic Sea. (Puestow et al, 2013)

One of the latest applications of LiDAR technology was demonstrated onboard the Sampo icebreaker during the Kemi Arctic 2015 oil recovery exercise (24–26 March 2015 in Kemi, Finland). The technology was provided by Ocean Visuals AS and it has been launched by ICD together with LDI Innovation and Faster Imaging (Figure 23).



Figure 23. Light Detection and Ranging (LiDAR) oil spill detection system by Ocean Visuals AS. (Image: SYKE/Jyrki Nikkilä)

According to the source (ICD, 2015), the basic components of the system will include laser sensors (Hyper-spectral Laser Induced Fluorescence – HLIF LiDARS), capable of selectively detecting part per million concentrations of oil in water, integrated real-time spectral- and metadata processing, on-line communication with NOC and visualization of information for decision making. The system will be developed for unattended continuous day and night operations with minimal technical maintenance.

Since it was not possible to use oil during the Kemi Arctic 2015 exercise, the performance of the system could not be verified.

2.5.4.1 Atmospheric and marine LiDAR

The experimental LiDAR system, called ATMospheric and MARine LiDAR (ATMARIL-3), was developed for atmospheric-optical and hydro-optical measurements from the carrier platform (e.g. aircraft, vessel, etc.). This LiDAR is capable of revealing an oil film on the water surface and chlorophyll/phytoplankton in the water. When short laser radiation pulses enter the water, they are dispersed and illuminate various heterogeneities (e.g. polluting hydrosols, fish), which are detected by the laser locator. The optical signal reflected from the heterogeneities is received, detected and processed by various algorithms. The LiDAR consists of an optomechanical transmitter-receiver, a laser with power supply and cooling systems, an analog-digital converter and a computer. The system makes it possible to account for the influence of above-water atmosphere, including atmospheric precipitations, to reduce the effect of mirror glares resulting from micro-roughness and to adjust the LiDAR parameters to changing conditions and different tasks. (LOOKNorth, 2014)

2.5.4.2 LED based detector

The Russian company Lumex has developed an active IR sensor for environmental monitoring and detection of oil pollution on water. The KRAB-1 detector is based on three infrared Light-Emitting Diodes (LEDs) to generate light beams (similar to laser) and a single channel receiver system (Figure 24).



Figure 24. KRAB-1 detector of oil film on the water surface. (Puestow et al, 2013)

Signal processing capabilities are built into the microprocessor of the unit and the detection of oil on water is based on the difference in the coefficients of light reflection for oil and water. The device can be calibrated for different environmental conditions to reduce the impact of wind waves and background light on the measurement results. The instrument can be mounted on vessels or platforms and can detect oil slicks with thicknesses greater than 0.5 μm over distances up to 25 metres. The instrument supports the generation and transmission of information products in real-time using wireless communications. (LOOKNorth, 2014)

2.6 Experimental sensors

2.6.1 Acoustic sensors

Sound or acoustic waves consist of two types: compressive or longitudinal waves and transverse waves. A transverse wave (or shear wave) is a moving wave consisting of oscillations perpendicular to the direction of travel. Longitudinal waves propagate by means of compression and decompression in the direction of travel. Longitudinal waves are waves that have the same direction of vibration as their direction of travel. These two types have different movement in ice. (Fingas and Brown, 2013)

The acoustical properties of ice are variable. Compressive waves travel almost three times as rapidly as transverse waves, although the speed varies significantly with the type of ice. The attenuation of acoustic waves is also affected by ice type. Sound is strongly attenuated with increased salinity and increased frequency. A frequency of about 200 kHz is about the maximum usable with typical multi-year ice. The speed of the compressive and transverse waves decreases as the salinity increases. The acoustic impedance of air and different types of ice also vary, with the impedance of ice being about twice that of water. (Fingas and Brown, 2013)

According to the reference (Fingas and Brown, 2013), standard acoustic units designed for metal and concrete inspection could be used for oil-in-ice detection. Several studies have shown that acoustic means of detecting oil under ice show potential. However, these technologies were not commercialised or developed further. One difficulty is the logistics of deploying transducers to a clean ice surface (Figure 25).



Figure 25. Acoustic transducers placed on sea ice for a field test to detect oil under ice. (Fingas and Brown, 2013)

Underwater acoustic measurements of the ice/water surface have been used for many years and it is a prime method for under-ice roughness determination. The method may also be useful for detection of oil under ice, as it has been suggested that oil/water and oil/ice interfaces may be detectable and also that the oil would change the underwater ice profile. (Fingas and Brown, 2013)

Although acoustic sensors can be used to detect oil under ice, there are several challenges for deployment. The acoustic sensor (i.e., transducer) must be directly coupled to the ice surface due to the relatively high attenuation of sound in air. This may be achieved by freezing the sensor into the ice surface or by coupling the transducer to the ice through a layer of liquid (seawater or anti-freeze) and the ice must also be snow-free. When operated above the ice surface, acoustic sensors are strictly surface-based systems and cannot be deployed from vessels or aircraft. (Puestow *et al*, 2013)

2.6.2 Nuclear Magnetic Resonance (NMR)

NMR spectroscopy is a technique used to characterise the magnetic properties of a material system. When a material is placed in a well-defined magnetic field, the magnetic dipoles in the specimen are aligned along a known direction. Subjecting the material to an electromagnetic pulse perturbs the magnetic dipoles away from equilibrium. Once the electromagnetic pulse ends, the dipoles return to equilibrium, producing a measurable electromagnetic signal in the process. This electromagnetic response is partially dependent on the material, allowing NMR to image materials based on their magnetic properties.

The earth's magnetic field is highly uniform and can be used for NMR with exciting and emitted electromagnetic pulses in the radio frequency range. At these frequencies the electromagnetic fields can penetrate rock, soil and ice. The

penetration depth depends on the dimensions of the loop antenna used to produce and receive the electromagnetic signal and the material properties. A penetration depth of 1–2 metres requires a loop antenna with a diameter of approximately 5 metres. This technique has been used successfully to detect subsurface water aquifers, which is unsurprising since water exhibits a strong NMR response.

Preliminary work has been done to assess the potential for using aerially-deployed earth field NMR for detecting oil under ice in experimental conditions using loop antenna slung from a helicopter. Initial findings suggest that the electromagnetic response obtained from oil is sufficiently different from water to allow oil detection. Additionally, the relatively high rigidity of ice and snow results in NMR responses over much shorter timescales than those of oil and water, and thus they do not interfere with oil spill detection.

NMR imaging requires sophisticated computer control of the NMR phase and timing parameters and complex processing techniques, such as multi-dimensional Fourier transform. The acquisition time in imaging mode is long, for small objects in laboratory setting varying from 90 minutes to more than 3 hours. Much shorter integration times are required for the system to be operationally feasible. Recent work has focused on improving antenna portability to facilitate aerial deployment, removing dead time between individual measurements to shorten the overall imaging time, and improving Signal-to-Noise Ratio (SNR) to reduce the probability of false alarms. It is anticipated that less than 10 minutes of total imaging time is achievable under operational conditions. Arctic field testing and validation with a full-scale prototype are expected within the next two years (Puestow *et al*, 2013).

The reference (Fingas and Brown, 2013) also notes that recent work on NMR shows promise in oil detection applications, and large-scale field units are being built.

2.6.3 Trained dogs

The utilisation of trained dogs, i.e. canine detection, is a rapid, straightforward, proven concept based on sound scientific principles. The canine sense of smell is at least as sensitive as commercial gas analytical instruments. A trained SCAT (Shoreline Clean-up Assessment Tech) field team consists of a canine, handler and SCAT team lead. The team can provide an efficient, versatile, rapid, reliable, cost-effective and real-time support tool for a SCAT program to locate surface and subsurface oil in a wide range of environmental settings. (API, 2016). The findings presented in the reference were related to shoreline, inland and pipeline scenarios.

A canine's ability to detect surface and sub-surface oil varies as a function of several factors, including the training method and inherent qualities of the canine, health and fitness, welfare and handler motivation. The greatest challenge to independent testing and certification of an Oil Detection Canine (ODC) team is to create a test that is as representative of the operational situation as possible (Bunker, 2017). According to the discussions in the AMOP (Arctic and Marine Oilspill Program), K2 Solutions Inc. has some plans to perform canine tests in arctic conditions including the presence of ice and snow.

Trained dogs are effective for locating oil spills in soil (Huppunen *et al.*, 2012) as well as in ice and snow (Brandvik and Buvik, 2009). In the field test reported by Brandvik and Buvik, the dogs (border collie and dachshund) managed to pinpoint the exact location of smaller oil slicks of 400 ml of weathered oil placed in a snow-covered hole in ice for one week. Dogs also managed to determine the dimensions of larger oil spills by indicating the borders of clusters of smaller oil spills (10 metre spacing). Using triangulation of the detected oil plume, a large 400 litre spill was located up to 5 km downwind of the spill location.

The use of dogs will probably be limited in offshore spill scenarios due to logistical challenges and safety concerns with deploying personnel on sea ice. Additionally, there is no evidence that dogs can reliably detect oil embedded in or under ice. By contrast, trained dogs have considerable potential for application on land fast ice and large ice floes, and they should be considered for detecting oil covered by sediment or snow in shorelines. In the context of arctic shoreline response, dogs may also contribute positively to the engagement of local stakeholders, since dogs constitute an important element of the social and economic fabric of northern communities. (Puestow *et al*, 2013)

2.6.4 Visual observations

Aerial visual observation uses the human eye as the primary sensor. Because it is one of the simplest sensing techniques and its platforms can be rapidly deployed, visual observation often serves as the backbone of a surveillance program during a response. Trained observers can provide interpretation of visual oil signatures as well as spatial patterns related to appearance and relative thickness. Aerial visual observation can be used in both a preventive (prior to an environmental event) and a reactive (during a response) mode, and is typically one of the first types of surveillance data received.

Visual observation is effective in daylight hours and in relatively calm weather environments. It is not effective at night time (typically not deployed at night for safety reasons and a lack of visibility) and during rough weather. In rough weather conditions the launching of aircraft or other manned platforms is limited due to safety restrictions. Accurate observations are also difficult when the water surface is highly disturbed. False positive observations can be reported if observers are not trained. (API, 2013)

Gas sniffing and leak detection is discussed in the reference (Fingas and Brown, 2013). The authors noted that many oils have a significant volatile component, which may penetrate ice to the surface and possibly be detected using sensitive gas-sniffing techniques. However, field tests have not been successful, since too little volatile material actually penetrates the ice and is diffused in the air to enable detection. The sniffing method might work when the oil is freshly spilled and if it contains a large amount of methane.

2.7 Multi-sensor data integration

The parallel use of multiple sensors with complementary characteristics can minimize uncertainties associated with single sensors and facilitate the generation of enhanced, comprehensive information products, while allowing visual interpretation of imagery to remain a central element of oil spill surveillance. The trained observers have an important role during the early stages of a spill to deploy clean-up resources in the most effective and efficient manner. Visual analysis and interpretation by a trained operator implicitly integrates information from different sources according to the cognitive abilities and experience of the observer.

Although visual interpretation works well for extracting qualitative information, generating quantitative information from diverse data sources and their dissemination to downstream users requires the use of automated systems. Data fusion provides a useful framework for integrating observations from multiple remote sensors. Fusing information from various sources generates meaningful information products of higher quality than could be obtained from single data sources only and requires a range of methods to accurately integrate co-registered or geocoded image data sets at pixel, feature and decision levels (Puestow *et al*, 2013)

2.7.1 Operational multi-sensor systems

Integrated systems of multiple sensors are increasingly used for operational monitoring of oil spills and discharges. Specially equipped and dedicated aircraft using a combination of SLAR, UV/IR, FLIR, image and video cameras have emerged as a typical payload for maritime monitoring. In some cases, the basic sensor set is extended by LFS and MWR systems and the integration of other datasets, such as satellite imagery and Automatic Identification System (AIS) data, is increasingly enabled. (Puestow *et al*, 2013)

In Germany, maritime oil spill surveillance in the North Sea and the Baltic Sea is accomplished using two dedicated and specially equipped Dornier Do 228 aircraft. Equipped with Optimare's MEDUSA maritime surveillance system, the sensor set comprises SLAR, UV/IR, FLIR, MWR and LFS together with FLIR and digital still and video cameras. In this configuration the SLAR is used for far-range detection of potential slicks with a swath width of 60 km, while the other sensors are used in the near range to describe the slick and extract oil properties, including classification and thickness with swath widths of 500 m (UV/IR, MWR) and 150 m (LFS), respectively. The data streams are displayed on a central operating console, which is the primary interface with the operator for data manipulation and product generation. (Puestow *et al*, 2013)

In order to avoid overwhelming data streams, various analysis tools, e.g. oil spill scene analysis system (OSSAS) as part of the MEDUSA system, are used to automatically generate information from multi-sensor data including raw UV/IR imagery, area of the oil spill, maps showing intermediate and thick areas within an

oil slick, the centre of its area and specific size parameters. An example of an oil slick captured by the five different sensors is presented in Figure 26.

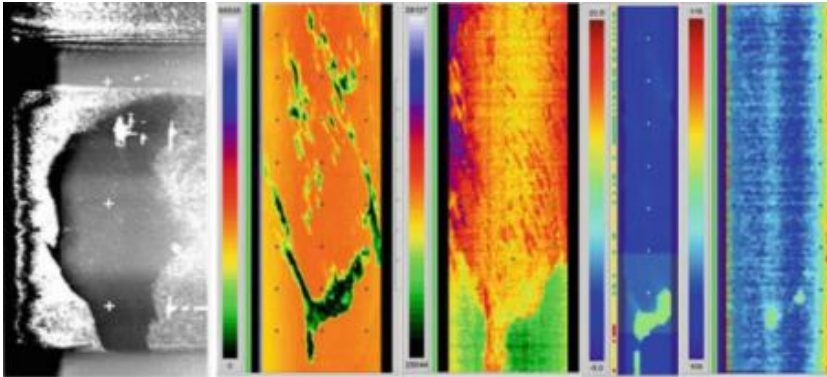


Figure 26. Oil pollution event observed using the MEDUSA systems with concurrent acquisition of SLAR, IR, UV, LFS and MWR imagery. (Puestow *et al*, 2013)

OSSAS also generates oil thickness products by merging UV/IR and LFS data. In this case, the UV signal is correlated with LFS-derived optical thickness and scaling-up is performed from the narrower LFS swath (150 m) to the spatial coverage of the UV sensor (500 m). Figure 27 shows an example of the fused UV/IR and LFS data, with extrapolated optical thickness as a measure of oil film thickness and UV and IR spill contours. (Puestow *et al*, 2013)

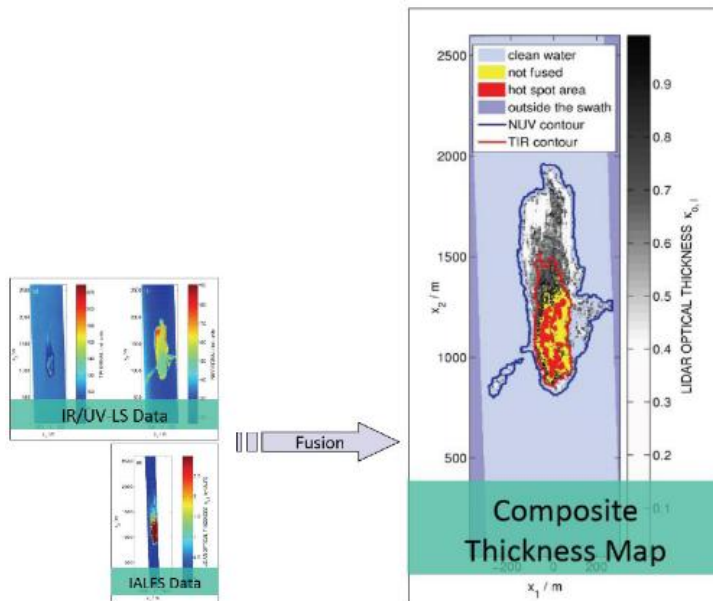


Figure 27. MEDUSA composite thickness map generated with OSSAS. (Puestow et al, 2013)

The Swedish Space Corporation has also developed and installed more than 80 operational aerial monitoring suites since 1976. The latest MSS 6000 comprises a combination of SLAR, FLIR, IR/UV-LS, as well as still and video cameras. Data flows from imaging sensors and other equipment, including direction finder, search radar and AIS, are accessible to the operator via a dual operator console. The system further supports the integration of digital nautical charts and satellite SAR images.

Depending on user requirements, information products can be generated in a variety of formats, including reports, map products, image maps and video feeds. All information generated can be disseminated in real-time to command centres and ground crews using high-speed INMARSAT communication. In addition to oil slick products, MSS 6000 supports vessel tracking and identification.

MEDUSA and MSS600 are permanent installations, whereas a mobile system developed by Ocean Imaging combines multispectral and TIR sensors to be mounted on aircraft of opportunity. The system consists of a DMSC MK2 progressive-scan CCD camera with four selectable narrow (10 nm) spectral bands within the spectral range of 400 to 950 nm, together with an IR-TCM640 un-cooled micro-bolometer measuring emitted radiation from 7.5 to 14 μm . The spatial integration of the two sensors is based on a combined differential GPS and inertial measurement unit with a circular positional error of 2 m, resulting in an RMS error of less than 6 m. At an altitude of 3800 m, the ground resolutions are 2 m (multispectral) and 4 m (TIR), with a swath width of 2048 m. A more detailed

description of the systems is presented in the reference (Svejkovsky and Muskat, 2009).

Another multi-sensor system presented in the reference (Puestow *et al*, 2013) is Aptomar's SECurus, which is a ship-mounted situational awareness and decision support tool comprising TIR and digital video sensors installed on a stabilized pointing unit that allows for images to be collected in all weather conditions. The system complies with Norsk Oljevernforening for Operatørselskap (NOFO) requirements for oil recovery vessels on the Norwegian continental shelf. In addition to spill response, the SECurus system is applicable to maritime surveillance and search and rescue operations. (Puestow *et al*, 2013)

2.7.2 Conceptual systems

The reference (Puestow *et al*, 2013) describes three different prototype systems targeted for oil spill application. These systems include FLS[®]-SUV (a LIF-based technology), an oil spill identification system and a method for detecting oil in water using optical and thermal video sensors.

Laser Diagnostic Instruments (LDI) has developed a system based on the FLS-SUV fluorescent LiDAR. The FLS[®]-SUV is a compact hyperspectral LiDAR (Light Detection and Ranging system) based on the Laser Induced Fluorescence (LIF) method.

The FLS[®]-SUV LiDAR is based on a Ultra-Violet (excimer) laser and hyperspectral detector. A pulsed laser beam senses the water body remotely. The resulting time-gated echo-signal is collected, spread into a spectrum and recorded by a detector. Read-out of the comprehensive LIF spectrum per every laser pulse allows detailed analysis of its spectral shape by recognition of specific spectral patterns characteristic for oil and oil products and other chemicals in water. The processing chain of LiDAR and classifier data is shown in Figure 28.

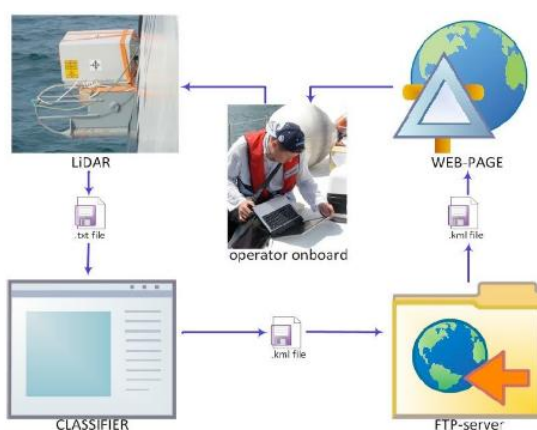


Figure 28. The data process flow of the FLS-SUV LiDAR system. (Yarovenko et al, 2011)

The device is used onboard a vessel or stationary platform for observation of coastal waters and detection of oil and organic pollution. It is able to measure the concentration of oil in water from trace amounts (ppm levels) on the water surface. The detection distance is up to 25 m, and the device can be operated continuously during day and night. Minimum detectable oil concentration is 1 ppm and minimum oil thickness in water is 1 μm . (Yarovenko, *et al*, 2011)

The latest version of the FLS-SUV LiDAR was demonstrated in the Kemi Arctic 2015 oil recovery exercise in March 2015.

An oil spill identification system for offshore structures or ships was described in Puestow *et al* (2013). The system comprises a combination of 36 GHz and/or 90 GHz MWR and radar sensors, although other sensors could also be integrated (e.g. UV/IR). Data collected from all sensors are transmitted to a control station for processing and analysis. Automated pattern recognition routines generate information products, which are transmitted to end users using available communication channels. Alternatively, raw images can be transmitted and subjected to operator interpretation at the control station or a remote location.

The third system presented in the reference (Puestow *et al*, 2013) is a method for detecting oil on water using a combination of vessel or platform-mounted optical (i.e. visible and NIR) and thermal video sensors. The thermal sensor registers EM radiation in the spectral range of 7–14 μm and the sensor configuration provides a video stream monitored by an operator at a remote location. Individual frames are subjected to an analysis of temperature contrast, spectral contrast and thickness contrast to extract potential slicks. The detection of a potential slick triggers an alarm for the operator. The system may integrate data streams from other sensors, such as visible light cameras, RF sensors, chemical sensors, Raman sensors or fluorescence sensors.

2.8 Application in ice-affected water

Although the performance of individual oil surveillance and detection systems in ice conditions is not yet fully understood, operational monitoring for oil slicks in ice environments will probably rely on the parallel use of multiple sensing technologies. While this would apply to above surface data from satellite-, airborne- and vessel- or platform-based sensors currently used in open water, data streams from submerged platforms, such as remotely operated vehicles (ROVs) and autonomous underwater vehicles (AUVs), may be deployed to perform under-ice surveillance.

Integration in a multi-sensor network for oil spill monitoring requires accurate geo-referencing and co-registration of all datasets. Image co-registration is required to ensure the alignment of images from different sensors over the same region. Geo-referencing ties the imagery to the geographic reference system used during a response effort and is usually achieved by GPS measurements. Geo-referencing is necessary in order to use remote sensing-based products with other spatial data within a dedicated GIS platform. Even in cases where detection products are not

images, they should be associated with geographic coordinates and be available in a suitable GIS-compatible format to facilitate their downstream use.

Ideally, raw sensor output acquired by multiple surveillance systems should be converted into information products that are meaningful and easily interpreted by response personnel and decision makers. Automated generation of information products would streamline the interpretation process and minimize variability due to varying operator experience. It would also allow for generation of information from a vast amount of input data in near real-time without overwhelming an operator.

Effective communication is a critical element of OSR, especially with respect to the rapid transmission and dissemination of spill information products. Maritime communications largely rely on geostationary communications satellites orbiting the earth above the equatorial line (e.g. INMARSAT). While the theoretical coverage of such systems extends to 81°N, signal instability can occur at latitudes as low as 70°N due to the satellite's low elevation angles and the associated susceptibility to signal attenuation. In practice, at latitudes higher than 75°N, satellite communication is essentially restricted to using IRIDIUM satellite telephony. Over shorter distances, LOS (Line-of-Sight) communication via VHF is possible, as are HF and MF, albeit with significant bandwidth limitations. (Puestow *et al*, 2013)

In fact, digital HF radios can provide communication over thousands of kilometres with limited capacity. In addition, 4G radios and ISM radios have recently also been used for high capacity short distance communications for maritime applications.

The ICEMAR initiative aims to address the issue of the limited communications bandwidth and demand on resources from multiple users by implementing intelligent delivery of information content to vessels operating in the Arctic. The ICEMAR system uses user location, area of interest and data compression together with available communications channel bandwidth to deliver information efficiently. ICEMAR is being developed primarily for ice-related information, but once operational it can be used to deliver any type of spatial information product, including spill reconnaissance products, in a wide range of data formats (e.g. SIGRID-2, S-57, GEOTIFF, JPEG, NETCDF, etc.). The ICEMAR architecture is presented in Figure 29.

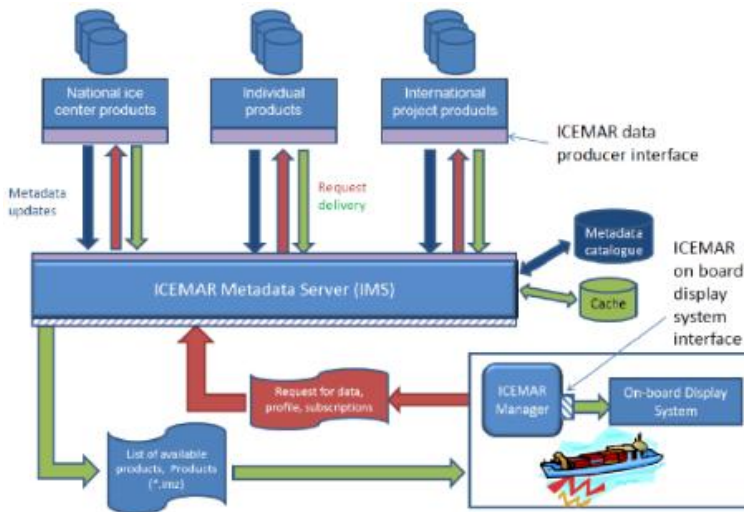


Figure 29. The ICEMAR architecture. (Hall, 2012)

Across the Arctic and other ice-affected areas, national ice services rely routinely on satellite imagery to generate ice information products in NRT (Near Real-Time). While the primary data source for ice charting is SAR imagery, data from optical satellites are also used to aid interpretation, especially if radar images are not available.

For spill response in ice-affected areas, satellite imagery can provide useful information on ice conditions and provide situational awareness. Depending on sea state and illumination conditions, it can also provide a synoptic view of major spill events. A number of satellite systems acquire data systematically (e.g. LANDSAT, MODIS and AVHRR). Automated systems can be implemented to download and geo-reference all available imagery for a given area of interest.

Ongoing acquisition of satellite imagery can be useful during response activities, since a search for imagery would not be required and the data are already readily available in a GIS compatible format. The future European satellite missions SENTINEL-1 (SAR) and SENTINEL-2 (optical) will be designed to collect data systematically and will be available in NRT via online archives. A steady stream of optical satellite imagery could also be exploited by developing nested approaches to extrapolate high-resolution observations from ship-borne or aerial sensors to the larger spatial footprint of a satellite image. (Puestow *et al*, 2013)

2.9 Mode of operation

Airborne oil spill remote sensing is normally divided into two different modes of operation: far-range detection and near-range monitoring. Far-range detection often uses airborne imaging radar systems usually covering swaths of several tens of

kilometres. These detection options are insensitive to weather and natural illumination. Suspicious structures detected by airborne radar are subsequently investigated on-site using near-range sensors.

Near-range monitoring of oil spills includes mapping of relative and absolute oil layer thickness, as well as classification of the type of oil. This mode of operation is typically limited to swaths of several hundreds of metres at flight altitudes in the range of 300–1000 metres. There are a number of well-established near-range sensors, such as IR and UV sensors, visible sensors, camera systems, MWRs and LFSs. (Partington, 2014)

The report of Puestow *et al* (2013) covered platforms situated on or above the surface. Table 5 summarises type of platform, distance from the surface, typical sensor spatial coverage and resolution. Additionally, Autonomous Underwater Vehicles (AUVs) and Remote Operated Vehicles (ROVs) can be used for a platform of remote sensor technology.

Table 5. Remote sensing platforms. (Puestow *et al*, 2013)

Platform	Distance from the surface	Sensor spatial coverage	Sensor spatial resolution
Satellite	Several hundred kilometres	ca. 100–10 000 km ²	From 0.5 to > 250 m
Airborne (helicopter, airplane, UAV, aerostat)	From tens metres to kilometres	Up to 1 000 km ²	From centimetres to metres
In the field (e.g. ship, rigs)	Centimetres to metres	Up to 10 km ²	From centimetres to metres
Contacted, on the surface (water, oil or ice)	N/A	Point measurement	From millimetres to metres

The distance from the surface is an important consideration since it indicates whether information must be collected in situ or not. For example, airborne platforms can provide coverage up to 1000 km² with a resolution of the order of metres or better depending on the system and its distance from the surface. These platforms are capable of carrying a range of relevant sensors, and decisions must be made regarding trade-offs between resolution, coverage and reliability of detection. (Puestow *et al*, 2013)

Remote sensing systems can also be classified by the resolution of the system. Three major types of resolutions dictate how effective a system will be for a response event: temporal, spatial, and spectral. Temporal resolution is used to describe how frequently data are gathered, spatial resolution describes the ground representation for a particular data set, and spectral resolution reflects the number and bandwidth of discrete bands in which data are collected.

Systems that obtain imagery from distances closer to a surface may provide better spatial resolution of a smaller area of view, while systems acquiring imagery from greater distances typically provide poorer spatial resolution of a much larger

area of view. Most satellite or high-altitude systems may be useful for initial detections of medium-sized spills or mapping of larger spills. Shoreline assessment and detection of small spills, especially those near coastal areas, usually require the higher resolution that lower altitude systems may provide.

Aerial remote sensing systems are typically designed to look vertically downward, toward the nadir (nadir is the point directly below the sensor). The majority of remotely sensed imagery used for mapping and environmental remote sensing is obtained with a vertical sensor, one that records an image with a downward-viewing angle of less than 3 degrees. The viewing angle of an oblique image is tilted upwards towards the horizon, and the images are typically taken with hand-held, digital, single reflex cameras or sensors mounted within gimbals. (API, 2013)

2.10 Summary of sensor technologies for oil detection

The reference (Puestow *et al*, 2013) provides a review and evaluation of surface remote sensing technologies for detecting and monitoring oil in the presence of ice and under conditions of low visibility. The reviewed technologies include the following:

- Optical sensors: cameras and multispectral sensors, UV sensors and hyperspectral sensors;
- IR sensors and radiometers: TIR sensors, MWRs;
- Radar sensors: SLAR and SAR systems, Marine Radar, GPR;
- Laser and fluorosensors: fluorosensors, TDLS, LURSOT, LiDAR;
- Experimental sensors: Acoustic Sensors, NMR Spectroscopy, trained dogs.

Optical (visible, multispectral and UV) and TIR are routinely used in oil spill monitoring, and visual interpretation of still and video camera output remains an important element of operational surveillance. When using optical methods, trained operators should be used in order to avoid confusion with other phenomena than oil spill. Visible methods have been widely used in the mapping and characterising of oil on water, but little validated information exists to describe their use in different ice conditions.

A weakness of optical systems is their reliance on good visibility, which will be limited in arctic conditions. TIR has fewer visibility limitations. Capabilities of optical systems can be enhanced using illumination, referred to as active systems in Table 6.

MWRs are being used primarily for pollution control and enforcement. Their performance in ice conditions is unknown.

Airborne laser fluorosensors have the unique ability to detect oil on different surfaces including ice, with a high degree of certainty, to classify oil type and to determine the thickness of thin slicks. Despite their advantages, LFS systems are not widely used in pollution control. LFS instruments require dedicated aircraft and

are restricted to relatively low flying altitudes and have correspondingly narrow spatial coverage due to power limitations.

Non-UV LiDAR sensors have shown promise for detecting oil with generally lower costs and increased availability compared to LFS systems.

TDL technologies are capable of oil detection. However, they may face two major challenges in ice environments, i.e. the need for deployment in the field and the expected time delay between spill occurrence and sensor deployment. Puestow *et al* (2013) did not consider them a priority for further research.

The LURSOT concept to extract oil thickness from an array of multiple lasers was successfully demonstrated, but development of the initial experimental system was not continued. Thus there is no LURSOT system in operation today.

The utility of radar sensors to detect oil under ice conditions is probably limited. However, satellite, airborne and field-based radar systems are extremely useful in characterising and mapping the general ice environment, tracking movements of ice and guiding deployment of surveillance equipment. Additionally, they do not rely on illumination to operate, and in the case of satellite-based imagery the dependence on weather conditions is minimal. Therefore, radar sensors should be considered as a critical element of any suite of sensing technologies deployed for spill response in ice-affected waters.

The application of GPR to detect oil under ice and snow is a relatively recent development. The use of ground-based units for detecting oil under ice is considered optional and the research continues on airborne systems with frequency modulated continuous wave architecture.

Acoustic sensors may offer the possibility to detect oil under ice, but only as in-situ deployment. In addition to logistic challenges, the interpretation of acoustic signal is not trivial due to inhomogeneity in the ice cover that may affect detection.

NMR was proposed as a means to detect oil under ice. Present work is focused on improving the operational maturity of the technology, including development of a helicopter-based system and improving SNR of the detected signal.

According to the references (Puestow *et al*, 2013; Dickins, 2010; Brandvik and Buvi, 2009), trained dogs are capable to detect buried oil under snow and in soil. Dogs could be used near local communities due to the field deployment requirement.

A summary of the technology evaluation conducted in the study (Puestow *et al*, 2013) is presented in Table 6 and performance scenarios are given in Table 7.

Table 6. Technology evaluation summary: expected detection performance. (Puestow et al, 2013)

Technology	Among Pack Ice ice concentration			On ice	Under ice/ snow or encapsulated	Low visibility		
	< 30%	30–60%	>60%			Blowing snow	Darkness	Rain or Fog
VIS, MS, UV, HS	Green			Green	Red	Red (Active systems)		
TIR	Green			Green	Red	Orange	Green	Orange
MWR	Green	White		White	Red	Green		
SAR, SLAR Marine radar	Green	White		White	Red	Green		
GPR	Red	White		White	Orange	Green		Orange
LFS	Green			Green	White	White	Green	Red
TDL	Red	Orange		White	Red	Orange	Green	Orange
LURSOT	Green	White		White	Red	White	Green	White
LiDAR	Green	Orange		Orange	White	Red	Green	Red
Acoustic	Red			Red	Orange	Red	Green	Red
NMR	White			White	White	White		
Dogs	Red		White	Green	Orange	White	Green	White

The expected levels of performance are the following:

- **Green box:** The technology is proven and fully validated, and its performance and limitations under the current scenario are well understood.
- **Orange box:** The technology is potentially applicable, partial validation may have taken place but the technology has not been comprehensively validated for performance under the given scenario.
- **White box:** The likely performance of the technology is not known; it has never been tested under the given scenario.
- **Red box:** The technology is not applicable to the given scenario.

Table 7. Performance scenarios according to Puestow et al (2013).

Performance scenarios	Description
Detection of oil among pack ice	Ice concentration < 30%: at sea ice concentrations less than 30%, oil is generally considered to be unaffected by the presence of ice; the performance of detection technologies is expected to be similar to that in open water conditions.
	Ice concentration 30–60%: the movement of oil and the ability to detect it are affected by the presence of sea ice.
	Ice concentration > 60%: the oil is expected to move with the ice; oil is present in between ice floes and is mixed with slush and brash ice.
Detection of oil on ice	The oil is present on the ice surface or on melt ponds.
Detection of oil under ice, snow or encapsulated in ice	The oil is under the ice, encapsulated within the ice or on the ice surface covered by snow.
Detection of oil in low visibility	Darkness Blowing snow Rain or fog

The following paragraph presents a summary of the most appropriate confirmed and potential technologies for application in different ice and visibility scenarios by Puestow *et al* (2013).

- a) Pack ice concentration < 30%:
 - Optical imagery, including visible, MS, UV, and HS sensors;
 - TIR scanners and FLIR sensors;
 - MWRs;
 - SAR, SLAR and marine radar and
 - Laser fluorosensors and LiDAR.
- b) Pack ice concentration 30–60%:
 - Optical imagery, including visible, MS, UV and HS sensors;
 - TIR scanners and FLIR sensors and
 - Laser fluorosensors and LiDAR.
- c) Pack ice concentration > 60%:
 - Optical imagery, including visible, MS, UV and HS sensors;
 - TIR scanners and FLIR sensors and
 - Laser fluorosensors and LiDAR.
- d) Detecting oil on ice, on the surface of sea ice or on melt ponds:
 - Optical imagery, including visible, MS, UV and HS sensors;
 - TIR scanners and FLIR sensors;
 - Laser fluorosensors and LiDAR and
 - Dogs.
- e) Detecting oil under ice or snow, or encapsulated in ice:
 - Acoustic sensors;
 - Dogs; and
 - Drilling.

Active research is being undertaken using airborne and NMR systems, and it is anticipated that field testing of NMR will become available within two years.

LFS can potentially be used to detect oil under smooth ice and should be considered for further evaluation.

f) Detection in darkness:

- Passive optical systems, including visible, UV, and HS sensors, require sunlight to operate.
- Other systems, including active optical systems, can be used in darkness.

The reference (Puestow *et al*, 2013) notes that TIR sensors require a measurable temperature difference between oil and the surrounding water or ice, and this differential is initiated by the absorption of solar irradiation. At night, the temperature between oil and the surrounding area will equalize, and thermal imaging will become less applicable due to decreased temperature difference.

g) Detection in blowing snow:

- Microwave radiometers;
- SAR, SLAR, Marine radar;
- GPR and
- Acoustics

Thermal and FLIR systems as well as optical systems would have decreased visibility due to blowing snow. However, when the system is deployed on a platform operating within a short distance from the surface, these systems may provide meaningful information. Radar systems (e.g. SAR) can operate in snow; however, detecting oil spills will be limited in high sea states.

h) Detection in fog or rain:

Performance of IR and FLIR cameras in fog and rain depends on three factors:

- Atmospheric conditions (category of fog or rain);
- The type of IR sensor (its wave range) and
- Properties of the observed oil spill including size, temperature difference to water or ice background and oil type.

Performance of optical systems is significantly limited by fog and rain. Oil spill detection capabilities in open water by SAR and SLAR systems are also be affected by rain, as rain changes the ocean surface roughness in a similar way that oil spills dampen capillary waves.

The following technologies can operate in rain and fog (Puestow *et al*, 2013):

- SAR, SLAR, Marine Radar;
- GPR;
- TIR and FLIR;
- MWRs and
- Acoustic.

Hyperspectral imaging (HSI) is generally considered as not applicable for oil detection under ice. Polak *et al* (2016) wanted to challenge this statement by testing HSI combined with signal processing and classification techniques in a small-scale laboratory experiment with sea ice and engine lubrication oil (Figure 30).

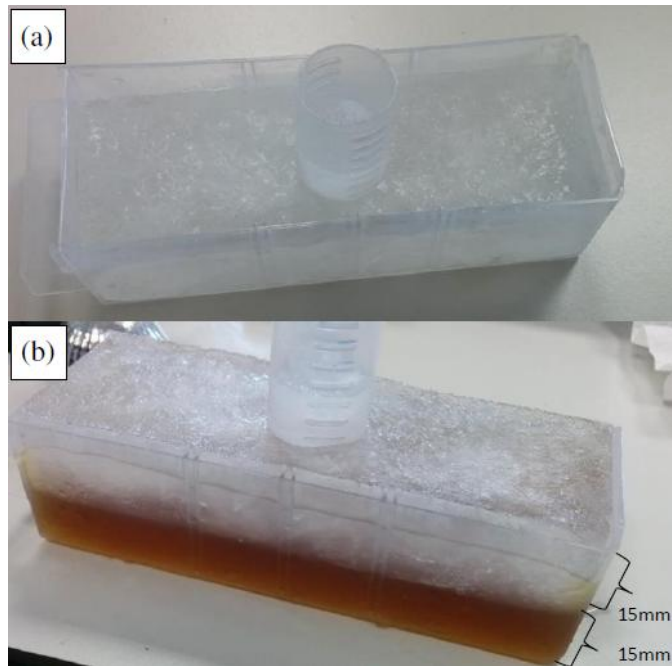


Figure 30. Small container with sea ice (a), and engine lubrication oil introduced under the ice (b). (Polak *et al*, 2016)

Polak *et al* (2016) performed the tests with two different imaging hardware: a passive HS camera operating in the NIR wavelength (900–1700 nm), and an active, laser based, mid-infrared (MIR) (2500–3750 nm) HS imager also featuring short-range of NIR band (1490–1850 nm). In the experiment the detection was tested through a 15 mm ice layer for the passive system, and an 80 mm layer for the active system.

The results indicated that HSI empowered by signal processing techniques is able to detect oil underneath a thin layer of ice. The oil under ice scenario could be correctly distinguished from the pure ice case based on the data from both employed HSI cameras. The results served as a proof of concept for a feasibility study, which will quantify the limits of HSI detection by addressing the issue of maximum ice thickness under which HSI can detect oil, and the minimum detectable oil layer thickness under ice. The presented results were sufficient to obtain funding for a feasibility study from The International Tanker Owners Pollution Federation Limited (ITOPF). (Polak *et al*, 2016)

In the reference (Dickins, 2010), several sensors and systems for oil detection were screened and assessed. These include airborne remote sensing, satellite systems, the combination of airborne and surface systems, surface-based systems and evolving technologies.

The matrix of different sensors for remote sensing of oil spills in ice according to the platform and the oil/ice configuration with a mix of pack ice and fast ice is presented in Table 8.

Table 8. Different sensors for remote sensing of oil in various ice and platform configurations. (Dickins, 2010)

Platform	Ice surface		AUV	Shipborne		Airborne					Satellite
Sensor	Dogs	GPR	Sonar	Marine radar	FLIR	GPR	Visible	UV	FLIR	SLAR	SAR
OIL ON ICE											
Exposed on cold ice surface	Y	N/A	N/A	N	Y	Y	Y	N	Y	N	N
Exposed on spring melt pools	Y	N/A	N/A	?	Y	N	Y	?	Y	?	N
Buried under snow	Y	Y	N/A	N/A	N	Y	N	N	N	N	N
OIL UNDER ICE											
Smooth fast ice	?	Y	Y	N/A	N/A	Y	N/A	N/A	N/A	N	N
Deformed pack ice	?	?	Y	N/A	N/A	?	N/A	N/A	N/A	N	N
OIL IN ICE											
Discrete encapsulated layer	?	Y	N	N/A	N/A	Y	N/A	N/A	N/A	N	N
Diffuse vertical saturation	?	?	N	N/A	N/A	?	N/A	N/A	N/A	N	N
OIL BETWEEN ICE FLOES											
1–3/10 concentration	N/A	N/A	N	Y	Y	N	Y	Y	Y	Y	Y
4–6/10 concentration	N	N/A	N	?	Y	N	Y	?	Y	?	?
7–9/10 concentration	?	N/A	N	N	Y	N	Y	N	Y	N	N

LEGEND	
Likely	Y
Possible	?
Not likely	N
Not applicable	N/A
Blocked by dark/cloud/fog/precipitation	

The following observations from Table 8 were made by (Dickins, 2010):

- Very few sensors have demonstrated a capability to detect and map oil under or trapped within rough offshore pack ice. Sonar carried under the ice on AUVs may have potential in the future to deal with this scenario.
- GPR – surface or airborne – is the only sensor currently capable of detecting isolated oil pockets trapped beneath or within a solid ice sheet or on the ice surface under snow. Limitations and unknowns centre its performance in warm saline ice and/or rough rubble and rigging.

- Extrapolating from the proven ability to detect slicks at sea, existing airborne sensors developed for open water applications are expected to perform reasonably well in open drift ice (1–3/10). In heavier ice concentrations the capabilities of different sensors will depend largely on the scale of the openings and slick areas among the floes, oil thickness and wave effects.
- Some form of IR sensors used from the surface, vessel, aircraft or helicopter is possibly the most flexible technology for detecting oil between floes or exposed on the ice surface, recognising the constraints of darkness and cloud/fog. Recent systems with integrated X-band Marine radar with passive or active IR sensors have shown promise in trials with spills on open water in Norway and could provide equivalent spill mapping capabilities in very open sea covers.
- Given the limitations of cloud cover and darkness, visible satellite sensors cannot be relied on in an emergency to provide reliable coverage.
- The latest generation of SAR satellites are theoretically capable of resolving targets close to one metre in size, but their ability to discriminate between natural wind-roughened water between floes and the modified sea surface affected by the presence of oil is still unknown. Direct spill detection from SAR satellites and airborne SLAR/SAR systems may be possible for large spills in very open drift ice (< 4/10), and under moderate surface wind conditions (approximately 5–10 m/s).
- During freeze-up in autumn and early winter, any detection of oil among ice with SAR/SLAR sensors will be complicated by the presence of grease ice – the earliest smooth stage of ice crystals at the water surface. The presence of grease or new ice in conjunction with an oil spill on the water will produce almost identical signatures in the radar imagery, making identification of an oil slick difficult or impossible.
- Trained dogs can reliably detect very small oil volumes and map oiled boundaries on solid ice and in sediments on arctic shorelines under extreme weather conditions. The future utilisation of dogs in this role will require established standards for training of new dogs and their certification, established procedures to protect the animals and long-term agreements with recognised dog training institutes. Cooperation with local Arctic communities should be explored to fully realise the potential of the dogs in this new role. The oil detection capability can also be added to skills already routinely exercised with dogs for other cold climate emergencies such as avalanche search and rescue.
- Future arctic oil spill contingency plans need to account for the operational constraints of aircraft range and endurance limitations (availability of alternative airfields), weather limits, crew duty cycles, satellite reliability and reprogramming time and the likelihood of competing demands in limited remote sensing resources.

The key messages of the study (Dickins, 2010) were the following:

- A flexible combination of sensors operating from aircraft, helicopters, vessels, satellites and the ice surface are recommended for future arctic oil spill emergency preparedness.
- The most useful remote sensors and systems for spills in ice are expected to be aircraft and vessel-based FLIR for oil on the surface in a broad range of ice concentrations, trained dogs on solid ice, GPR operated from helicopters and the ice surface for oil under snow or trapped in the ice, and SLAR and satellite-based SAR for large slicks on the water in very open ice covers.
- The current generation of all-weather SAR satellites can play a valuable support role in mapping detailed ice conditions and directing marine resources.
- Existing commercial GPR systems can be used from low-flying helicopters to detect oil trapped under snow on the ice and to detect oil trapped under solid ice.
- Detecting isolated oil patches trapped among closely packed ice floes is a major challenge with any current remote sensing system, especially during periods of extended darkness, low clouds or fog. The most effective solution is to deploy closely spaced GPS tracking buoys to follow the ice and the oil.
- Trained dogs can reliably detect very small oil volumes and map oiled boundaries on solid ice and in sediments on arctic shorelines under extreme weather conditions.
- New technologies may enhance the ability to detect oil over a broader range of arctic spill scenarios in the near future. These include NMR, UAVs, AUVs and next generation GPR optimised for the oil in ice problem.
- The optimum combination of remote sensing technologies depends heavily on the spill characteristics and prevailing weather and ice conditions and
- Arctic spill contingency plans need to account for the operational constraints of aircraft and helicopter endurance, weather and the likelihood of competing demands in limited remote sensing resources.

Cardo Entrix (2012) performed a study which focused on research and emerging trends in surveillance technologies for OSR. The study included published, peer-review papers related to remote sensing technology between the years 2000–2012. Based on the findings, the conclusions were the following:

- A system or product that combines a variety of sensors and/or data would provide the most utility across the greatest number of response activities. More research should be conducted to design new or improve current combined sensor technology.

- Satellite imagery provided valuable data during response operations. Satellite acquisition processes and satellite technology capabilities should be investigated further.
- The sharing of remote sensing data via GIS not only within response groups, but also with the media and public, proved to be a useful tool. This process should be refined and included in response planning.
- Although many new technologies provided useful and unique data, aerial observation surveys remain one of the most practical and effective methods for surveillance of a large spill.
- More R&D into remote sensing technology for spill response needs to be conducted in general, but technologies currently in the developmental stages need to be field-ready before the next large spill.
- Both novel and established remote sensing technologies provided a wide range of valuable data, but were not always utilized due to an overabundance of the data or a lack of means to employ it.
- Therefore, the process of remote sensing itself, as well as the application of resultant data, during a spill response needs to be established and included in future planning efforts.

It is worthwhile to note that Cardno Entrix (2012) did not have any special focus on the issues relevant for arctic OSR.

The knowledge of how the oil would be detected if released into ice-affected waters is very restricted. The limited availability of light in the Arctic for much of the year limits the utilisation of optical remote sensing technologies. Underwater sonars and hyperspectral techniques using autonomous underwater vehicles, as well as SAR and UV techniques using satellite sensing, show potential as technologies for oil spill detection in the Arctic. However, the understanding of how these technologies could be deployed to detect oil in various ice conditions requires further studies. (CEOS, 2014)

2.11 Options for chemical detection

Unlike hydrocarbons, there is limited research on the detectability of hazardous and noxious substances (HNS) at sea using remote sensing (Angelliaume *et al*, 2016). This section focuses on the chemical detection technologies demonstrated in field conditions, thus excluding technologies utilised only in laboratory environments.

According to Harig *et al* (2005), various analytical methods, including mobile gas chromatography/mass spectrometry (GC/MS), infrared spectrometry, and hand-held sensors such as photoionization detectors, are applied for on-site analysis. Moreover, a system containing a combination of sensors, the portable gas detector array (GDA 2) comprising an ion mobility spectrometer in combination with a photoionization detector, an electrochemical cell, and two semiconductor gas

sensors, is applied by the analytical task forces. However, all these methods require the collection of a sample, which may be dangerous. For a complete assessment of the situation, information about the position and the size of the gas cloud is essential.

One option for identification, quantification, and visualization of potentially hazardous gas clouds from long distances is Scanning Infrared Gas Imaging System (SIGIS). This is a scanning imaging remote sensing system based on the combination of an IR spectrometer with a single detector element and a scanner system (Figure 31).



Figure 31. SIGIS 2-system mounted in an emergency vehicle in Germany. (Bruker, 2017)

The system measures a selected area and visualizes a chemical image overlaid on a video image as a result of the automatic analysis. SIGIS 2 systems are applied in industrial facility surveillance, environmental applications, atmospheric research and volcanology, and are part of the equipment of emergency response forces. Since the SIGIS 2 is a passive remote sensing system, no external light sources or reflection optics are needed. (Bruker, 2017)

Due to its rugged construction and special shock absorbing mounts, the SIGIS 2 can be operated in helicopters and motor vehicles. In addition to toxic industrial compounds (TICs), chemical warfare agents (CWAs, optional) can also be detected and visualized from long distances. The size of the unit is approximately 1190 x 580 x 365 mm, and the mass is 65 kg. SIGIS 2 can be operated with 110/230 V AC voltage or battery. Typical power consumption during measurement is < 100W and

battery supply runtime is 6 hours. The operational temperature is from 0 °C to 49 °C with the option of -20 °C to 49 °C. SIGIS 2 has demonstrated the detection and identification of ammonia being discharged from a stack at a distance of approximately 1.5 km. (Bruker, 2017)

Another example of a product designed for detection of gas plumes is Hyper-Cam by Telops (Figure 32). This is a hyperspectral imaging system which combines spatial, spectral and temporal resolution and is capable of remote detection, identification and quantification of TICs. (Telops, 2017)

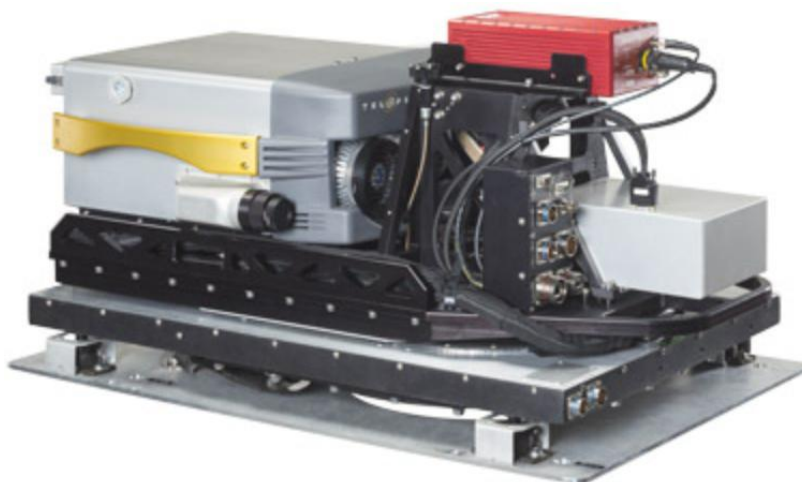


Figure 32. The Hyper-Cam by Telops mounted on an airborne platform. (Telops, 2017)

The Hyper-Cam allows standoff chemical detection at a distance of up to 5 km. It enables the user to measure different spectra, and then compare the measured spectrum with the signatures of known gases and solids. Constituents and properties of a target can then be easily identified. Telops provides different configurations of the Hyper-Cam with spectral ranges of 3–11.8 μm . The power consumption is 180 W and weight 31 kg. (Army Technology, 2017; Telops, 2017)

Angelliaume *et al* (2016) reported the findings of an experimental field measurement campaign which focused on remote sensing of six chemicals and non-hydrocarbon oil products using airborne sensors. The target substances included rapeseed oil, fatty acid methyl esters (FAME), toluene, heptane, xylene and methanol. The results indicated that rapeseed oil, FAME and xylene were detected by SAR imagery. The non-detectability of the remaining three chemicals could be due to the high volatility of these products or by an impact into the water column that physically does not affect the backscattered signal at microwave frequency. However, Angelliaume *et al* (2016) concluded that using SAR data with a suitable wavelength, i.e. 9.6–9.9 GHz for X-band and 1.25–1.4 GHz for L-band, it

can be possible to define the characteristics of the slick along a spectrum ranging from thin surface films to thicker emulsions.

NHL University of Applied Sciences in the Netherlands has prepared comprehensive oil and chemical spill response manuals, which can be accessed via their website. The manual for chemical spills includes e.g. the descriptions of detection, sampling and monitoring technologies when the substance is on the sea floor, in the water column, floating or in the air. The manual also includes strategies on measuring the physical and chemical properties of hazardous substances and discusses the need to gather on-scene information by measurement or observation. (NHL, 2017)

Widely used options for chemical detection in field conditions contain the following instruments (VTT, 2015):

- Indicator tubes provided by e.g. Dräger, Kitagawa, MSA and RAE Systems,
- Compact handheld analysers, e.g. MX6 IBrid, RAE Systems, MBFuma, Sulfuma and Phosfuma, Dräger X-am 7000, Fumiscopes, ChemPro 100i, City-Tech sensors and GasAlert detectors and
- Gas analysers such as gas chromatographers, electrochemical cells, and analysers based on thermal conductivity, methods based on IR and mass spectrometry.

In addition to the abovementioned products, several other companies offer their own products or act as an agent for products targeted for various remote sensing missions. These companies include e.g. Detector Ltd, Beup Automation Ltd, Patria and Optimare.

Commercially available products intended for on-site remote sensing were field-tested by Syke and VTT in arctic conditions with several target chemicals. These options included the products of Aeromon Ltd, Dräger, Environics Ltd and 3M. The outcomes of those trials are presented in section 6.2.

3. Deployment platforms

Remote sensing technology can be deployed to different platforms. Depending on the size, location and time of the incident, different types of data can be gathered from different platforms. The platforms currently used for remote sensing technology deployment are satellite systems, aircraft systems, UAS, tethered balloon systems (aerostats) and surface vessels (API, 2013).

3.1 Surface vessels

Remote sensing devices used on surface vessels support direct response actions to oil on water. The platforms may be ships, boats, barges or buoys. Any number of sensors can be deployed that may increase the interface with floating or subsurface oil. Examples include visual observations, radar systems and thermal sensors. Trained observers on board vessels can also verify the presence of oil and direct resources to removing oil from the surface of the water.

Surface vessels are very agile and can be manoeuvred to locate oil. Observation instruments are often mounted on the highest point on the vessel in order to provide the maximum viewing distance. Manned vessels can be manoeuvred to find oil and remain in the oil-affected area, based on data from the sensing instruments. (API, 2013)

The advantages of surface vessels are that they have an increased interface with the thickest oil based on remote sensing data and visual means, they are versatile and they can be manoeuvred to remain in a desired location, instrumentation and sensors can easily be changed to meet needs and weather conditions, the probability of detecting oil is very high, human presence on manned vessels enables the presence of oil to be validated by visual means, and surface vessels can provide a much longer “time on station” (e.g. hours to days) in the area for observations together with other platforms.

The disadvantages of surface vessels are that they are limited to small coverage areas in the immediate vicinity of the vessel and they have limited usefulness in high seas due to sensor movement at the high point of the vessel. Additionally, some oil-combating technologies (e.g. booms and arms) have limited operational capabilities in high seas and in heavy ice conditions, which also limits the operational capabilities of smaller vessels.

Surface vessels with appropriate sensors can locate and remove oil from the water surface, and they can track oil on the surface or subsurface. Appropriate use of sensors can place removal equipment into the thickest oil, increasing the interface and achieving the best collection results. The ability to detect oil is a complex function of sea state and conditions, ice conditions, oil types, and sensor view angles. (API, 2013)

The OSR vessel Louhi (Figure 33) represents state-of-the-art technology in responding to marine oil and chemical spills. It has the capacity to store

approximately 1 200 m³ of recovered oil and approximately 200 m³ of chemicals. Its sweeping width is approximately 42 metres.



Figure 33. OSR vessel Louhi, state-of-the-art oil and chemical recovery vessel during the Kemi Arctic 2015 exercise. (Image: SYKE/Jyrki Nikkilä)

During the Kemi Arctic 2015 exercise the installed three heavy duty ice brushes were operated from the deck of the vessel (Figure 34).



Figure 34. Heavy duty ice brushes in operation during the Kemi Arctic 2015 exercise. (Images: VTT/Jukka Sassi)

In addition to Louhi, the waterway vessel Letto (Figure 35) also participated in the exercise. The size of the recovered oil storage tanks is 42 m³, the shaft power is 2500 kW and the lifting capacity of the crane is 20 t.



Figure 35. The waterway vessel Letto during the Kemi Arctic 2015 exercise. (Image: SYKE/Jyrki Nikkilä)

3.2 Manned aircraft systems

Airborne platforms have traditionally provided the most effective platform for OSR, being adaptable specifically to the task in question. They are usually manoeuvrable and potentially capable of being deployed at very short notice to one or more locations simultaneously. Some aircraft are equipped with pre-integrated sensors that can be used for OSR. Some of these can be used to host portable sensor packages. (Partington, 2014)

Different manned planes can be tasked to deploy observers and specialised observation equipment. Aircrafts have a much better chance to find and track oil when compared to some other systems, due to their ability to change direction, altitude and course when needed. (API, 2013)

The Finnish Border Guard operates Dornier 228 aircraft in oil response missions to support oil combating vessels during response actions (Figure 36).



Figure 36. Dornier 228 equipped with Side-Looking Airborne Radar (SLAR) and IR/UV scanner. (Image: The Finnish Border Guard)

The reference (Partington, 2014) summarises the minimum requirements for aircraft to be used as a platform for OSR as follows:

- Compliance with local and international aviation regulations (and associated certification);
- Flight permissions;
- Required permissions and approvals allowing an airborne operator to install and operate a given sensor on board a given aircraft platform (regardless of the location where the aircraft is flying);
- Flight plan that relates to oil spill observation requirements;
- Good downward visibility for surface surveillance (manual and/or sensor);
- Slow speed capability;
- Effective communications with vessels or ground (robust, continuous and with sufficient bandwidth, which might be direct or via satellite);
- Adequately trained and equipped personnel, for operating the platform (in situ or remote) and sensors and/or making manual spill observations;
- Sensor suite incorporating a minimum of digital camera or video for recorded observations of the spill, with positioning information and with a data link to the oil spill control centre; and
- High accuracy dynamic positioning system including GNSS (Global Navigation Satellite System), gyro and inertial sensors integrated with the sensor suite.

The advantages of aircraft detection systems are that large areas can be surveyed in a relatively short time frame, aircraft are usually available at short notice (providing that contractual issues are agreed upon) and can be more cost effective, most types of remote sensors can be deployed on aircraft, multiple sensor types

may be deployed from a single aircraft and aircraft usually have multiple navigation aids that can assist in pinpointing locations.

The disadvantages of aircraft systems are that weather and daylight/darkness must be suitable for the type of aircraft and sensors being utilized, safety margins for operation need to be determined and adhered to, and regional flight rules may dictate operating conditions for aircraft (e.g. visual flight rules).

Remote sensing equipment should be in a “universal” package that can be deployed on any type of aircraft. Specifications of a remote sensing package are needed prior to locating the appropriate aircraft and the air speed operational parameters (if any) of the remote sensing equipment. Some equipment may require that operator/operators be present on the aircraft.

Some remote sensing equipment is too bulky and can be used only from the dedicated aircraft on which it is installed. Furthermore, the remote sensing operation must be coordinated with other aircraft activities (e.g. overflight, dispersants and observer).

The remote sensing package must have the necessary method of data capture and communications that can send information to the command centre from the aircraft. Some remote sensing packages have self-contained data capture that must be downloaded after the flight, which can delay interpretation and use of the data. (API, 2013; Partington, 2014)

The reference (API, 2013) noted that safety considerations are paramount and the pilot of the aircraft should be consulted on all the aspects of the operation before the observation flight. All the personnel attending to the flight must be thoroughly briefed beforehand on the safety features of the aircraft and procedures to be followed in the event of an emergency.

3.3 Satellite systems

Satellite systems are space borne platforms that host a variety of sensors. Many civilian satellites have been acquiring and archiving imagery for nearly 40 years. Data gathered by the satellite platform are transmitted to teams on the ground, who then process and interpret the data to support decision making.

Sentinel-1, the first in the family of Copernicus satellites, will be used to monitor many aspects of our environment, from detecting and tracking oil spills and mapping sea ice to monitoring movement in land surfaces and mapping changes in the way land is used. It will also play a crucial role in providing timely information to help respond to natural disasters and assist humanitarian relief efforts (Figure 37).



Figure 37. Sentinel-1 satellite platform. (Image: ESA/ATG medialab)

The newer satellite systems have spatial resolutions as low as 50 cm and systems like these can revisit a specific target daily. Multiple SAR systems are currently in orbit. An overview of operational optical satellite systems is presented in Table 9.

Table 9. Operational optical satellite systems. (Puestow et al, 2013)

Instrument	Resolution [m]	Swath [km]	Revisit [days]
LANDSAT 5, 7, 8	15–30 (MS) and 120 (TIR)	185	16
MODIS	250–1000	2330	1–2
MISR	275–1000	360	2–9
DMC	20–30	600	Near daily
SENTINEL-2	10–60	290	Near daily
QuickBird	0.6–2.4	16.4	1–3.5
Worldview-1/2	0.5–1.8	16.4	Near daily
Geoeye	0.41–1.35 (MS)	15.2	2.1 days

The advantages of satellite systems are that they can potentially cover a large area in a short period of time, data may potentially be transmitted via the internet almost immediately, many radar satellites are useful in detecting large offshore spills and spotting anomalies, and some operational commercial satellites can be tasked to respond to emergencies within a range of 90 minutes to 4 hours.

The disadvantages of satellite systems relate to the following aspects: the timing and frequency of overpasses by satellite systems may not be optimal for the situation, clear skies are needed to perform optical work, the probability of detecting oil may be low, developing algorithms to highlight oil slicks is difficult and extended time may be required to convert data into actionable information. In some situations,

data can be collected in hours, when bounded by different situational factors, but actionable information may take days.

The reference (API, 2013) noted that the ability to detect oil may be a complex function of conditions, oil types and view angles, and to be successful, these techniques generally rely on ancillary data such as suspected position or other satellite data.

The limitations of optical systems are most severe for satellite-based systems, whereas aerial and ship-borne systems may be operated in cloudy conditions. Due to these restrictions, optical sensors need to be combined with other technologies to offset their limitations. (Puestow *et al*, 2013)

VTT Technical Research Centre of Finland Ltd launched its small and lightweight hyperspectral camera into space with the Aalto-1 nanosatellite on 23rd June 2017. This tunable spectral imager operating in the visible and near-infrared spectra can measure in a wavelength range of 500–900 nanometres. The camera is half a cubesat unit (0.5U) in size, or 5 x 10 x 10 cm (Figure 38).

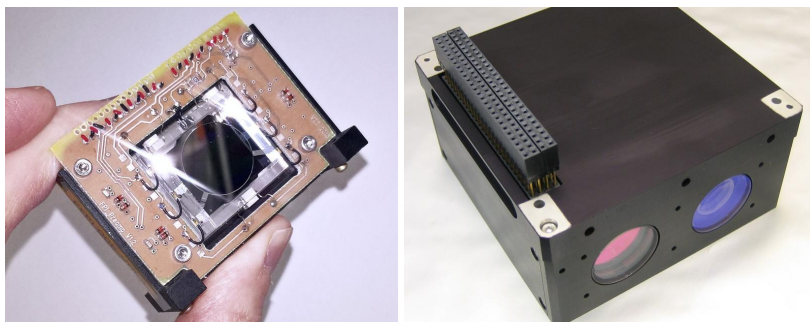


Figure 38. The tunable spectral imager by VTT.

The key advantage of this technology is that the measurement wavelengths are software programmable, and thus the same camera hardware can easily be scaled to different applications, even after the launch.

Hitherto, hyperspectral imaging has only been possible with instruments in traditional, large satellites, but VTT's technology now makes it possible to perform hyperspectral imaging from small satellites. VTT's hyperspectral technology can also be customized for other wavelength ranges and specific needs.

The number of launches of small satellites has grown significantly, enabling much faster technical advances in comparison to traditional space industry. In addition to that, space services on Earth have pushed the boundaries for non-space industries. This enables the creation of data-based services for industries which are not traditionally involved in space, such as agriculture and insurance. (VTT, 2017)

The Finnish company ICEYE is developing an SAR microsatellite radar imagery constellation which can measure local data with more rapid cycles than traditional instruments. This enables unprecedented access to SAR data without restrictions related to location or time. With the full constellation they aim for an average of 3

hours delay from order to acquisition. ICEYE can provide imagery with very short lead times. They provide frequent revisits, rapid mosaicking of larger areas with high resolution, and cooperate with other satellite operators and data providers to provide complementary data layers (ICEYE, 2017). The current status of the SAR technology limits its utilisation in dynamic ice-oil-water conditions. In open water conditions, in ice concentrations less than 30% and in low visibility conditions SAR is able to detect oil (Table 6).

3.4 Unmanned Aerial System (UAS)

UASs have a proven recent history of use for military applications, but are now being promoted increasingly for civilian purposes. An Unmanned Aerial Vehicle (UAV), also known as a drone, refers to a pilotless aircraft, a flying machine without an onboard human pilot or passengers. As such, 'unmanned' implies total absence of a human who directs and actively pilots the aircraft. Control functions for unmanned aircraft may be either onboard or off-board (remote control). This is why the terms Remotely Operated Aircraft (ROA) and Remotely Piloted Vehicle (RPV) are also in common use. The term UAV has been used for several years to describe unmanned aerial systems. (Limnaios, 2014; Partington, 2014)

Recently, the most highly ranked international organizations such as the International Civil Aviation Organization (ICAO), the EUROCONTROL, the European Aviation Safety Agency (EASA), the Federal Aviation Administration (FAA), as well as the US Department of Defence (DoD), have adopted the term UAS or Unmanned Aircraft System as the correct and official term. The changes in the acronym are caused by the following aspects (Limnaios, 2014):

- The term "unmanned" of the UAS refers to the absence of a pilot from the flying part of the system;
- The term "aircraft" signifies that UAS is an aircraft and as such properties such as airworthiness will have to be demonstrated;
- Finally the term "system" was introduced because of the fact that UAS is not just a vehicle but a (distributed) system consisting of ground control stations, communication links and launch and retrieval systems in addition to the aircraft itself.

The term Remotely Piloted Aircraft Systems (RPAS) is also used in conjunction with UAS.

Nowadays and after many years of development, UAS are reaching the critical point at which they could be applied in a civil/commercial scenario. The potential civilian applications can be categorized into five groups (Limnaios, 2014):

- Environmental (or earth science) applications: remote environmental research (i.e. magnetic field measurement, ice thickness monitoring etc.), atmospheric monitoring and pollution assessment (i.e. stratospheric pollution monitoring, CO₂ flux measurements etc.), weather forecasting,

geological surveys (i.e. mapping of subsidence and mineral distribution, oil search, etc.).

- Emergency applications: firefighting, search and rescue, tsunami/ flood watch, nuclear radiation monitoring and catastrophe situation awareness, humanitarian aid delivery, etc.
- Communications applications: Telecommunication relay services, cell phone transmissions or broadband communications are examples of communication applications.
- Monitoring applications: homeland security (marine and international border patrol, coastal monitoring, law enforcement etc.), crop and harvest monitoring, fire detection, infrastructure monitoring (oil/gas lines, high voltage power lines, pipelines, etc.) and terrain mapping (forest mapping, remote sensing of urban areas, etc.).
- Commercial applications: photography, precision agriculture-chemical spraying, transportation of goods and post, etc.

UAS have the potential to fill an important gap in surveillance capability from fixed wing aircraft to almost in-situ scale. Some can fly at very low altitudes with high degrees of flight flexibility and with no human exposure. They are therefore complementary to manned aircraft and satellites. (Partington, 2014)

Regarding the application of UAVs in OSR, UAVs are a relatively new option for deploying remote sensors. UAVs come in two types: fixed wing and rotary wing. UAVs come in all shapes and sizes, from long-range, high-endurance models to small, human-portable UAVs with ranges of a few miles. A large UAV offers outstanding performance and capability (carrying VIS, IR, and SAR sensors), but at a high cost (\$20–\$30 million per unit) (API, 2013).

Examples of various UAVs from different manufacturers are presented in Figure 39. Figure 40 illustrates the range and payload capacities of various types of UAVs.



Figure 39. Examples of UAVs: the Altair by General Atomics Aeronautical Systems Inc. (left), Skeldar V-200 by Saab Aerospace (middle), and the T-Hawk™ Micro Air Vehicle from Honeywell (right).

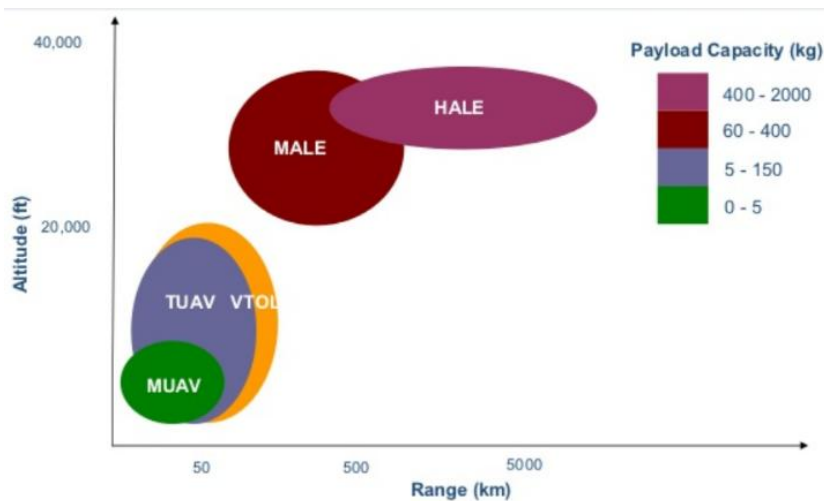


Figure 40. Range and payload capacities of different UAVs. HALE: high altitude long endurance; MALE: medium altitude long endurance; TUAV: tactical UAV; VTOL: vertical take-off and landing; MUAV: mini and micro UAV. (Partington, 2014)

A family of smaller, lighter UAVs offers a more balanced approach between capabilities and costs for OSR. These UAVs are propelled by gasoline-powered engines, are capable of programmed or manually controlled flight, and require minimal space for launch and recovery.

UAV systems generally include a ground station used to program missions, make in-flight adjustments and receive, process, display, and potentially disseminate real-time imagery and imagery products. The smaller UAVs can be packaged with their ground station to fit into a mid-sized sport utility vehicle, and they typically involve relatively simple assembly and user-friendly operation. Operational sensor packages which are small enough to meet payload restrictions for small UAVs include panchromatic (VIS) and IR imagers.

Advantages and potential of the UAVs (not all types of UAVs) are the following (API, 2013; Partington, 2014):

- Various ranges of UAVs available for OSR;
- UAVs can fly lower than aircraft and generate imagery of high spatial resolution;
- UAVs can fly below low clouds, removing that obstruction from the field of view;
- The cost of some UAVs is significantly lower than that of some other platforms;
- Launch and recovery requirements help UAVs reach some places inaccessible to other aircraft;

- UAVs can be deployed rapidly;
- Some UAVs can be operated remotely by pilots who can operate in shifts if required;
- Significant health and safety benefits to not deploying manned aircraft in some areas, such as the Arctic;
- UAVs are less noisy, smaller, and less disturbing or annoying than manned aircraft and
- Some UAS can be used as communications platforms as well as remote sensing platforms.

Disadvantages with the UAVs are that (API, 2013; Partington, 2014):

- Payload capacity limits the sensors currently available for operations;
- Local aviation and/or government regulations restrict the use of commercial UAVs;
- Allocation of the EM frequencies for UAV communication is limited and sensitive to interference (i.e. need for frequency bands for UAV use);
- Possible export regulations for larger UAVs (range >300 km, payload capacity >500 kg);
- Possible extreme operating conditions (e.g. darkness, low temperatures, high winds, rain) limits their use;
- High development and procurement costs;
- Detection sensors and components are not designed to be deployed in UAVs and
- Slow speeds and short-duration flights may limit the amount of data collected.

The ability of UAVs to capture, process, and integrate imagery from multiple sensors increases the utility and timeliness of obtaining useable event intelligence. On some systems, quantified information can be directly downloaded, processed, analysed and web served to the command and control or response assets. (API, 2013)

Partington (2014) concluded that limited numbers of UAVs are available for rapid deployment, since many of them are experimental or prototype systems and the availability of UAV units for OSR has been estimated on an optimistic basis. Additionally, the challenges of UAVs are significant and distinct from those of manned aircraft, and reflect the lack of maturity of the technology for operational uses. However, Partington (2014) estimated that UAVs will provide another platform for OSR in the coming years, since UAVs are evolving rapidly in terms of technology and commercial and legal landscape.

During the Kemi Arctic 2015 oil recovery exercise, Air Intelligence Finland Ltd demonstrated their drone, which was equipped with IR and video cameras (Figure 41).



Figure 41. The drone operated by Air Intelligence Finland Ltd during the Kemi Arctic 2015 oil recovery exercise. (Image: SYKE/Jyrki Nikkilä)

The wind limit for their system is from 8 to 12 m/s depending on the mission and requirements. For example, the quality of video decreases when the wind speed exceeds 12 m/s. During the exercise the wind speed was 3–4 m/s and the air temperature 4–5 °C.

The payload capacity for installed sensors is a maximum of 2.5 kg. Operational time in cold conditions (-20 °C) is approximately 20 minutes for one set of batteries, providing that the batteries are stored and recharged in warm conditions. The change of batteries takes a maximum of 2 minutes, after which the drone is ready to fly again.

During the Kemi exercise, the sight distance between the drone and the icebreaker Sampo was a maximum of 500 m at 150 m altitude. (Ehnqvist, personal communication, 2015)

3.5 Autonomous Underwater Vehicle (AUV) and Remote Operated Vehicle (ROV)

AUVs are robots which travel underwater without requiring input from an operator, controlled and piloted by an onboard computer. The systems consist of the body, sensors, navigators, propulsion, power supply and remote receiver (e.g. laptop), and they can be equipped with a wide variety of sensors. An example of an AUV is presented in Figure 42.

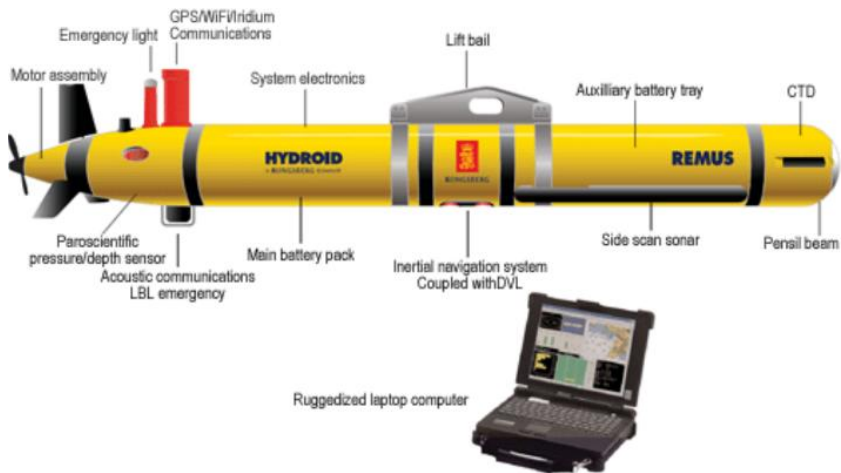


Figure 42. REMUS-600 AUV system by Kongsberg Maritime.

ROVs are tethered underwater robots that allow the operator to remain in a comfortable environment while the ROV works underwater. An ROV system comprises the vehicle, a group of cables for signal and power transfer, a handling system to control the cable dynamics, a launch system and associated power supplies. ROVs can be equipped with video and still camera, lights and additional equipment, e.g. samplers and various sensors. An example of an experimental ROV is presented in Figure 43.

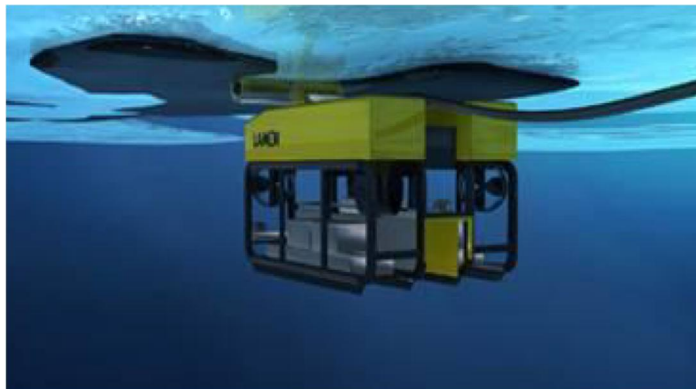


Figure 43. An experimental ROV by Lamor Corporation.

One of the latest examples in the field of AUV development is the HC-Sentinel glider. It is an autonomous underwater glider equipped with an ultra-low power mass spectrometer for real-time subsea hydrocarbon pollution detection (Figure 44).



Figure 44. Underwater photo of HC-Sentinel after being deployed from a surface vessel. (Camilli, 2017)

HC-Sentinel, a modified Slocum glider, is an integrated platform intended to serve as a low cost, long-range exploration tool for detecting hydrocarbon pollution in marine environments. Due to its minimalistic architecture, the operational costs have decreased to orders of magnitude lower than conventional subsea leak detection vehicles. Since HC-Sentinel does not require an attending surface vessel, it is able to perform leak inspections and surveys for longer durations than conventional AUVs. It can also be used in sea states in which surface vessels could not operate, i.e. severe storms and hurricanes.

HC-Sentinel weights 85 kg in air, and can be deployed and recovered by two persons from a small rigid inflatable boat. The vehicle is designed to operate to a maximum water depth of 1 000 metres with a maximum endurance of 3 days before requiring recharge. Its payload mass spectrometer is capable of detecting hydrocarbons at trace levels. The average speed over ground is approximately 0.37 m/s. (Camilli, 2017)

The Finnish Meteorological Institute (FMI) is using a Slocum G2 glider from Teledyne Webb Research, called “Uivelo”, for the monitoring of water quality in the Baltic Sea area (Figure 45).



Figure 45. Slocum G2 glider “Uivelo” in the workshop at FMI together with the main pilot Kimmo Tikka. (Image: VTT/Jukka Sassi)

“Uivelo” is equipped with various sensors, e.g. ctd for temperature and salinity, oxygen optode and a fluorometer for chlorophyll *a*, turbidity and coloured dissolved organic matter (CDOM). The glider can dive down to 200 m and the continuous operation time in the Baltic Sea environment is up to two months (Tikka and Alenius, personal communication, 2017). In addition, the Marine Systems Institute (MSI) at Tallinn University of Technology is utilizing a similar Slocum G2 glider mainly to acquire high-resolution vertical sections of different parameters in connection with certain processes under investigation. The glider “Mia” records temperature, salinity, chlorophyll *a* fluorescence, dissolved oxygen and turbidity. (BOOS, 2016)

The BOOS Vision 2020 in the service development segment foresees that the Baltic Operational Oceanographic System (BOOS) and its members will be the main providers of operational oceanographic services for local, national, regional and European users in the Baltic Sea area. The main goal in the field of in-situ observations is to develop further the multi-platform interdisciplinary network of real-time observations to meet the requirements of the Copernicus marine service, marine environment monitoring, climate change studies, maritime affairs and marine research and innovation. It includes the development of the network of Baltic Sea Argo floats, establishment of the Baltic Sea glider port and initiation of the programme of long-term glider sections in the Baltic Sea. (BOOS, 2016)

On the European level, utilization of the gliders is promoted by the European Gliding Observatories (EGO) network, which consists of academic and industrial partners. The EGO network aims to facilitate glider experiments through networking and support within the EGO community. It also collects information about worldwide glider activity, references, tutorials, technical notes and links, and supports the development of software related to gliders (EGO, 2017).

Another example of the utilization of gliders in the monitoring of marine environments is the Argo programme. It was initiated in 1999 as a pilot project endorsed by the Climate Research Program of the World Meteorological Organization, the Global Ocean Observing System (GOOS), and the Intergovernmental Oceanographic Commission. The Argo network is a global array of more than 3500 autonomous instruments, deployed over the oceans, reporting subsurface ocean properties to a wide range of users via satellite transmission links to data centres (Argo, 2017). The “Uivelo” glider is included in the Argo network.

The advantages of AUVs and ROVs include the following:

- Operational time limited only by operators (ROVs) and battery power (UAVs);
- Can be used for oil detection under ice when equipped with e.g. sonar sensors;
- Highly manoeuvrable and can cover wide surveillance areas;
- Allows detailed examination of the target area;
- Depth range limited by the length of umbilical cable (ROVs) and battery capacity (AUVs);
- Various systems available due to oil and gas exploration in the Arctic;
- Applications for underwater oil removal in design phase and
- In case of lost equipment or accident, no loss of life.

The disadvantages of AUVs and ROVs include the following:

- Limited experience in arctic conditions;
- Cables may cause severe problems when operated in rough ice conditions;
- Equipment quite expensive;
- Requires reliable and robust communication platform;
- Operation requires trained persons and
- Effectiveness can be limited by water turbidity or darkness if adequate illumination is not provided.

3.6 Aerostats

Tethered balloon systems (aerostats) are tethered balloons (or other lighter-than-air craft) that gain lift through the use of buoyant helium gas, deployed from mobile or permanent platforms. They can therefore be considered either as airborne or in situ remote sensing platforms. They are capable of being deployed to an altitude of up to 6 000 m and so can provide excellent tactical support to an area of operations, potentially covering a few hundred km. Dependent upon their configuration, aerostats are capable of providing 360° unrestricted sampling. Such systems may

also permit immediate download to multiple users, thereby minimizing data latency and turnaround time.

These platforms can take significant sensor payloads, potentially up to 2 500 kg. Communications can be wireless and can be used to control the sensors as well as to receive the observations, or in some cases may be via a wire to enhance data transfer capacity. The large size and weight-carrying capacity of some systems allow them to support a broad range of sensors that will greatly extend the operational observation capabilities of response assets (Figure 46).



Figure 46. Examples of tethered balloon systems: Aerophile Group (left), and SPEC Ltd ready for deployment at the South Pole (right).

Installed visible, thermal and other spectral sensors can greatly enhance the ability to provide quantifiable information to responders by viewing an area several miles around the platform, depending on the operational height of the balloon.

These systems are intended to function in a manner similar to planes with aerial observers. A variety of sensor types may be attached to a helium-filled balloon using a tether and winch system attached to a platform. The sensor can be wirelessly controlled from a computer and deck station on the platform. It transmits a signal wirelessly back to the mother ship and surrounding vessels.

The balloons are generally powered by a battery with an expected duration of 24 hours, and there may be an option for using a wire to transmit power and signal to and from the camera. (API, 2013; Partington, 2014)

Advantages of the tethered balloon systems are as follows:

- Relatively cost effective, primary costs are often the sensors rather than the platform;
- Can fly below low clouds, removing that obstruction from the field of view and thus providing almost continuous observations;
- Increases the height of observation compared to boat-based observers;

- Can be deployed from a moderate-size ship or from land and deployment can be rapid;
- Communication can be wireless;
- Can operate 24 hours per day, with few weather limitations and
- Less regulation limitations compared to UAVs.

Disadvantages with the tethered balloon systems include the following:

- Operating the system to its full capability can require extensive training;
- High winds can degrade the system's capabilities;
- Obtaining adequate volumes of helium for larger balloons may be difficult in some areas and
- Limited experiences in arctic oil detection operations.

The tethered balloon must be operated under the local aviation regulations. Tethered balloon systems may provide a tool for resource management, allowing task force leaders to observe other vessels within the task force and check for positioning and adherence to tasks. The tethered balloon may also be used to develop a communication relay system by carrying repeating equipment. The majority of the costs for these platforms are associated with the sensor/camera system. (API, 2013)

According to the reference (Puestow *et al*, 2013), a compact aerostat system "Ocean Eye" (Figure 47) can carry a high-resolution camera and IR sensor to monitor spills from altitudes up to 150 m.



Figure 47. An aerostat system "Ocean Eye". (Maritime Robotics, 2015)

Both airborne and space-borne sensors, including SAR, SLAR, infrared- and visible-range imaging, microwave radiometers, and laser fluorosensors can be used. The various sensors use different physical attributes of the oil and the surrounding environment to detect the presence of oil. The applicability of a given detector depends on such factors as the size of the spill, ambient weather conditions, time of day and accessibility of the geographic region. (Puestow *et al*, 2013)

Utilisation of the tethered balloons was discussed e.g. in the JIP 2 and International Association of Oil and Gas Producers (OGP) workshops. The general opinion was that they might offer one platform to enhance the situation awareness of the spill area close to the combating vessels when equipped with IR and video cameras.

4. HSE issues in field operations

The Finnish authorities have specific industrial safety guidelines for accidental oil and chemical spill response. The instructions are an integrated part of the Health, Safety and Environmental (HSE) procedures which define the actions for safe oil and chemical spill response. The instructions supplement the legal acts and regulations set by the relevant authorities, but they do not replace or disprove them.

The instructions include the legal framework of industrial safety both on the international and national levels. They define the responsibilities of each management level, including the persons who perform the actual response actions. They have a specific focus on different oil and chemical types and they emphasise the supervision of the work. Occupational health care, first aid preparedness issues and the required actions in the case of an accident are also discussed.

The instructions provide tools for the identification and risk evaluation of damage and hazard caused by equipment, lifting and moving of heavy loads, falling, electric shock, noise, steam, heat and UV radiation and environmental conditions (e.g. temperature, wind), exposure to chemicals, oils and oil mist, and the fire risk caused by different oil qualities. In addition, the issues related to a risk of disaster, work ergonomics, properties of various oil types, options for recovery in different oil spill cases, chemical and physical exposure and protection equipment are discussed. (SYKE, 2015)

5. Wireless data transmission

In addition to gathering the relevant data with multiple sensors, the functional systems must have means to transfer the data to processing computers and human beings that will make decisions on how to act. The data can be processed locally in order to reduce the information load in the network. There are many factors affecting the implementation of the communication link, including e.g. whether the sensors are located in a vessel, if they are fixed, in a drone or in a satellite.

Maritime users are typically mobile, and also affected by wind, weather and waves. This poses a range of challenges that a fixed land-based user will never encounter. For communication purposes, the maritime sector can be divided into three parts (Løge, 2013).

- 1) Small vessels which will experience substantial rolling motion already in small waves and fair weather. These vessels will need low gain antennas to communicate, and directional use will be difficult.
- 2) Large and stable vessels and installations that can take advantage of maritime very small aperture terminal (VSAT) satellite solutions.
- 3) Fixed and quasi-fixed offshore installations such as oil platforms and drilling rigs. Users in this group have more in common with terrestrial users than other maritime users.

An especially problematic area for communications, due to the current lack of supporting infrastructure, is the Arctic. Table 10 shows which kinds of communication systems can be used in these areas. It is possible e.g. to have a drone connected with LTE to the ship that transfers the data over a satellite link to the shore for further processing and decision-making.

Table 10. Communication systems for the Arctic regions.

	System	Characteristics	Polar area (>80°N)	Sub-Polar area (70–80°N)
Terrestrial system	HF, MF	Messages and voice, recently IP-based communications	Products available, long coverage, limited data rates	Products available, long coverage, limited data rates
	VHF, digital VHF	Voice and very narrowband data	No base stations currently, VDES under development	Few base stations
	GSM, 3G	Voice and narrowband data	No base stations	Very few base stations
	LTE/4G, WiMAX	Voice and broadband data	No base stations	Insignificant deployment
Satellites	GEO and GSO	Moderate to high latency	Mostly unavailable, MUOS system demonstrated	Limited availability and quality
	LEO	Currently few hundreds of kbps, low to high, variable latency	Stability and limited quality. Requires constellation of at least tens of satellites	Stability and limited quality

More specific challenges are described briefly in the following paragraphs.

Security and authorization: The data should be well protected so that it cannot be accessed or modified by unauthorised users. Thus, only authorized stakeholders have access to data. A good cybersecurity solution for the end-to-end link should be implemented so that there are no weak points anywhere in the communication path. Especially crucial is to protect the control link from the shore control station (or from the ship control station), if there is one, so that there is no access to the control link from outside and no possibility to take possession of remotely controlled aircraft or vessel by hijackers.

Reliability: Transmitted and received data should be as specified, not corrupted or otherwise useless for end-users. Interference management is important to improve reliability. The communication link can be protected from intentional jamming and other interference by use of intelligent mechanisms such as changing the operational frequency under interference. Redundant radio links in general also improve the reliability in the case of communication equipment breaks. The cybersecurity solution should be strong enough to prevent additions/modifications to the data. A good example of bad protection is the automatic identification service (AIS) data that is used to track the movements of ships. It has been shown that a hacker can very easily add “ghost ships”, remove ships from the system, and change information concerning ships such as location, heading and speed. This should be prevented.

User interface: For the functional user interface, only the required data should be shown. The demands of a human being and his/her cognitive capacity should be taken into account. This is currently being studied quite intensively in the area of autonomous ships, e.g. to find out how many ships one person can handle simultaneously.

Data processing: Extraction of useful information from the raw data may require a considerable amount of processing. Local processing reduces transmission requirements significantly. Sensor fusion can be used to combine data from different sensors locally and send the fused data over the wireless link. This is heavily dependent on the used sensor and communication technology choices. For example, hyperspectral imaging data requires extensive post processing before oil can be differentiated from other surface modifications such as waves. Local processing capability is dependent on the payload ability of the carrying equipment.

Accuracy of data vs. transmission distance and speed: A short distance communication link can usually support high capacity transmissions, and the further the receiver is from the transmitter the smaller is the throughput of the link. This means that depending on the sensor technology, the accuracy of transferred data is inversely proportional to the length of the link if the link capacity is the limiting factor. For example, video can be adaptively scaled according to the supported capacity of the link to always send the highest possible quality. It is also possible to aggregate data over multiple radio channels or even over multiple radio access technologies simultaneously, in order to achieve higher data rates. If very long communication links are needed, current options include only low data rate HF links

or satellites. Table 11 illustrates a comparison between different technologies, showing e.g. maximum bit rates and communication ranges.

Table 11. Comparison of various transmission technologies.

	802.11p for ITS	Wifi	LTE/4G	5G mmW	VHF digital radio	HF
Spectrum	5.9 GHz	2.4/5 GHz	450 MHz–3.7 GHz	24–86 GHz	30–300 MHz	3–30 MHz
Bandwidth	10 MHz	20/40 MHz	From 1.4 to 20 MHz	Up to few GHz	25 kHz channels, can be bundled together e.g. to 100 kHz	Up to 48 kHz
Max. bitrate	27 Mbps	600 Mbps	75/300 Mbps for UL/DL	Up to 20 Gbps	VDES: up to 307 kbps in ship-to-ship or ship-to-shore, 240 kbps for satellite link	Up to 240 kbps
Tx range	< 1 km	Typically < 100 m, up to 10 km with fixed service	Typically < 2 km, up to 70 km with directional antennas	< 10 m for 60 GHz Wifi, tens of kilometres with fixed links	Up to 85 km	Thousands of kilometres
Cost	Cheap	Cheap	Expensive	Cheap (Wifi), Expensive (Cellular)	Cheap	Cheap

Connectivity management: Often the data sent over the wireless links can be prioritized, e.g. some data is very delay-sensitive and should be transmitted before some other data. This is especially important when the capacity is limited and there is more data to be transferred than can be supported at the time of transmission. Thus, data is sent according to the quality of service (QoS) requirements over different times and radio technologies. The connectivity manager decides what data is sent over which route, ensuring that data reaches its destination with integrity and within latency requirements. An example is shown below, in which a remote operator from the shore control centre (SCC) is connected to the ship with several different technologies; a multi-hop connection over multiple ships is also possible (Figure 48).

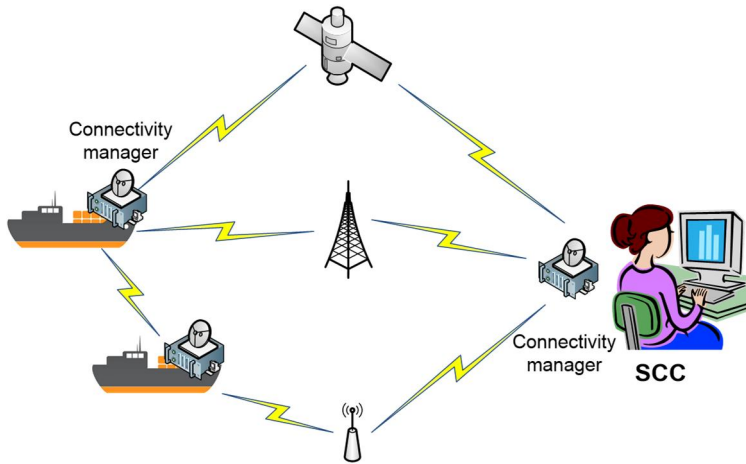


Figure 48. An example of connectivity management.

Estimated data transfer requirements are presented in Table 12. These estimates are based on experiences from autonomous ship studies.

Table 12. Data transfer estimates related to an autonomous ship.

System	Single file/Image (kB)	Update rate (Hz)	Compressed bit rate (kbps)
Radar/AIS plot	375	0.4	100
Video	200–500	1–10	150–1500
HD video	2600	2	800–1500
LiDAR	up to 200 000	1	1000–2000
Infrared	330	1–10	300–1000
Mechanical sensors	12	0.1–1	1–10
Control data	Remote control, rendezvous	1	1–10
General GMDSS data	Varies		10

It is anticipated that the transferring of e.g. video or LiDAR data requires more bandwidth than radar and IR. The control data between the ship and shore requires a significantly lower bit rate.

6. Recent field experiments in Finland

6.1 Oil detection field trials in Kalajoki (2016)

6.1.1 Description and objectives

In the operative oil spill response one of the challenges is to detect the released oil in ice-covered waters. It is essential for successful recovery options to locate the spilled oil, define the thickness of the oil layer, prevent the spillage from spreading and decide on appropriate recovery actions.

Limited visibility due to snow, fog or rain, darkness and challenging ice conditions hamper the oil detection. Various detection technologies can be utilised from different platforms such as satellites, aircrafts and surface vessels. In cases when the oil is located between ice floes or under the ice or snow, some of the currently utilised methods are insufficient, since each sensor technology has its limitations.

The objective of the field trials was to increase hands-on experience of the selected sensors and platforms in oil detection under arctic conditions. This included e.g. how different sensors can detect heavy fuel oil in prevailing weather conditions, and what are the limitations of the used platforms in terms of payload, wind, visibility and vibration.

The field trials were performed 14–15 March 2016 in cooperation with SYKE, the Centre for Economic Development, Transport and the Environment in Kokkola, Javal Ltd and VTT. The sensors were provided by Air Intelligence Finland, LDI Innovation OÜ, National Land Survey of Finland (NLS) and Rikola Ltd. The UAS platforms were provided by Air Intelligence Finland Ltd, and First Invest Ltd operated the helicopter.

6.1.2 Test arrangements

Test area

The test site was located in the Port of Kalajoki, 70 km north-east from Kokkola (Figure 49).

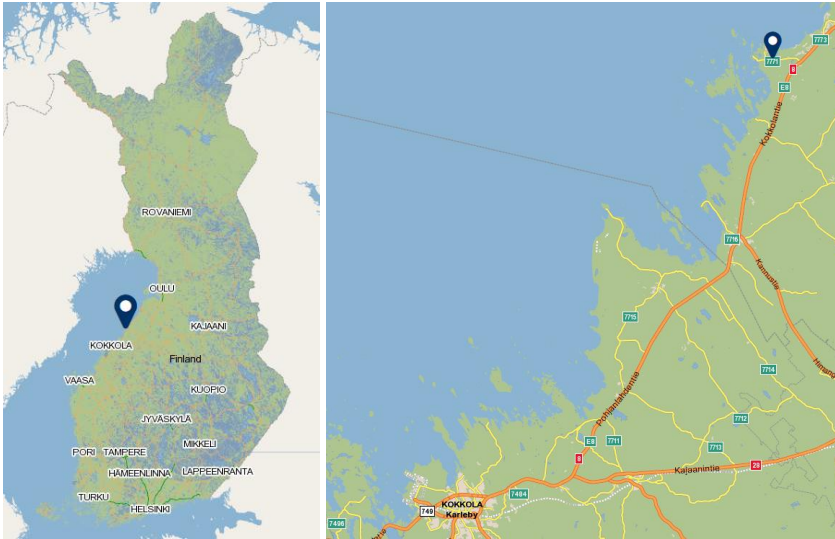


Figure 49. The location of the test site (amended from Fonecta map service, not to scale).

Three separate basins with different oil-ice concentrations were utilised. The sizes of the basins were: basin A; 5 m x 12 m = 60 m², depth 1 m, and basins B and C; 2.5 m x 6 m = 15 m², depth 1.5 m. During the tests the water depth was approximately 70 cm in basin A and 1.2 m in the basins B and C (Figure 50, Figure 51).

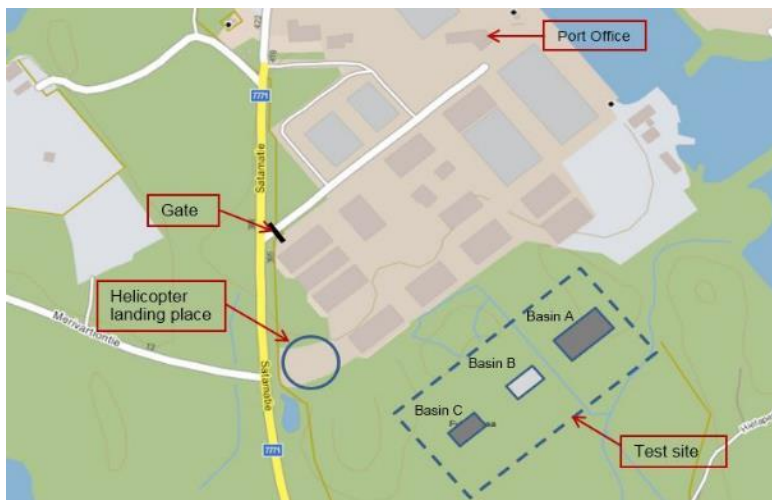


Figure 50. Map of the harbour area (amended from Fonecta map service, not to scale).

The distances between the basins were approximately 10–12 m, and the length of the test area was approximately 60 m. The basins were surrounded with ice and snow to imitate real oil spill conditions in which oil is spilled on the ice surface (Figure 51).



Figure 51. The test site with indication of the basin locations. (Image: VTT/Jukka Sassi)

Test oil

Heavy fuel oil HFO180 was used as the test oil. Before pouring the oil into the test tanks it was stored in a warehouse at a temperature of 32 °C. The sulphur content of the test oil was 0.9% and calculated viscosity at 50 °C is typically 170 mm²/s. The properties of the test oil are presented in Appendix A.

LDI Innovation took oil samples after the tests and their spectral signatures were recorded in the laboratory. The analyses indicated that the samples revealed rather modest fluorescence efficiency, probably due to their low content of polycyclic aromatic hydrocarbons (PAHs), which were not specified in the data sheet of HFO180. PAHs are responsible for oil fluorescence. The emission spectrum of fluorescence of the test oil samples is presented in Figure 52. (Babichenko, 2016)

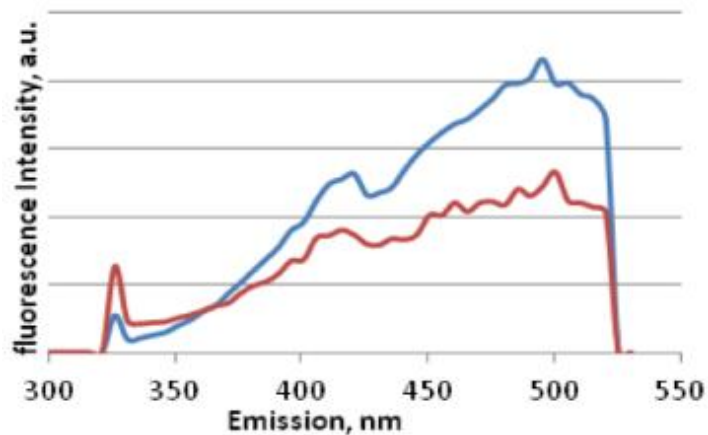


Figure 52. Fluorescence emissions spectra of HFO180 measured on the surface in the laboratory with lower (red) and higher (blue) oil film thickness. (Babichenko, 2016)

Figure 52 shows the emission spectrum of fluorescence of the oil samples at the excitation wavelength of 308 nm (laser emission wavelength of the OWL). It can be seen that the fluorescence band of oil is located in the spectral range longer than 450 nm, with maximal intensity at 500 nm, which generally corresponds well to typical spectral signatures of heavy fuels. (Babichenko, 2016)

Test execution

Day 1, 14 March 2016

The basin A (60 m²) was filled with sea water (salinity approximately 4 ‰, taken from the harbour basin) and ice with a ratio of approximately 30/70, i.e. ice 18 m² and open water 42 m². The nominal layer of 2 mm (approximately 150 l, ¾ of the 200 l barrel) of HFO180 was spread as evenly as possible on ice and on water (Figure 53, Figure 54).



Figure 53. The basin A in the morning of Day 1. (Image: SYKE/Jouko Pirttijärvi)



Figure 54. Aerial view of the basin A on Day 1. (Extracted from the video by Air Intelligence Finland)

The oil temperature was 13 °C when poured from the bucket of an excavator (Figure 55). The amount of poured oil was determined visually by checking the oil level inside the 200 l barrel before and after the pouring.



Figure 55. The 200 l oil barrel of HFO180 with a release lid in the bucket of an excavator. (Image: SYKE/Jouko Pirttijärvi)

The basin B (15 m²) was used as the reference basin without oil. The water/ice ratio was approximately 50/50 (Figure 56).



Figure 56. Aerial view of the basin B. (Extracted from the video by Air Intelligence of Finland)

In the basin C (15 m²), the ice ratio was approximately 70/30, i.e. ice 10 m² and open water 5 m². The nominal layer of 2 mm (approximately 50 l, ¼ of the 200 l oil barrel) of oil was spread as evenly as possible on ice and water (Figure 57).



Figure 57. Aerial view of basin C with 50 l of oil on ice and on water. (Extracted from the video by AIF)

In the dark testing conditions, the locations of the three basins were signposted by several lights indicating the locations of the basins for the helicopter pilot. The lights did not illuminate the oil or ice on the surface of the basins, since they were positioned on ground level.

During the test trials the average temperatures of the oil, ice and water were measured with a Fluke 68 IR Thermometer from basin A (Table 13). The air temperature, wind and cloudiness data were acquired from the webpage of the Port of Kalajoki.

Table 13. The measured temperatures in Day 1.

Time	T _{air} [°C]	T _{ice} [°C]	T _{oil on ice} [°C]	T _{oil on water} [°C]	Remarks
10:40	-2	-2.4	-1.4	-0.7	30 minutes after oil was poured.
13:30	-1	-1.1	1.5	5.3	Sunny weather, cloudiness 44%, wind 2.56 m/s NW.
14:55	-1	-2.1	0.2	4.6	Partly sunny, cloudiness 45%.
18:10	-2	-1.8	0.8	-0.7	Partly sunny, cloudiness 48%.
21:30	-3	-0.9	-1.3	-1.4	After sunset, dark.

During Day 1 the following sensors were demonstrated (Table 14). Sunset was around 18:15.

Table 14. The sensors and platforms used during Day 1.

Time	Sensor	Platform	Remarks
13:30–13:45	Hyperspectral camera	UAS	Camera by Rikola Ltd.
13:55–14:15	OWL™ LiDAR	Helicopter	LiDAR by LDI Innovation OÜ, altitudes from 30 to 100 m, speed from 24 to 100 km/h.
14:35–14:50	No sensor	Helicopter	Iceye Ltd checked the vibrations caused by the helicopter and the usability of the helicopter as a platform for their radar sensor.
15:00–15:25	Video camera and Optris TIR	UAS	Two UAS, both sensors by Air Intelligence Finland, battery replacement to other UAS during the flight.
18:35–19:10	Blue-Hawk™	UAS	Sensor by LDI Innovation OÜ. Sensor (3.8 kg) was too heavy for the UAS, instead it was operated handheld in basin A.
21:00–21:10	OWL™ LiDAR	Helicopter	LiDAR by LDI Innovations Ltd., several flights over the test site, assistant on ground with a laser indicator to indicate the locations of the basins.

Day 1 was finished at 22:15 after all the test trials were completed and the equipment was prepared for the Day 2 trials.

Day 2, 15 March 2016

The same three basins with the same oil/ice concentrations and oil quantities were utilised during Day 2, with the modification that all the three basins were covered with a snow layer of approximately 5 mm (Figure 58). Thus the oil and ice were mainly covered with snow and slush. The snow cover was generated by using a heavy duty snow blower installed in a tractor (Figure 59).

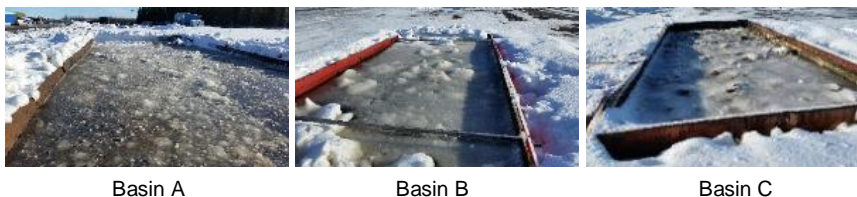


Figure 58. All the three basins with snow cover. (Images: VTT/Jukka Sassi)



Figure 59. Snowing of the test basins in progress. (Image: SYKE/Jouko Pirttijärvi)

The measured temperatures and demonstrated sensors with selected platforms are presented in Table 15 and in Table 16.

Table 15. The measured temperatures during Day 2.

Time	T _{air} [°C]	T _{snow on ice} [°C]	T _{oil on ice} [°C]	T _{oil on water} [°C]	Remarks
9:35	0	0.9	0.6	0.7	Cloudiness 30%, wind 5,67 m/s SW.
9:50	0	0.2	0.3	0.4	
10:30	-1	-0.2	-1.9	2.7	

Table 16. The sensors and platforms demonstrated during Day 2.

Time	Sensor	Platform	Remarks
10:20–10:30	Hyperspectral camera	Helicopter	Camera by Rikola Ltd, two speeds approximately 10 km/h and 30 km/h.
11:10–11:15	Hyperspectral camera	Handhold	Operated as handhold by Hakala/NLS.
11:25–11:30	Hyperspectral camera	UAS	Camera by Rikola Ltd, visually estimated altitudes 5, 10 and 20 m, same setting as in the helicopter in Day 2 and in UAS in Day 1.

Day 2 was finished at 12:15 after all the test trials were finalised and the sensors dismantled from the UAS and helicopter.

6.1.3 Platforms

Two different platforms were used for the sensor mounting, i.e. unmanned aerial system (UAS) and a helicopter.

Unmanned aerial system (UAS)

The UAS type used in the test trials was a Videodrone X8 with the remote control console and the operator (Figure 60).



Figure 60. The UAS used in the test trials with the video camera mounted, and the remote control console with the video controls. (Images: VTT/Jukka Sassi)

According to ICAO during VLOS (visual line-in-sight) operations, the remote pilot or remotely piloted aircraft (RPA) observer must maintain direct unaided visual contact with the remotely piloted aircraft. (ICAO, 2015)

The wind limit for the UAS is around 10 m/s; harder wind speeds cause exceeding of the rectification limits of the gimbal, resulting in poor image quality.

The video camera used in the test trials was a Sony HDR-CX410. The power for the camera was obtained from the batteries of the UAS. The remote control console enabled online monitoring of the video camera image. Additionally, zooming and switching the camera on and off was possible. The batteries of the UAS were charged from the power supply, which was connected to the portable SDMO Pro 2000 inverter (Figure 61).



Figure 61. The inverter charging the batteries of the UAS. (Image: VTT/Jukka Sassi)

The UAS was operated by Air Intelligence Finland, which offers tools for aerial mapping and management for actors in the private and public sectors. The equipment consists of modern unmanned aerial vehicles (UASs) and unmanned aerial systems (UASs) with ground stations enabling real-time data gathering and exploitation. The platforms were operated by professional aviation experts with professional discretion. (Air Intelligence Finland, 2015)

Trafi's regulation OPS M1-32 defines that the maximum take-off load for a UAS is 25 kg and the maximum allowed flying altitude is 150 m. Exceptions from the requirements may be requested from Trafi in cases of extraordinary and urgent situations. (Trafi, 2015)

Helicopter

The helicopter was provided by First Invest Ltd and piloted by Hannu Koponen. The model was a Schweizer 300, with maximum payload of 75 kg. The sensor mounting racks were located on both sides of the helicopter (Figure 62). The electricity for the mounted sensors was generated by the inverter. The cabin has room for two persons.



Figure 62. The helicopter ready for test flights. The mounting racks were installed on both sides of the helicopter. (Images: Carelia Copters)

The helicopter has no precisely measured wind limit, but wind speeds of 15 m/s and more make a precise flight pattern difficult to maintain. If the mission requires very precise aiming, use of the helicopter might be very challenging or even impossible.

In the daytime the minimum required cloud altitude is 150 m and horizontal visibility is 500 m. In the night-time the required cloud altitude is approximately 1000 m and horizontal visibility is approximately 5 km. These distances apply to helicopters with visual flight rules (VFR), when a pilot operates an aircraft in weather conditions generally clear enough to allow the pilot to see where the aircraft is going. The pilot must be able to operate the aircraft with visual reference to the ground and by visually avoiding obstructions and other aircrafts.

Heavier helicopters, which are operated e.g. by the Finnish Border Guard and Mediheli, are operated under the instrument flight rules (IFR). IFR flight depends upon flying by reference to instruments in the flight deck and navigation is accomplished by reference to electronic signals. These helicopters can be operated in harsher meteorological conditions. (Hannu Koponen, personal communication, 2016; Instrument Flying Handbook, 2008)

6.1.4 Sensors

The sensors tested in the Kalajoki field test trials represented different technologies and suppliers (Table 17).

Table 17. The sensors demonstrated in the field tests.

Sensor	Company	Platform
Optris IR camera	Air Intelligence Finland Ltd (FI)	UAS
Oil in Water Locator – OWL™	LDI Innovation OÜ (EE)	Helicopter
BlueHawk™	LDI Innovation OÜ (EE)	Handhold
VIS/NIR hyperspectral camera	NLS (FI)	Handhold
VIS/NIR hyperspectral camera	Rikola Ltd (FI)	UAS and helicopter

A detailed description of each sensor is provided in the following sections.

Blue-Hawk™ and Oil In Water Locator OWL™

Blue-Hawk™ and Oil In Water Locator OWL™ sensors by LDI Innovation OÜ are both based on light-induced fluorescence (LIF) technology. In LIF technology, the sensing light generated by a UV light source hits the target and is absorbed by oil molecules, if present in the target. Absorbed light energy is re-emitted by the oil molecules in a spectral range characteristic for such molecules. This re-emitted light (fluorescence) is recorded by spectral detector and analysed. The recorded fluorescence flux serves for oil detection and the spectral shape of the fluorescence emission serves for oil characterisation (as a “spectral signature” of oil).

The techniques employing the LIF method can be divided into fluorosensors, registering integral fluorescence in a selected spectral range, and spectral devices recording the fluorescence spectra with subsequent analysis. The use of pulsed light sources with synchronous detection of fluorescence makes possible the application of this technique in day and night time.

Blue-Hawk™ is a non-contact fluorosensor of LDI Innovation OÜ for oil on water detection based on a pulsed UV light emission diode (LED) and spectral detector. The sensor registers specific fluorescence without recording its spectra and is therefore able to detect oils, although it does not have an oil differentiation capability. The sensor produces an alarm when the oil signal exceeds a pre-set warning level. Its sensitivity allows detection of oil films with minimal thickness of only a few micrometres, subject to the type of oil.

Very light weight and low power consumption make Blue-Hawk™ applicable on board small drones for oil pollution inspection on site. It operates with a battery, and has an integrated GPS module and optional GSM communication channel for alarm and coordinated transmission. For such operation the sensor is equipped with an additional video-camera to record underlying objects in flight. The technical data of the Blue-Hawk™ fluorosensor is presented in Table 18. (Babichenko, 2016)

Table 18. Technical data of the Blue-Hawk™ fluorosensor. (Babichenko, 2016)

Sensing distance	Max. 15 m	
Power consumption	2.5 W	
Dimensions	Ø 10 cm, length 24.5 cm	
Weight	1.5 kg/3.8 kg with battery and communication module	

The Blue-Hawk™ sensor was installed on the UAS and it was equipped with a down-facing video camera (Figure 63).

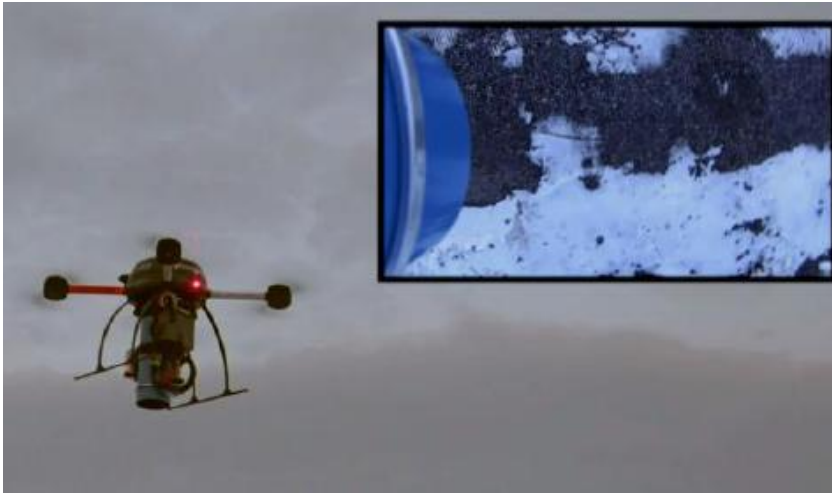


Figure 63. The UAS with Blue-Hawk™ sensor and video camera installed. (Image: LDI Innovations OÜ)

Within a few seconds (10–20 sec) after take-off it was noticed that the total weight of the sensor exceeded the payload limit of the UAS. Therefore, the UAS was piloted back to land and the test was interrupted. Additionally, the legs of the UAS were too short. The sensor was then tested as a handheld setting in the basin A, but the centre of the basin could not be inspected (Figure 64).



Figure 64. BlueHawk sensor installed on UAS but operated as a handheld set-up due to excess payload. (Images: VTT/Jukka Sassi)

Hyperspectral camera

The hyperspectral imagery was captured by the novel hyperspectral camera based on the tunable Fabry-Pérot interferometer (FPI) produced by Senop Ltd (former Rikola Ltd) (Figure 65). The hyperspectral camera was demonstrated both with the helicopter and UAS.



Figure 65. The hyperspectral camera by Rikola Ltd installed in the UAS on Day 2. (Image: VTT/Jukka Sassi)

The camera collected spectral information by capturing small rectangular images of a size of 648 by 1010 pixels. The camera had a focal length of 9 mm and a pixel size of 5.5 μm . The properties of the spectral bands can be tuned in order to obtain suitable spectral information for the analysis task. In this experiment, 50 spectral bands were used. The spectral settings (central wavelengths and the full width of half maximum (FWHM)) are given below. Senop Ltd took care of the data capture.

Central wavelengths of the bands [nm]: 524.64, 531.946, 539.285, 545.426, 552.826, 560.258, 566.478, 573.972, 581.498, 587.796, 595.384, 601.733, 609.381, 615.78, 623.49, 629.94, 657.933, 664.254, 671.856, 679.476, 685.84, 693.493, 699.885, 707.571, 713.99, 720.421, 728.156, 734.615, 742.383, 748.869, 755.369, 763.184, 769.711, 776.25, 784.114, 790.681, 797.261, 805.173, 811.78, 818.4, 826.36, 833.007, 839.667, 846.339, 854.362, 861.062, 867.775, 874.5, 881.237, 889.339.

Full width of half maximum (FWHM) [nm]: 15.5, 15.27, 15.06, 14.91, 14.73, 14.57, 14.45, 14.31, 14.17, 14.07, 13.94, 13.83, 13.7, 13.59, 13.45, 13.32, 13.5, 13.45, 13.38, 13.3, 13.23, 13.13, 13.05, 12.94, 12.85, 12.76, 12.65, 12.56, 12.46, 12.38, 12.3, 12.22, 12.16, 12.1, 12.05, 12.02, 12.0, 11.99, 12.0, 12.03, 12.08, 12.15, 12.23, 12.33, 12.49, 12.64, 12.82, 13.02, 13.25, 13.56.

When analysing spectral peaks on a graph, full width at half maximum (FWHM) is a useful way of characterizing the shape and overall value of a peak. FWHM is given as the wavelength difference between the two points on either side of the maximum at which the intensity is at half of the peak's maximum value. This provides not only a measure of a peak's height, but also its width. Similarly, the full width at quarter maximum (FWQM) may be used to characterize the spread of a peak. (<http://oceanoptics.com/glossary/#>)

The FPI hyperspectral camera operates on a tunable filter principle. The individual bands are not exposed at the same moment, and thus when operated from a moving platform the bands forming the hypercube are not aligned. In the worst cases, if the platform speed is too high with respect to the flight height, the full object spectrum is not obtained. In the Kalajoki campaign, the helicopter flew in different altitudes. Data from the highest altitude provided full spectral data and was thus suitable for hyperspectral analysis. The flight height was approximately 36 m and the GSD (geometric standard deviation) was 2.2 cm. (Honkavaara and Rosnell, 2016)

In dark conditions a hyperspectral camera requires active illumination systems, i.e. artificial lighting from the helicopter or other platform.

Oil in Water Locator – OWL™

Oil in Water Locator – OWL™ by LDI Innovation OÜ is a compact HLIF LiDAR of Ocean Visuals AS. It is a laser-based spectral device for oil in water detection and characterisation. The term LiDAR stands for Light Detection And Ranging, and indicates a capability of performing the sensing remotely. The hyperspectral LIF (hyperspectral laser induced fluorescence) LiDAR stands for the laser system detecting detail and comprehensive spectral response of water to the laser pulse. Due to this feature, HLIF LiDAR can directly detect and differentiate various oil products in water, including water containing ice.

The OWL™ is designed as a robust single box unit to operate in the open environment. The housing filled by nitrogen at overpressure contains sensing laser (UV emission, 308 nm), optical telescope for collecting induced fluorescence, and hyperspectral detector (512 channels in UV and VIS spectral ranges) for recording the HLIF spectra. The sensing pulses follow with a pre-set pulse repetition (PPR) rate up to 100 pulses per second. The HLIF spectra are recorded per each laser pulse and analysed in real time for oil spectral signature. The oil findings are accompanied with GPS coordinate and time, and reported to the local/remote server. The technical data of OWL™ is presented in Table 19.

Table 19. Technical data of OWL™LiDAR. (Babichenko, 2016)

Sensing distance	Max. 75 m	
Power consumption	150 W/1500 W arctic	
Dimensions	65 x 45 x 37 cm	
Weight	40 kg	

The device operates in unattended mode controlled by an integrated microcontroller. According to Babichenko (2016), the OWL™ is a most compact LiDAR of its type, designed for operation at a distance up to 50 m with oil in water detection sensitivity down to the part-per-million level. It is able to detect and differentiate oil films on water, oil emulsion in water column, and submerged oil under the water surface. (Babichenko, 2016)

OWL™ was operated by LDI Innovation OÜ. The laser of the LiDAR needed heating for approximately 15 minutes before the test flight. During the Kalajoki exercise the OWL™ was installed on the helicopter (Figure 66).



Figure 66. OWL™ by LDI Innovation OÜ in the Kalajoki exercise. The green spot indicates the laser beam. (Images: LDI Innovation OÜ (left) and VTT/Jukka Sassi)

The OWL™ box was fixed on the frame outside the cabin in nadir facing mode with a direct line of sight to the surface. It was powered by an onboard generator with a power converter and connected by cable to an in-cabin PC for data storage and visualization. The operation of HLIF LiDAR does not depend on the ambient illumination conditions because it utilises its own light source laser for measurements. To confirm the detection capabilities in different light conditions, the measurements were made in day and night time.

Several flights over the test area were performed during Day 1, also in dark conditions. The flight altitude varied from 30 to 100 m and the speed from 24 to 100 km/h. The helicopter also hovered above the target area.

The LiDAR operated with PPR in a range of 10–25 pulses per second depending on the flight speed. Every single HLIF spectrum was stored and processed. It should be noted that the laser beam had a fixed position, and therefore the beam pointing to the targets was made only by helicopter movement, which required a skilful pilot. For this reason, the laser beam did not cross the targets at every passage. Nevertheless, the targets were hit many times and corresponding signals have been recorded, analysed and reported. (Babichenko, 2016)

The HLIF LiDAR of LDI Innovation OÜ was also demonstrated in the Kemi Arctic 2015 exercise as a surface vessel installation (Figure 67).



Figure 67. Light Detection and Ranging (LiDAR) oil spill detection system by Ocean Visuals AS during the Kemi Arctic 2015 exercise. (Image: SYKE/Jyrki Nikkilä)

The performance of the sensor could not be verified since the use of oil was not permitted during the exercise.

Optris PI 400 IR camera

The Optris PI 400 IR camera (Figure 68) was provided by Air Intelligence Finland. It calculates the surface temperature based on the emitted infrared energy of objects. The two-dimensional detector (FPA – focal plane array) allows measurement of an area, which will be shown as a thermal image using standardized palettes. The radiometric processing of the picture data enables the user to make a suitably detailed analysis with the PI Connect software. (Optris, 2016)



Figure 68. Optris PI 400 IR camera. (Optris, 2016)

The weight of the camera with lenses is 320 g and the dimensions are 46 x 56 x 90 mm (Figure 69).

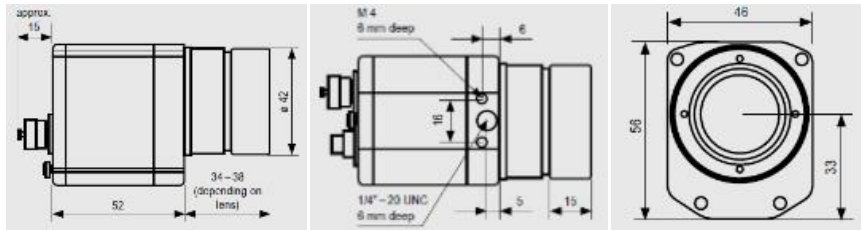


Figure 69. The dimensions [mm] of the Optris PI 400 IR thermometer. (Optris, 2016)

Thermal image recording in real time is up to 80 Hz, meaning that the display and recording of thermal images at full optical resolution can be performed at measurement speeds of 80 frames per second. The optical resolution is 382 x 288 pixels. The thermal ranges are -20–100 °C, 0–250 °C and 150–900 °C, with 200–1500 °C being an option. The spectral range of the camera is 7.5–13 μm . The power supply for the camera is 5 VDC powered via a USB 2.0 interface. (Optris, 2016)

6.1.5 Results

Blue-Hawk™

The field tests with Blue-Hawk™ were interrupted since the sensor was too heavy for the UAS to carry for more than 10–20 seconds. However, according to Babichenko (2016), the oil detection capability of Blue-Hawk™ at distances up to 15 m has already been demonstrated by numerous tests in its stationary installations, including operation in some harbours of the Baltic Sea.

Since the sensor was pre-adjusted for a distance of 10–15 metres for the UAS installation, its operation in handheld mode was optically out of focus in the distance of approximately 1.5 metres (Figure 64). Hence all signals were lower than they should be. The sensor measures the integral intensity of fluorescence and the measured oil fluorescence is added to signals from snow/ice/water as in Figure 87. In the hand-held operation this was not possible since only the fluorescence from oil was detected.

The tests confirmed that Blue-Hawk™ can be mounted in a UAS device and during the short flight the sensor transmitted signals correctly to the ground PC. (Babichenko, 2016)

Hyperspectral camera

The data from the hyperspectral camera was analysed by Eija Honkavaara and Tom Rosnell from Dimensium Ltd. The data was measured when the camera was installed both on the UAS on Day 1 and on the helicopter on Day 2.

The analyses from the UAS flight indicated that the important difference between the three basins was the ice concentration, being 30% in the basin A, 50% in basin B and 70% in basin C (Figure 2). From the UAS flight, one frame taken as close as possible from each basin was analysed: frame K00030 from the basin A, K00142 from basin B and K00376 from basin C.

The on-site reflectance calibration was made with the 50% Spectralon reflectance panel to the frame K00008. The coefficients are presented in Figure 70.

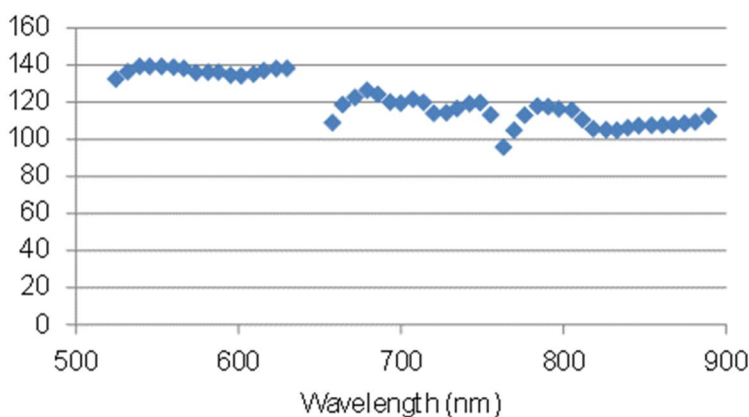


Figure 70. Reflectance calibration. (Honkavaara, 2016)

On the y-axis the coefficients (DN) are presented based on the formula $DN = a \cdot Refl$. The nominal reflectance value of 0.5 was used in the calculation.

According to Puestow *et al* (2013), oil has no specific absorption bands in the VIS and NIR spectral range (400–800 nm). The oil detection on water relies on differences in contrast between the oil and the surrounding oil-free water (Figure 71).

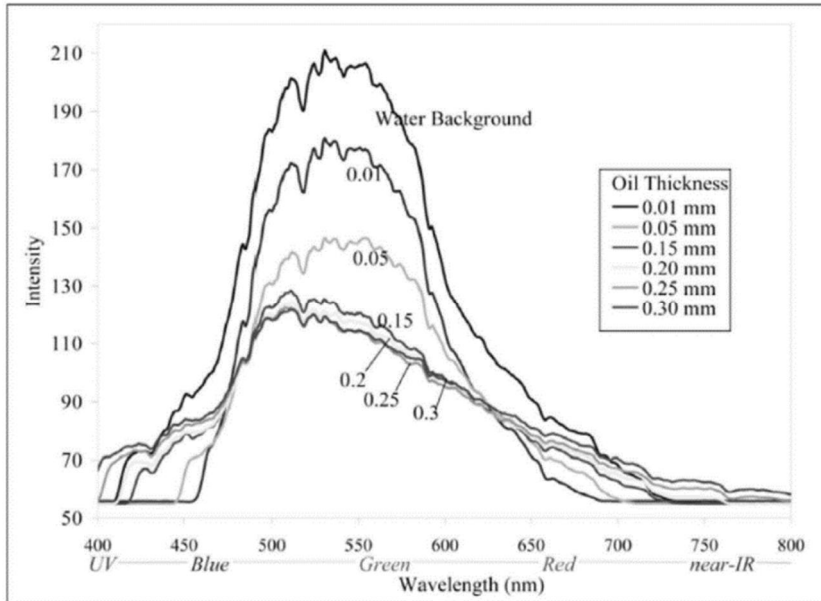


Figure 71. Thickness dependence of the VIS-NIR range reflectance of Alaska North Slope crude oil. (Svejkovsky et al, 2012)

The difference in reflectance between oil and water increases for shorter wavelengths and the contrast may be enhanced by filtering out any response above 450 nm and by using cameras positioned at the Brewster angle of water (i.e. at an incidence angle of 53°) in conjunction with a horizontal polarising filter.

Honkavaara (2016) and Svejkovsky *et al* (2012) noted that prior knowledge of reflectance properties would be useful in detecting the thickness of oil layers. This data could be gathered from specific spectral libraries from the sea area in question. This would require a visit to the area before the utilisation of a hyperspectral camera.

During the UAS flight, around ten spectral samples from water and snow were taken from each basin, totally 60 samples. The reflectance used in the test was calculated in a 3 x 3 pixel window for water and in a 1 x 1 pixel window for snow. In the spectra from the water samples a deviating reflectance value was observed at 650 nm and it was omitted from the further analyses (Figure 72).

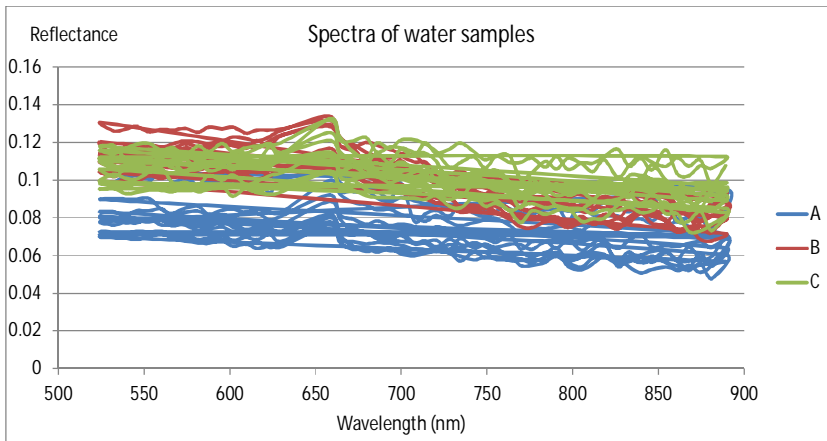


Figure 72. Spectral ranges of the water samples. (Honkavaara, 2016)

The separate (Figure 72) and the average spectral analyses from water (Figure 73) indicated that in the basin B (no oil) the decline in the reflectance values was more sudden when compared to basins A and C. This was an expected result, but less notable than the difference presented in Svejkský *et al* (2012) in Figure 71.

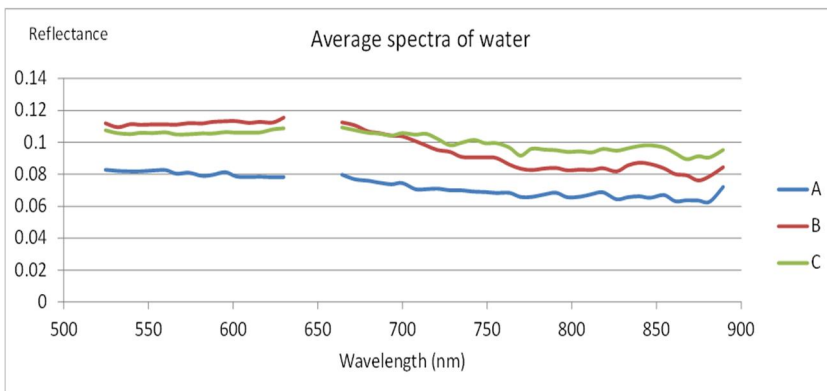


Figure 73. Average spectral ranges of water. (Honkavaara, 2016)

Regarding the spectral ranges from snow (Figure 74), the reflectance from the basin A was higher compared to basins B and C. Additionally, the decline in reflectance values was more intense in basins A and B. (Honkavaara, 2016)

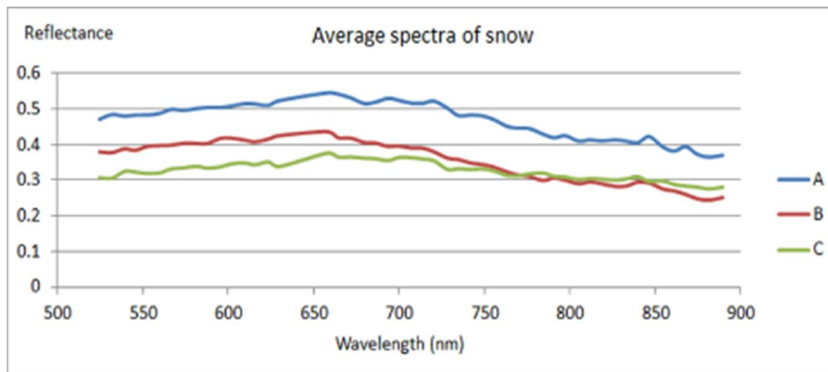


Figure 74. Average spectral ranges of snow. (Honkavaara, 2016)

Thus, the presence of oil can be noticed in the reflectance values: in oil-free surfaces the decline is more evident. The different ice concentrations in the basins may have influenced the result.

The hyperspectral camera was also demonstrated with the helicopter during Day 2, when all the three basins were covered with snow and slush. In cases where the oil is covered by snow or slush, the camera cannot detect the oil. However, if the oil shimmers through the snow or slush, the camera may detect the oil (Honkavaara, personal communication, 2016). According to Puestow *et al* (2013), hyperspectral cameras cannot detect oil under snow or ice or in low visibility conditions (Table 6).

The steps in the data processing and analysis of the helicopter flight were as follows:

- 1) Image calibration based on laboratory calibration information,
- 2) Image georeferencing,
- 3) Image calibration to reflectance,
- 4) Mosaic calculation and
- 5) Spectral data analysis.

Senop Ltd provided calibrated hyper cubes (step 1) and Dimension Ltd took care of the steps 2–5, which are described in the following paragraphs.

Georeferencing

The georeferencing process included the image orientation and object surface model generation. The processing was carried out using the Agisoft Imagescan Professional Imagegrammetric software. The helicopter flight had been carried out from a very low flight altitude with a relatively high speed, and thus there were significant misalignments between individual bands. Processing was performed separately for each basin by including all the bands in the single processing. This processing thus provided exterior orientations for all bands, and separate band matching was not necessary. The reprojection errors were 0.6–0.8 pixels, which indicated good accuracy of georeferencing.

Image calibration to reflectance

From the helicopter flight, the data sets of each basin were processed separately. The following hypercubes were used:

- Basin A: cubes K00412, K00414;
- Basin B: cubes K00450, K00452 and
- Basin C: cube K00490.

Examples of individual band images of each basin A, B and C are shown in Figure 75.

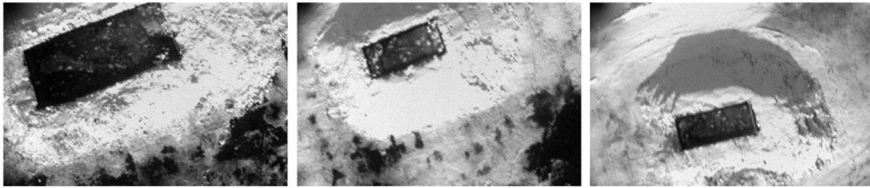


Figure 75. Individual band images of basins A, B and C from the helicopter flight. (Honkavaara and Rosnell, 2016)

The transformation from the image digital numbers (DN) to the reflectance (Refl) was performed using a scaling factor, a . $Refl = a DN$. The scaling factor was calculated by using the white Spectralon reference panel having a reflectance of 0.5.

The white-reference data was captured from the ground altitude before the helicopter flight. The Spectralon image and the a -factors are shown in Figure 76.

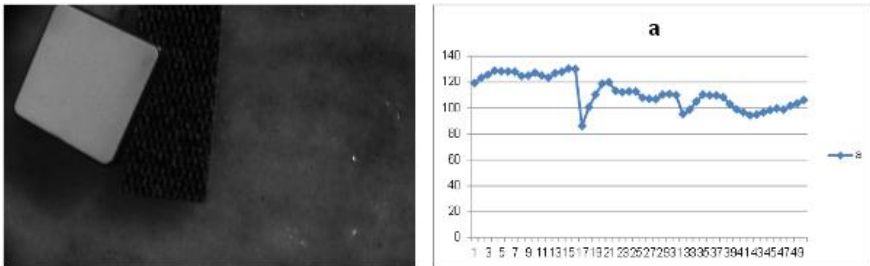


Figure 76. The white Spectralon reflectance reference (nominal reflectance 0.5) (left), and the normalization factors to transform DN to reflectance (right). (Honkavaara and Rosnell, 2016)

Mosaic calculation

The reflectance mosaics were calculated utilizing the image orientation data, the digital surface models and the reflectance transformation factors. The GSD of the mosaics was approximately 3 cm for the basins B and C and 6 cm for basin A.

Quality of the mosaics was good. The final mosaics and magnified 3-band zooms are shown in Figure 77.

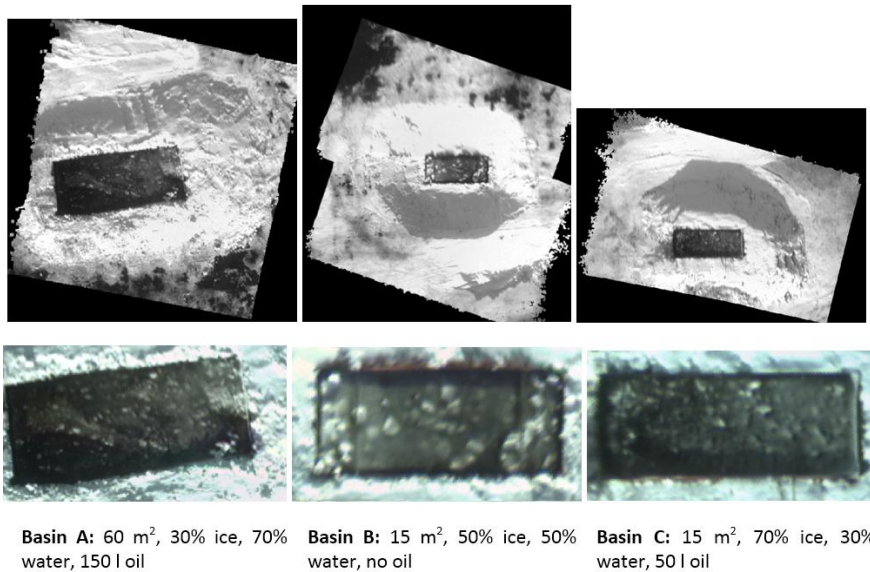


Figure 77. Top row: full image mosaics for single bands. Bottom row: RGB (approximately) band combination of each basin. (Honkavaara and Rosnell, 2016)

Spectral data analysis

Spectra were sampled from each basin. Different object areas were visually identified from each basin and 10 spectra were taken from each object area (a total of 80 spectra). The object areas were classified as (Figure 78):

- 1) Snow in the water: the snow and ice blocks that appeared to be above the water level.
- 2) Snowy water: the areas where snow appeared to be below or mixed with the water.
- 3) Dark water, no snow: Based on visual assessment, dark areas in the basins were identified where the snow was not visible. This could also be the shadow of the side of the basin. These areas were found only in the basins A and C.

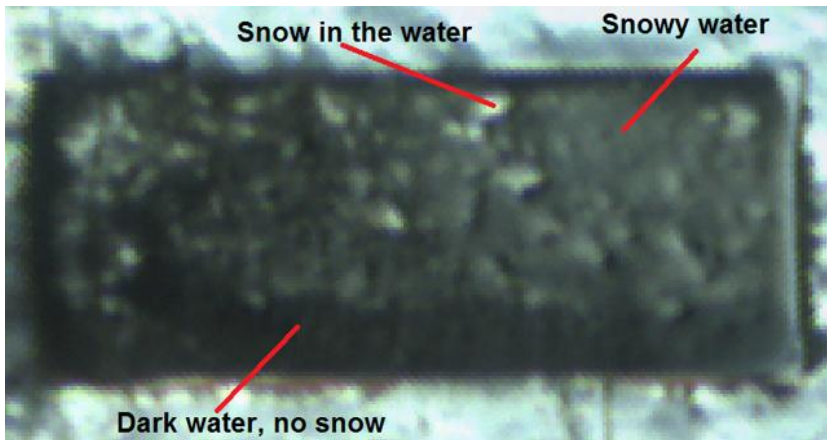


Figure 78. Different object areas in basin C: snow in the water, snowy water, dark water, no snow. (Honkavaara and Rosnell, 2016)

The spectral data sampled from the image mosaics are shown in Figure 79 and the averaged spectra are shown in Figure 80. The first observation is that the reflectance values were higher than expected. A possible reason for this could be that the illumination conditions during the white reference measurement and the data capture were different. The data set did not enable analysis of illumination conditions; irradiance measurements during the data capture are necessary in order to be able to manage the illumination changes. Another potential reason for the high reflectance values of the water is that there was some new snow in the basins; the helicopter flights were performed on Day 2, when the test basins were covered with snow. However, it appears that the illumination was stable during the helicopter data capture over different basins, and thus the data values from different basins are comparable and relative analysis is feasible.

The averaged spectra indicated that basin C had brighter values for the snowy water and dark water than basin A; this could be due to the fact that there was more snow in basin C (70%) than in basin A (30%) (Figure 80). The snowy water was the brightest in basin B (without oil) and the snow reflectance values were at the same level as in basin A. The drop of the reflectance was the strongest in basin B without oil.

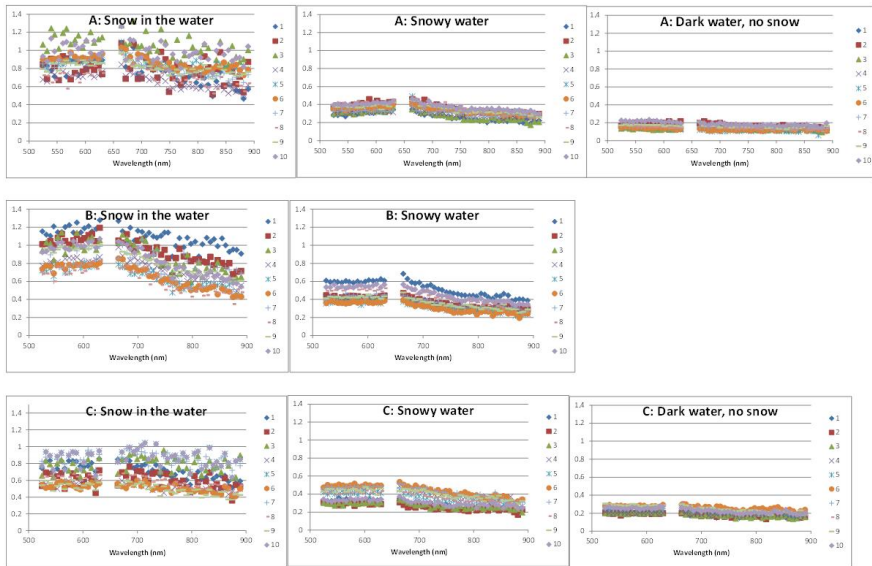


Figure 79. Individual spectra for each object and basin. From the top: basins A, B and C from the left: snow in the water, snowy water and dark water, no snow. (Honkavaara and Rosnell, 2016)

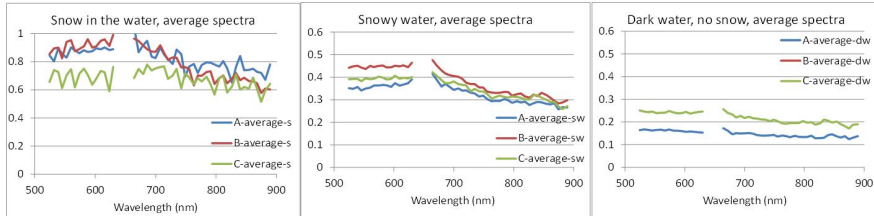


Figure 80. Average spectra, from the left: snow in the water, snowy water and dark water, no snow. (Honkavaara and Rosnell, 2016)

The expected behaviour is that water with no oil would be brighter in the visible spectral range, and both clean and oily water should be equally dark in the NIR wavelengths. This will cause a greater relative drop of the spectra for the clean water. This was evaluated by calculating indices based on yellow and NIR range spectral values:

$$\text{Index}_{Y_NIR} = R_Y/R_{NIR}, \text{ where:}$$

- R_Y is yellow (550–600 nm) and
- R_{NIR} is NIR (750–800 nm) spectral range reflectance calculated from the average reflectance.

For comparison, the corresponding indices for the drone data captured one day earlier are given. The indices were consistently the highest for the basin B that did not have any oil (Figure 81). The drone and helicopter-based indices were consistent particularly in the basins A and B. (Honkavaara and Rosnell, 2016)

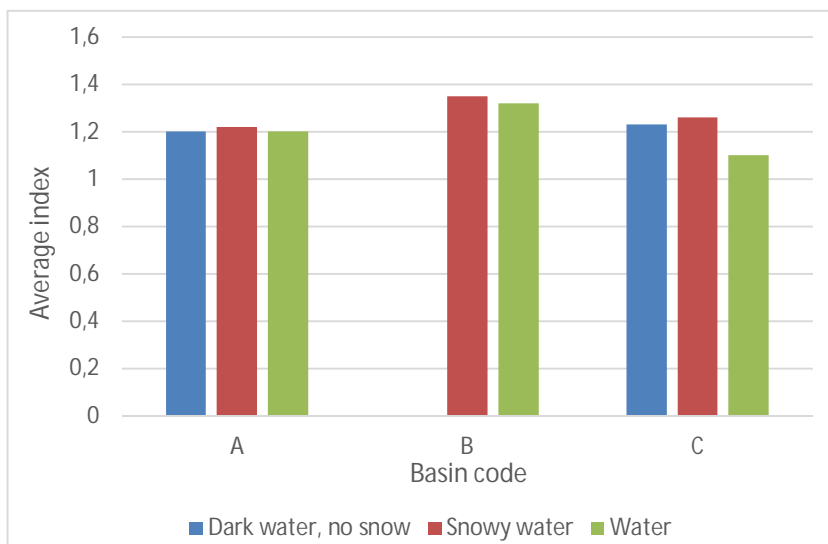


Figure 81. Average indices calculated from the drone data for snowy water objects in basins A, B and C. (Honkavaara and Rosnell, 2016)

Although the data collected by the hyperspectral camera requires expertise and time to be analysed, it is expected that during the next 5 to 10 years the progress in computer vision and software development will offer possibilities for online analyses. Further processing of the data would offer 3D images of the test basins. 3D images have been utilised e.g. in forest inventories. NLS develops the hyperspectral cameras and the imaging tools in cooperation with Senop Ltd. (Honkavaara, personal communication, 2016)

Optris IR thermometer

Optris identified the oil in basin A during day-time conditions on Day 1 (Figure 82). The temperature difference between oil on water and ice was approximately 4 °C, and between oil on ice and ice was approximately 2 °C (Table 13). In the Optris image the temperature can be checked by moving the cursor to the desired location in the image. The highest temperature of the selected area is shown in the right upper corner of the picture. When compared to Figure 53 it seems that the thickest oil layer was detected.

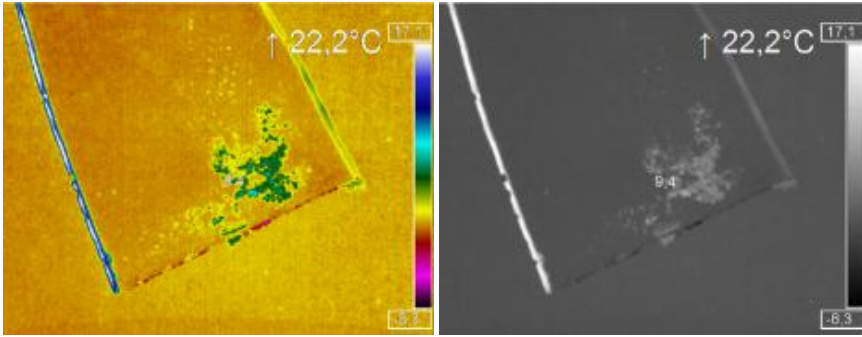


Figure 82. Optris IR thermometer image from the basin A illustrated with two different colour palettes. The warmest surface temperature of the oil was 94 °C, whereas the warmest place in the picture was 22.2 °C in the frame of the basin. T_{air} was approximately -1 °C.

Interestingly, Optris detected hardly any oil in the other parts of basin A (Figure 83 and Figure 84).

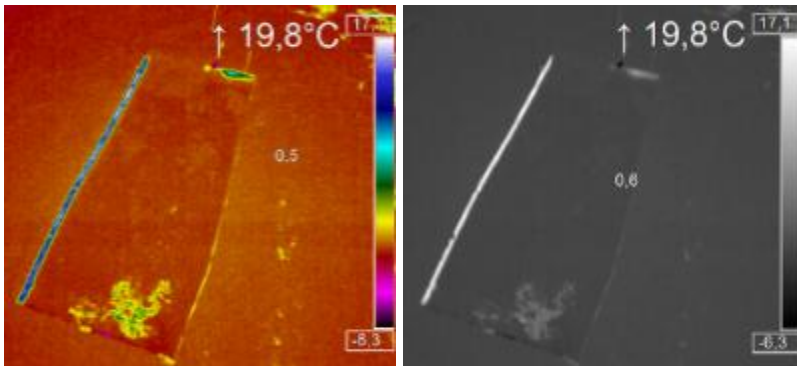


Figure 83. Optris IR thermometer image with two different colour palettes from the basin A.



Figure 84. Basin A in TIR images and an optical picture. Only the thickest layer of oil was detected by Optris.

In the basin B, apparently no oil was detected by Optris but the temperature difference between water and ice was observed (Figure 85).

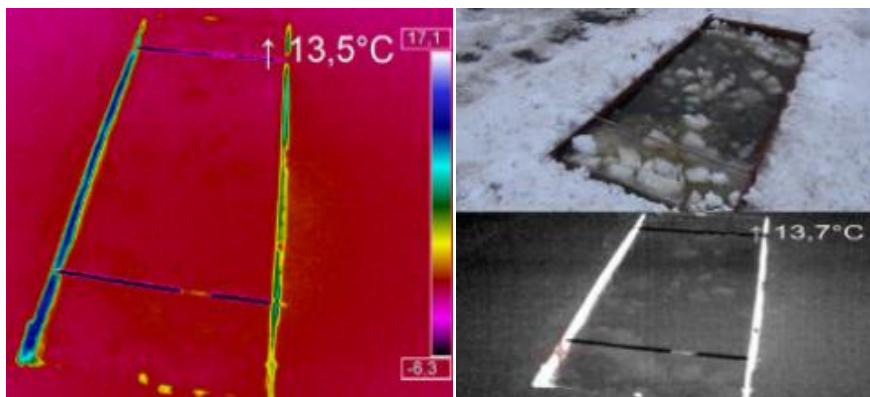


Figure 85. Optris IR thermometer image from the basin B where no oil was present. The temperature difference between ice and water can be detected as dark and light areas.

Optris did not detect any oil in basin C, although there was oil. Furthermore, Optris did not distinguish any difference between the basin and the packed snow surrounding the basin (Figure 86). This was confusing, since there was plenty of oil present in the basin and the difference between packed snow and oil/ice in the basin was visually apparent.

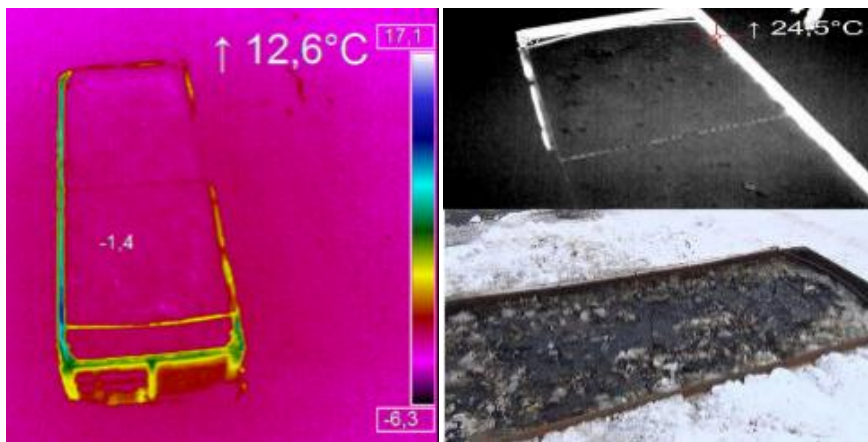


Figure 86. Optris image from the basin C. No oil was detected from the target area.

This observation could be the result of several factors. The time used for the imaging of one basin (average of one minute) might have been too short for oil detection in basin C and also in basin A, since only the thickest layer of oil was detected in basin A. Furthermore, the angle of the IR camera toward the basins might not have been optimum for oil detection in the prevailing conditions. A better result might have been achieved by imaging the basins for a longer time directly above the basins instead of from a tilted angle. Ideally, different imaging angles might have been tested in order to determine the best possible angle. The target areas should also have been larger.

Imaging in sunlight is not the best option, since the bright light hinders the utilisation of different contrast settings of the image analysis software. The best time for IR imaging is the evening, when the temperature differences between the substances have not been normalised.

An experienced Optris IR thermometer operator can adjust the palettes and temperature ranges in the Optris IP Connect software in order to find the best combination of settings for the prevailing conditions. Optris must be switched on for 10–15 minutes before the actual imaging of the target area, in order to allow the temperature of the camera to normalise. (Keränen and Mikkola, personal communication, 2016)

Optris was not tested during Day 2, when the basins were covered with snow. Puestow *et al* (2013) concluded that TIR sensors cannot detect oil which is under ice or snow or encapsulated.

OWL™

The HLIF spectra measured by OWL™ contained spectral patterns of oil and CDOM in water. Water, ice and snow manifested themselves by the characteristic signal of inelastic (Raman) light scattering on water molecules (Figure 87).

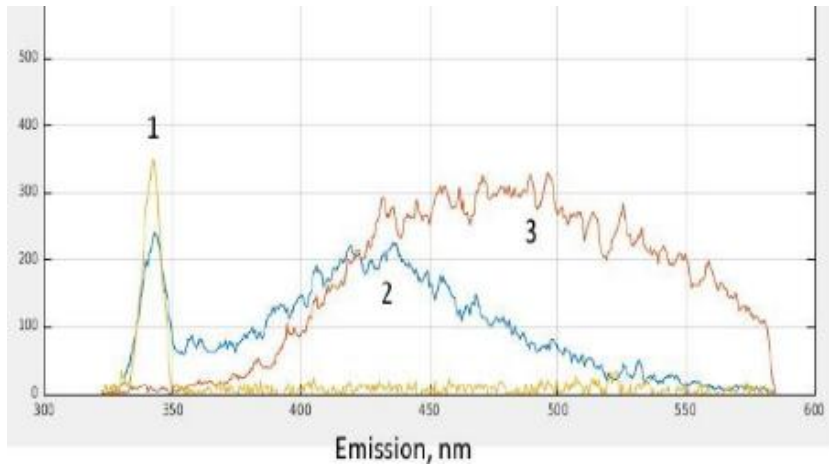


Figure 87. Examples of HLIF spectrum measured during the flight: yellow (1) – spectrum of Raman scattering of laser emission on ice and snow; blue (2) – spectrum containing Raman scattering (1) and CDOM (2) of seawater; brown (3) – Fluorescence of oil (3) mixed with water, ice and snow. (Babichenko, 2016)

At the slowest flight speed of 24 km/h and PPR equal to 10 pulses per second, the HLIF LiDAR provided spatial resolution of 0.6 m, thus making approximately 60 measurements along the study area. At higher speed the number of measured HLIF spectra of the targets decreased. The readings during the flights are presented in Figure 88.

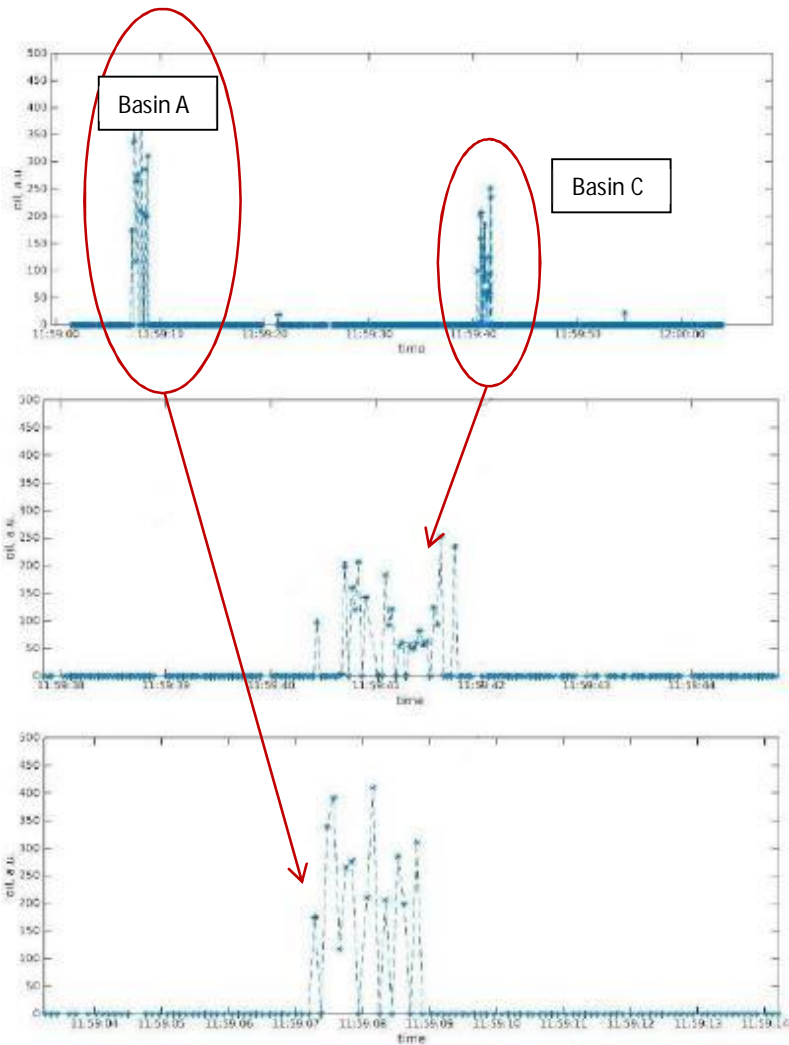


Figure 88. Oil readings during the flight in the daytime. (Babichenko, 2016)

The results indicate that the first set of non-zero readings corresponds to the first crossing of the oil target at 11:59:07. Another overflight at 11:59:41 also corresponded to the oil target. The difference in the oil fluorescence intensity in detector counts on the y-axis can be explained by the fact that the laser beam did not hit exactly the same spot during the two overflights.

The time readings in the x-axis differ from the readings presented in Table 14 due to different time settings in the sensor and the wrist watch.

Since OWL™ operates with invisible UV sensing light, it is equipped with an additional green pointing laser for dark condition operations. This pointing laser helps the pilot to hit the target area more precisely (Figure 89).



Figure 89. The view of the oil basin from the helicopter cabin in the dark conditions. (Babichenko, 2016)

The two peaks in Figure 90 correspond to the oil readings from basins A and C, while basin B did not generate any readings as there was no oil in that basin.

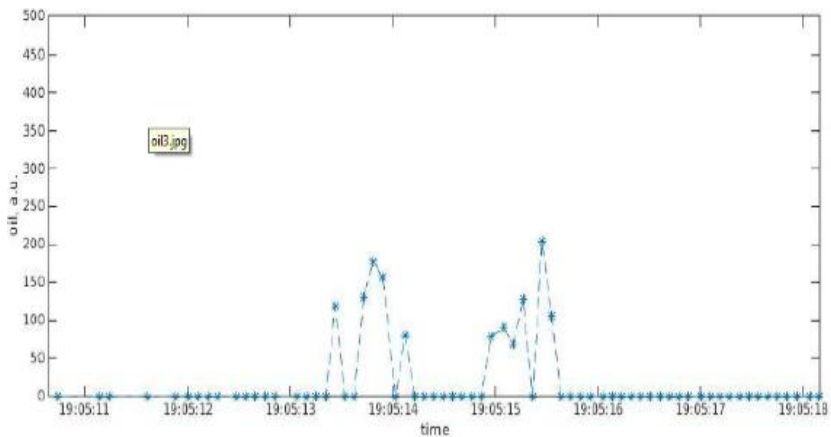


Figure 90. The oil readings during the flight in dark conditions (Babichenko, 2016).

The test trials on board the helicopter served mainly to demonstrate the sensing capability of the HLIF technology in flight. (Babichenko, 2016)

Puestow *et al* (2013) concluded that LiDAR is sensitive to waves and it may work in ice-covered waters. The backscattered signal of clean water is “flat” and the signal of diesel oil is clearly notable in wind speed of 0.28–1.39 m/s (Figure 22). During the Kalajoki trials the effect of wind and waves could not be verified due to the small size of the target areas.

6.1.6 Conclusions

The field trials in the port of Kalajoki were arranged in order to obtain valuable hands-on experience of the applicability of the selected sensors and platforms for oil detection operations in arctic conditions.

Regarding the platforms, moderate wind conditions were favourable for Videodrone X8 UAS and the flying operations could be performed as planned. The wind limit for the UAS is around 10 m/s; stronger wind speeds cause exceeding of the rectification limits of the gimbal, leading to poor image quality. The maximum payload is around 3.5 kg, since 3.8 kg was too heavy for a longer (>20 sec) period of flying time. The operator must have direct unaided eye contact to the UAS. Attention must be paid to charging of the batteries in order to avoid additional interruptions during the monitoring sessions.

A heavyweight UAS would enable higher payload, longer operational time and also beyond visual line-of-sight (BVLOS) operations. This option should be discussed with the other stakeholders with intentions to invest in and operate UAS in BVLOS mode, in order to ensure cost effective and multipurpose investment.

The helicopter had some challenges to hit the targets in the rather small basins, especially when flying at higher altitudes. In a real situation this would obviously not be a problem since the target area, i.e. where the oil has been spilled, is much larger. A heavier helicopter would enable more space for sensors and sensor operators, but the downside is the higher operational costs. According to Hannu Koponen (personal communication, 2016), a Robinson R44 would be one option for a heavier helicopter while keeping the operational costs reasonable. On the other hand, Schweizer 300 offers 4-hour operational time with sensor and operator load and it is agile when operating in a small area like in the port of Kalajoki.

In cases when the operational area is more than 300 m from the shoreline, the helicopter must be equipped with floats. This installation limits the use of the sensors due to the visual block caused by the floats on both sides of the helicopter.

The Blue-Hawk™ sensor was too heavy for the UAS and the trial was stopped, but the sensor can be installed on a suitable UAS. The previous experiments conducted by LDI Innovation OÜ with stationary installations have indicated that the sensor is able to detect oil at a distance of up to 15 m.

The helicopter and UAS-based low altitude data capture provided hyperspectral image data in the visible to NIR spectral ranges with a 2 cm GSD. The very high spatial resolution datasets provided the possibility to identify different areas in the water in very high detail, such as ice blocks above the water, plain water etc. In practical applications, by selecting appropriate flight altitude the feasible resolution can be selected. With higher flight altitudes and lower spatial resolution, better efficiency can be obtained for the data capture. The higher spatial resolution datasets provide very good object classification and reduce the spectral mixing. (Honkavaara and Rosnell, 2016)

The results showed differences in spectral data collected in basins with different characteristics. Detailed analysis of the spectral properties was difficult because appropriate reference data of different object areas were not available (e.g. plain

water, snow, oil). The indices that eliminated the impacts of differences caused by the environment and processing from the data showed consistent results. When comparing the indices, the helicopter data capture showed good agreement of the spectral data in the different basins. (Honkavaara and Rosnell, 2016)

There were some uncertainties in the data analysis of the hyperspectral camera. Especially, interpretation of data sets that had variable amounts of both snow and oil was uncertain; it was not possible to separate impacts of all variables in the data sets. More comprehensive reference data would help to make more reliable conclusions. A fundamental approach would be to carry out laboratory measurement of plain oil and different mixtures of oil and water, as well as snow. In outdoor conditions, the gradual increasing of amount of oil in the basins with different proportions of ice, and repeated measurements at each stage would enable controlled analysis of the impact of oil on spectral properties of the mixed ice and water. (Honkavaara and Rosnell, 2016)

Furthermore, controlled remote sensing data capture is needed for making reliable analyses. It is important to eliminate impacts of all external factors from the analysis in order to obtain full advantage of the spectral data. In particular, calibrated and stable sensors and monitoring of the illumination conditions is necessary in order to obtain comparable spectral data from different times. Future UAS-based data capture systems will provide this possibility. (Honkavaara and Rosnell, 2016)

Although the data collected by the hyperspectral camera requires expertise and time to be analysed, it is expected that during the next 5 to 10 years the progress in computer vision and software development will offer possibilities for online analyses. Further processing of the data would offer 3D images of the test basins. 3D images have been utilised e.g. in forest inventories. NLS develops the hyperspectral cameras and the imaging tools in cooperation with Senop Ltd. (Honkavaara, personal communication, 2016)

OWL™ HLIF LiDAR detected the oil in both basins and confirmed that the technology is suitable for a helicopter platform. When operating in dark conditions, a UV target light is needed in assisting the pilot and operator to hit the target area.

The Optris IR thermometer identified the thickest oil layer in basin A but did not detect oil in basin C. An average time of one minute above the target area might not be sufficient for the image collection, and the imaging should have been made from directly above the basins. Optris was not tested in the conditions in which the basins were covered with snow. It was assumed that the oiled areas were too small for the proper testing of IR sensor technology, as was also the case with the hyperspectral camera.

According to Partington (2014), TIR sensors are useful for detection of oil during day and night and for classifying oil thickness >10 µm. The ability of thermal sensors to detect oil depends on its thickness, type, degree of emulsification and time of day, and detection will not be effective during rough weather.

6.2 Chemical detection field trials and demonstrations in Kuopio (2016)

6.2.1 Description and objectives

The objective of the trials was to acquire hands-on experience with different sensors in chemical detection under arctic conditions. The field test trials were performed at the test area of the Emergency Services College (ESC) in Kuopio (FI) between 31 October and 2 November 2016. The preparations for the field tests were made in the afternoon of 31 October, the actual test flights were conducted on 1 November, and the demonstrations were carried out on 2 November.

The trials were conducted in cooperation between SYKE, ESC and VTT. The sensors were provided by Aeromon Ltd, Environics Ltd and the Finnish Institute of Occupational Health (FIOH). The drones used as the mounting platform for the sensors were provided by Air Intelligence Finland Ltd (AIF).

Regarding the weather condition during the trials, the sky was partly cloudy and temperature was around zero (+1 – -1 °C) during the test days. The wind speed varied between 0 m/s and 3 m/s. No rainfall, sleet or snow occurred during the exercise hours. The experiments were video recorded and/or photographed by VTT, AIF, FIOH or sensor providers.

6.2.2 Platforms

Two drones were used during the exercise, i.e. Videodrone X8 and Airborne KX8 (Figure 91).



Figure 91. Videodrone X8 (left) with video and FLIR cameras mounted, and Airborne KX8 (right) with a weight of 3.5 kg to imitate a sensor payload. (Images: VTT/Jukka Sassi)

The operational time for the drone depends on payload and battery capacity. The maximum payload for Videodrone X8 is 3.5 kg with an operational time of approximately 10–15 minutes with the 10 Ah battery (Figure 92).

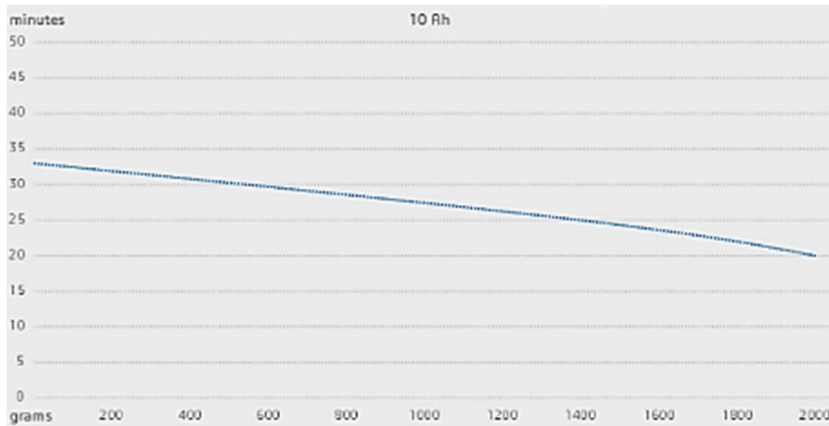


Figure 92. Operational times (Y-axis) of X8 with different payloads (X-axis). (Videodrone, 2016)

The Videodrone X8 has the following dimensions:

- Frame: width 58 cm, length 58 cm and height 37 cm and
- Weight 2.5 kg without the batteries.

The wind limit for Videodrone X8 is around 10 m/s; stronger wind speeds cause exceeding of the rectification limits of the gimbal, resulting in poor image quality. The type of the video camera used in the test trials was a Sony Handycam CX410, and the FLIR camera was an Optris PI 400 (see section 6.1.4). The Sony Handycam CX410 camera offers HD video resolution and it weighs 325 g. The full specifications can be downloaded from Sony (2017).

The Airborne KX8 drone has the following mechanical specifications (Airborne Mechatronics, 2016):

- Weight w/o batteries and payload: 5.7 kg;
- Frame dimensions: Width 66 cm, length 66 cm and height 22 cm;
- Diagonal size 80 cm and
- Main construction materials: Carbon fibre, aluminium, fiberglass.

The maximum payload for KX8 is 7 kg with a flight time of 8–14 minutes. It holds two batteries with 10 000 mAh capacity.

Most of the tests were performed with Videodrone X8; Airborne KX8 was demonstrated with the magnetometer from Radaai Ltd. Both drones were operated by pilots from AIF.

The maximum distance between the operator and the drone was approximately 40 m during the demonstration phase on 2 November 2016, when Airborne KX8 performed a pre-programmed test flight (grid) above the test site.

The regulation OPS M1-32 by Trafi defines that the maximum take-off load for a UAV is 25 kg and the maximum permitted flying altitude is 150 m. (Trafi, 2015)

According to ICAO during VLOS (visual line-of-sight) operations, the remote pilot or remotely piloted aircraft (RPA) observer must maintain direct unaided visual contact with the remotely piloted aircraft. (ICAO, 2015)

6.2.3 Target chemicals

The following chemicals were used as the target chemicals when the various sensor types were demonstrated:

- hydrochloric acid, HCl, (CAS no 7647-01-0);
- ammonia, NH₃, as 25% solution (CAS no 7664-41-7);
- o-xylene, synonym 1,2-dimethylbenzene, C₆H₄(CH₃)₂ (CAS no 95-47-6);
- m-xylene, synonym 1,3-Dimethylbenzene, C₆H₄(CH₃)₂ (CAS no 108-38-3);
- toluene, C₆H₅CH₃ (CAS no 108-88-3);
- benzene, C₆H₆ (CAS no 71-43-2);
- chloroform, CHCl₃ (CAS no 67-66-3);
- 1,1,2,2 tetrachloroethane, CHCl₂CHCl₂ (CAS no 79-34-5) and
- Acetone, CH₃COCH₃ (CAS no 67-64-1).

HCl and 25% ammonia were provided by ESC, and they were stored in 30 l canisters (Figure 93).



Figure 93. Two canisters of HCl acid and ammonia with the appropriate warning labels. (Image: VTT/Jukka Sassi)

The other chemicals were provided by SYKE, and they were stored in 500 ml Schott glass bottles (Figure 94).



Figure 94. The chemicals from SYKE were stored in glass bottles. (Image: VTT/Jukka Sassi)

6.2.4 Sensors

During the test trials, the following sensor types were demonstrated: BH-8 sensor module by Aeromon Ltd, Dräger detector tubes with Gilian LFS-113DC low flow sampler, ChemPro100i chemical detector by Environics Ltd, and SKC-226-01 sorbent tube together with 3M Organic Vapor Diffusion Monitor.

BH-8 by Aeromon Ltd

The Aeromon™ Emission Monitoring System consists of an RPAS-mounted BH-8 sensor module with an active sampling system, a data handling and communications computer and a web-based analysis platform, Aeromon Cloud Service. All the results are presented and visualized in real time.

Aeromon BH-8 is a light and modular gas sensor module designed for RPAS use (Figure 95).



Figure 95. Aeromon BH-8 module with its lid open (left) and mounted on a drone (right). (Aeromon, 2016)

The standard module can be equipped with 8 different gas sensors and the number of different target gases is currently 70. Gas samples are drawn into the measurement system with an active sampling system enabling continuous sampling during flight operations and non-continuous sampling for more detailed analyses. The BH-8 module is equipped with a GPS antenna to exactly position each sampling

point, enabling the gathering of high quality georeferenced data for a variety of emission measurements. The technical properties of the BH-8 module are presented in Table 20. (Aeromon, 2016)

Table 20. Technical properties of the BH-8 module. (Aeromon, 2016)

Properties	Value
Size	168 x 168 x 107 mm
Weight	850 g (fully equipped)
Gas sensor ports	8 pcs
Datalink	Satellite (Iridium)/Radio LOS/GSM modem
Sampling frequency	Adjustable, typically 0.5–5 Hz
Data storage	Aeromon Cloud Service database
GPS	Internal, 10 Hz update
Sample intake	Adjustable dynamic flow or sample capture
Sample filter	Quartz wool membrane
Mechanical interface	Customized for each platform
Environmental conditions	Between -20 – +50 °C, 15–85% RH, 80–120 kPa

Dräger indicator tubes by FIOH

Dräger indicator tubes are glass vials filled with a chemical reagent that reacts with a specific chemical or family of chemicals. A calibrated 100 ml sample of air is drawn through the tube. If the targeted chemical(s) is present, the reagent in the tube changes colour and the length of the colour change typically indicates the measured concentration (Dräger, 2016). An example of NH₃ tubes used in the Kuopio experiments is shown in Figure 96.



Figure 96. Two Dräger indicator tubes for NH₃, used (above) and unused (below). (Image: VTT/Jukka Sassi)

According to Dräger, over 500 gases or gas compounds can be measured with the tubes.

ChemPro100i by Environics Ltd

ChemPro100i uses an array of detection technologies to detect, classify and measure chemicals, enabling simultaneous detection of a wide range of chemicals (Figure 97).



Figure 97. ChemPro 100i handheld detector. (Environics, 2016)

ChemPro100i is an orthogonal detector, its heart remaining the Environics' unique open-loop Ion Mobility Spectrometry (IMS) sensor. The performance is improved with additional sensors that provide a wider range of detectable Toxic Industrial Chemicals (TICs) and improve false alarm rejection. (Environics, 2016)

SKC-226-01 sorbent tube and 3M Organic Vapor Diffusion Monitor 3520 by FIOH

Sorbent tubes are efficient and versatile tools for collecting gaseous samples of volatile organic compounds (VOCs). SKC-226-01 sorbent tube is a glass tube of 6 x 70 mm in size and contains coconut charcoal.

3M™ 3520 Diffusion Monitor is a passive sampling device designed to measure average concentrations of certain contaminants over a measured time interval. It can be used for either personal or areal monitoring. As a personal monitor, it is worn near the breathing zone of individuals exposed to potentially hazardous environments. The monitor contains two charcoal adsorbent pads for increased capacity. It is designed to be analysed by the user or by an independent laboratory. (3M, 2016)

Other detection methods

The reference (Widdowson, 2012) lists several methods, which can be used when determining chemical levels in containers. These include photo-ionisation detectors (PIDs), gas detection tubes, selective-ion flow-tube mass spectrometry (SIFT-MS) and thermal desorption-gas chromatography-mass spectrometry (TD-GC-MS).

PIDs are hand-held devices that provide quick response for a limited number of chemicals, including methyl bromide and phosphine. However, they cannot detect e.g. chloropicrin, sulfuryl fluoride or 1,2-dichloroethane, and they are non-selective for hydrocarbons. Thus, they need to be used together with other methods.

Gas detection tubes are glass tubes filled with a material that changes colour upon exposure to a particular chemical. The extent of the colour change provides an approximate measure of the concentration of the chemical, which varies depending on environmental conditions. Tubes are available for a range of the most commonly encountered chemicals.

SIFT-MS is emerging as the method of choice for rapid detection of fumigants from containers, as it is fast and provides a reasonably accurate indication of the amount of chemicals involved. Individual chemicals generally give distinctive “signatures”, and so comparison with a database allows identification. Detection limits are well below those specified for human health. The equipment is relative bulky, but can be housed in a mobile laboratory.

TD-GC-MS is well established and popular amongst analysts for detection of gases and vapours in a wide variety of situations. The air is collected in a gas sampling bag, canister or sorbent tube, and then sent to a laboratory for analysis. Detection limits, as for SIFT-MS, are well below those prescribed, and massive libraries of data are available, allowing identification and qualification of almost any chemical, although phosphine is difficult and requires a modification of the analytical method. This makes the method well suited for the comprehensive analysis of materials. The widespread use of TD-GC-MS by analysts also makes it ideal for offsite confirmation of measurements, routine calibration of other methods, and research-level investigations, such as those into the efficacy of container ventilation before opening.

The author in the reference (Widdowson, 2012) concluded that in many cases one or more methods need to be applied in order to be able to detect chemicals.

Experiments

Between 31 October and 1 November 2016, several different sensors and target chemicals were demonstrated. A summary of the performed demonstrations is presented in Table 21.

Table 21. Summary of the performed demonstrations.

Sensor provider	Sensor	Target chemical
Aeromon Ltd.	BH-8 module	NH ₃ , VOCs
FIOH	Dräger indicator tubes with Gilian LFS-113 flow sampler	NH ₃ , HCl
EnviroNics Ltd.	ChemPro 100i	NH ₃
FIOH	SKC-226-01 sorbent tube with passive 3M Organic Vapour Diffusion Monitor	Xylenes, toluene, benzene, chloroform, tetrachloroethane and acetone

Before the actual sensor testing, Videodrone X8 was tested with an indicator smoke to demonstrate the turbulence effect caused by the drone (Figure 98).



Figure 98. Videodrone X8 with the indicator smoke. (Image: VTT/Jukka Sassi)

Aeromon BH-8 module

The BH-8 module was equipped with an NH₃ sensor and a sensor panel of four different VOC sensors together with humidity (RH %), temperature (T) and pressure (p) sensors. The operational principles of the sensors are presented in Table 22.

Table 22. Sensor operational principles. (Aeromon, 2016)

Sensor	Operational principle
NH ₃	Electrochemical (EC) resolution enhanced
VOCs	Metal-oxide semiconductor (SC)
RH%, T, p	Piezo resistive micro electro mechanical structure

The module was mounted in Videodrone X8. The module was equipped with a 10 m long polyurethane tube in order to avoid the turbulence effect caused by the drone in the gas sampling point (Figure 99).



Figure 99. 10 m long polyurethane tube with a filter unit (right) attached to the sample intake. (Images: Aeromon, 2016)

Before the measurements, the sensor module was calibrated with certified test gases. An example of this procedure is shown in Figure 100.

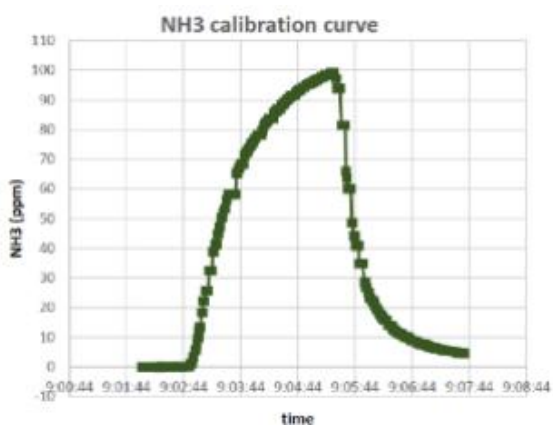


Figure 100. Signal for NH3 sensor with 100 ppm test gas. (Aeromon, 2016)

Aeromon's standard procedure includes the calibration of different sensors in the same ambient temperature, humidity and pressure where the actual measurement is conducted, in order to maximise the accuracy of the results. The zero level (clean air) together with the calibration gas concentrations define the scaling factors from raw signal to concentration for each sensor.

During the first flight, NH_3 was the target substance. In the beginning of the flight, the NH_3 canister was opened and the drone was piloted in a way that the sample intake was located in the proximity ($< 1\text{m}$) of the opened canister (green arrows in Figure 101 and Figure 102). The NH_3 level was increased to approximately 0.7 ppm.

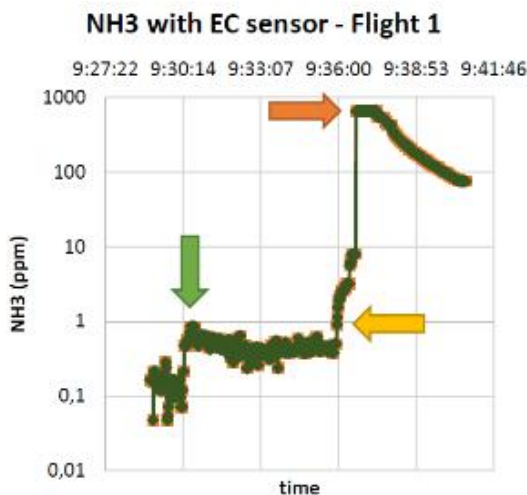


Figure 101. NH_3 concentration from the EC sensor. First, the NH_3 canister was opened (green arrow), then a small amount of NH_3 was spilled on the ground (yellow arrow), where after the sensor signal was saturated (orange arrow). (Aeromon, 2016)

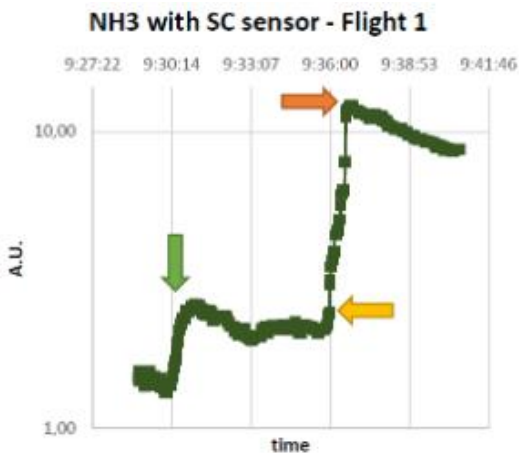


Figure 102. Signal in arbitrary units (A.U.) from the NH_3 sensitive SC sensor. First, the NH_3 canister was opened (green arrow), then a small amount of NH_3 was spilled on the ground (yellow arrow), where after the signal reached its maximum level (orange arrow). (Aeromon, 2016)

Next, NH_3 was spilled on the ground on purpose, which is marked with a yellow arrow in Figure 101 and Figure 102. Soon after the NH_3 was spilled, the EC sensor was saturated at 800 ppm (orange arrow in Figure 101). However, the SC sensor was not saturated, which can be observed from Figure 102 (orange arrow). This difference stems from the different operating principle between these sensors and the chosen measurement range for the EC sensor (optimized for low concentrations).

During the second flight, six different VOCs were used as target substances. The target substances were (in temporal order):

- 1) Chloroform (bottle open);
- 2) Toluene (bottle open in a bucket);
- 3) Xylene (bottle open in a bucket);
- 4) Benzene (bottle open in a bucket);
- 5) Acetone (bottle open in a bucket) and
- 6) Tetrachloroethane (bottle open in a bucket).

After the measurement with the first target compound (chloroform), a zinc bucket was added to increase the target compound concentration in the gas sample intake and to prevent the compounds from spilling if the nose of the sample intake hose touched and overturned the sample bottles (Figure 103).



Figure 103. The chemical bottles placed in the zinc bucket for identification. (Image: VTT/Jukka Sassi)

The drone was piloted in such a way that the sample intake was in the proximity (< 0.5 m) of the open target substance bottles. Between the measurements the drone and sample intake were flown approximately 10 m higher in order to ventilate the BH-8 sample chamber. The results can be seen in Figure 104.

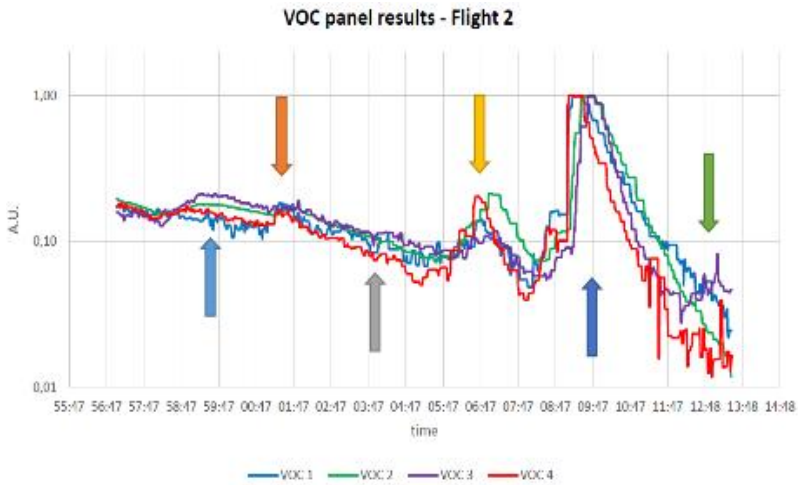


Figure 104. VOC panel response to the six different target VOCs. From left to right, chloroform (blue arrow), toluene (orange), xylene (grey) benzene (yellow), acetone (dark blue) and tetrachloroethane (green). (Aeromon, 2016)

Dräger indicator tubes with Gilian LFS-113DC low flow sampler

Two different experiments were carried out with the Dräger tubes: detection of NH_3 and of hydrochloric acid (HCl). Two Dräger indicator tubes for ammonia (NH_3 5/a CH 20501) were used together with the Gilian LFS-113DC low flow sampler (Figure 105).



Figure 105. Two Gilian LFS-113DC low flow samplers with detection tubes for ammonium, mounted in the Videodrone X8. (Image: VTT/Jukka Sassi)

Videodrone X8 was used as the platform, and it was directed towards an ammonium cloud near the building in the test site. (Figure 106).



Figure 106. The drone flying towards the ammonium cloud. (Extracted from the video by AIF)

One of the indicator tubes was positioned in such a way that the change in concentration could be noticed from the video screen of the drone operator and from the video recording.

In the experiment in which HCl was used as the target acid, the drone was equipped with a Gilian flow sampler and Dräger indicator tubes for HCl. The drone was piloted above a canister with HCl and above a cloth in which HCl was poured just before the experiment (Figure 107).



Figure 107. The drone flying near the cloth with HCl. (Image: VTT/Jukka Sassi)

The sampling was conducted both when the drone had landed on the cloth, and also when it was flying above the target.

ChemPro 100i

ChemPro100i by Environics Ltd was mounted in the Videodrone X8 and tested for NH_3 detection (Figure 108).



Figure 108. Videodrone X8 with ChemPro100i mounted. (Image: VTT/Jukka Sassi)

SKC-226-01 sorbent tube with Gilian LFS-113DC sampling pump and passive 3M Organic Vapor Diffusion Monitor type 3520

The SKC-226-01 sorbent tube was mounted in the Videodrone X8 drone together with a Gilian LFS-113DC sampling pump and a passive 3M Organic Vapor Diffusion Monitor type 3520 (Figure 109).

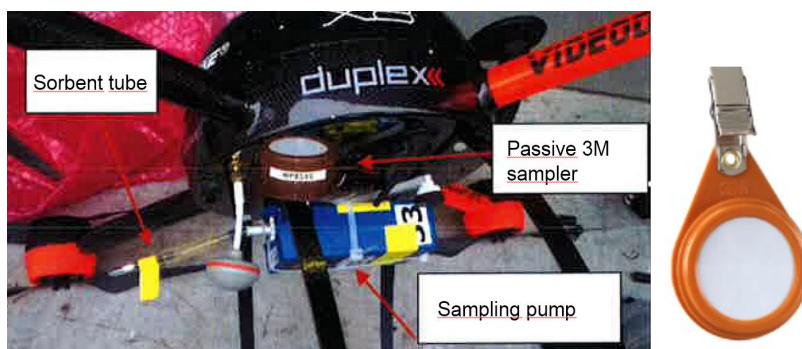


Figure 109. The sorbent tube, sampling pump and passive 3M sampler installed on the drone (left), 3M Organic Vapor Diffusion Monitor 3520 (right). (Images: FIOH/Mika Jumpponen, 3M)

The combination presented in Figure 109 was demonstrated in the detection of xylenes, toluene, benzene, chloroform, tetrachloroethane and acetone.

The bottles were placed inside a polystyrene box and the caps of the bottles (Figure 94) were opened. The drone was piloted over the box (Figure 110).



Figure 110. The drone with the sorbent tube, sampling pump and 3M passive sampler after landing over the polystyrene box for sampling. (Image: VTT/Jukka Sassi)

6.2.5 Results

During the pre-tests with the indicator smoke, it was clearly noticed that when the drone was approaching the target, the turbulence caused by the propellers pushed the smoke in the opposite direction (Figure 111).



Figure 111. The turbulence effect caused by the drone. (Image: VTT/Jukka Sassi)

This effect is problematic in situations in which a vapour sample should be taken. One solution is a long injection pipe attached to the sensor, enabling sampling without disturbance by turbulence.

During the first flight with the BH-8 module, the sensors were exposed to an increasing concentration of NH_3 . The NH_3 concentration in different stages (Figure 101 and Figure 102) of the flight was visualized in real time in the operator's computer until the EC sensor was saturated at the level of 800 ppm.

The responses to different compounds in the Aeromon's VOC sensor signals were quite diverse, e.g. no response for xylene and a high response to acetone. The reasons for this variation arise from the wind conditions (which altered during the test), the exact location of the sample intake at specific moments, vapour pressure of the target compounds and the differences in sensitivity in the VOC sensors which were chosen for this test. (Aeromon, 2016)

Figure 104 shows that that the Aeromon's sensor specific responses for different VOCs were different for each compound. Therefore, it is possible to distinguish different compounds from each other to a certain extent. However, this claim should be tested in a more stable environment with standardized target compound exposure methods, preferably in a laboratory environment. After the VOC panel is calibrated in this manner, the possibilities to distinguish different compounds from each other in field conditions can be increased considerably. (Aeromon, 2016)

The drone with ChemPro 100i detector hovered above the canister for few seconds, and the sensor clearly detected ammonia (Figure 112).



Figure 112. The ChemPro100i clearly detected ammonium. (Images: VTT/Jukka Sassi)

An ammonium concentration as low as 5 ppm can be detected by the human nose. Acute exposure guideline levels (AELG) for ammonia are the following (FIOH, 2016a):

- AELG-1: 30 ppm (21 mg/m³)/10 min
 30 ppm (21 mg/m³)/30 min
- AELG-2 220 ppm (160 mg/m³)/10 min
 220 ppm (160 mg/m³)/30 min
- AELG-3 2 700 ppm (1 900 mg/m³)/10 min
 1 600 ppm (1 100 mg/m³)/30 min

AELG-1 is the airborne concentration (expressed as ppm or mg/m³) of a substance above which it is predicted that the general population, including susceptible individuals, could experience notable discomfort, irritation, or certain asymptomatic non-sensory effects. However, the effects are not disabling and are transient and reversible upon cessation of exposure.

AELG-2 is the airborne concentration of a substance above which it is predicted that the general population, including susceptible individuals, could experience irreversible or other serious, long-lasting adverse health effects or an impaired ability to escape.

AELG-3 is the airborne concentration of a substance above which it is predicted that the general population, including susceptible individuals, could experience life-threatening health effects or death. (NOAA, 2016)

The harmful concentration of ammonium in the ambient air of a workplace is 20 ppm (14 mg/m³) /8 h or 50 ppm (36 mg/m³) /15 min. (FIOH, 2016a)

Both the SKC-226-01 sorbent tube and 3M Organic Vapor Diffusion Monitor detected that xylenes, toluene, benzene, chloroform, tetrachloroethane and acetone were vaporised in the air from the bottles. This means that both sensors can detect several different vaporised compounds. The results are presented in Table 23 and Table 24.

Table 23. The results for the SKC-226-01 sorbent tube. (FIOH, 2016b)

Compound	Result	Unit	HTP 8h	HTP 15 min	HTP portion
Acetone	1.4	mg/m ³	1 200	1 500	0.00
Benzene	0.7	mg/m ³	3.25		0.22
Butanes	1.9	mg/m ³	1 900		0.00
Xylene	< 0.2	mg/m ³	220		
Toluene	0.3	mg/m ³	81		0.00
Sum of HTP portion				total	0.22

Table 24. The results for the 3M passive monitor. (FIOH, 2016b)

Compound	Result	Unit	HTP 8h	HTP 15 min	HTP portion
Collection time	41	min.			
Acetone	2.7	mg/m ³	1 200	1 500	0.00
Benzene	1.1	mg/m ³	3.25		0.34
Butanes	1.4	mg/m ³	1 900		0.00
Xylene	0.5	mg/m ³	220		
Toluene	0.9	mg/m ³	81		0.1
Sum of HTP portion				total	0.35

The sampling time for the SKC-226-01 sorbent tube was 19.5 minutes and for the 3M diffusion monitor 41 minutes. The minor differences in the results can be explained by the different sampling methods (active vs. passive), sampling times and the locations of the sensors in the drone. (FIOH, 2016b)

The advantages of the SKC-226-01 and 3M diffusion monitors include the easy mounting and use of the sensors, especially in the case of 3M. Both sensors provide laboratory standard results from the samples, and several compounds can be analysed from the same samples. The disadvantages of the sensors are the time frame required for analyses and the limited preserving time of the samplers. (FIOH, 2016b)

When the Dräger indicator tube for ammonia was mounted in the drone and piloted near the building with ammonia, the installation enabled visual monitoring of the change in the colour of the adsorption material inside the tube, i.e. the increase of the ammonium concentration (Figure 113).



Figure 113. Extracts from the video by AIF with the optical camera mounted in Videodrone X8.

The increase in the ammonium concentration could be visually observed, and the maximum measured concentration was approximately 70 ppm.

The advantages of this method are that an approximate estimate of the ammonia concentration, or other predefined chemical, in the air can be defined quickly, and no samples need to be sent to a laboratory. This feature would be very useful for a rescue team when they need to estimate the chemical concentration of the target area before the actual rescue operation.

The downside of this method is that the rescue team must have prior information of the chemical in question. In addition, the preserving time of the samplers is limited. (FIOH, 2016b)

The acid indicator tubes mounted in the drone did not detect any acid above the canister or the cloth where HCl was poured, although the acid vapour was visible. Possibly the turbidity caused by the drone pushed the vapour towards the opposite direction, thus avoiding the acid sensors.

6.2.6 Demonstrations

In the afternoon of the second day of the seminar, four demonstrations were performed:

- Identification of acid containers inside a container with an optical camera,
- Identification of gas bottles under a canopy with an optical camera;
- Utilisation of an FLIR camera in the identification of hot spots in the multipurpose fire house during an artificial fire and
- Utilisation of the FLIR camera in an SAR exercise in which a person is lost in the forest.

Optical and FLIR cameras were mounted in the Videodrone X8 drone. The acid containers and gas bottles could be clearly identified from the video picture (Figure 114 and Figure 115).



Figure 114. Extractions from the AIF video of Videodrone X8 drone during the identification of acid containers inside the container. UN 1789 8 stands for hydrochloric acid (HCl).



Figure 115. Extractions from the AIF video of the Videodrone X8 drone during the identification of gas bottles under a canopy.

Although the cylinder label is the primary means of identifying the properties of the gas in a cylinder, the colour coding of the cylinder body provides a further guide. The colour applied to the shoulder, or curved part at the top of the cylinder, signifies the European standard colour coding. (AGA, 2016)

The aim of the new standard (EN 1089-3), which has replaced the old cylinder colour scheme (BS349), is to help improve safety standards within the gas industry. The shoulder colours inform about gas properties, but the most common pure gases have their own colours. (AGA, 2016)

The colour codes of different gas cylinders for pure industrial gases are presented in Table 25, for pure food gases in Table 26, for pure specialty gases in Table 27, and for gas mixtures in Table 28.

Table 25. Colour codes for pure industrial gases. (AGA, 2016)

Cylinder colours	Shoulder colours	Gas	Shoulder colours	Gas
 Black	 White	Oxygen	 Brown	Helium
	 Bright green	Air	 Blue	Nitrous oxide
	 Black	Nitrogen	 Yellow	Toxic and/or corrosive gases
	 Grey	Carbon dioxide	 Red	Flammable gases
	 Dark green	Argon		
Whole cylinder maroon	 Maroon	Acetylene		

Table 26. Colour codes for pure food gases. (AGA, 2016)

Cylinder colours	Shoulder colours	Gas	Shoulder colours	Gas
 Reseda green	 White	Oxygen	 Grey	Carbon dioxide
	 Black	Nitrogen	 Dark green	Argon

Table 27. Colour codes for pure specialty gases. (AGA, 2016)

Cylinder colours	Shoulder colours	Gas	Shoulder colours	Gas
 Silver grey	 White	Oxygen	 Brown	Helium
	 Black	Nitrogen	 Yellow	Toxic and/or corrosive gases
	 Bright green	Other inert gases	 Red	Flammable gases
	 Grey	Carbon dioxide	 Maroon	Acetylene
	 Dark green	Argon		

Table 28. Colour codes for gas mixtures. (AGA, 2016)

Gas	Shoulder colours
Inert	 Bright green
Fire intensifier/ oxidizing	 Light blue
Flammable	 Red
Toxic	 Yellow

From Figure 115 it can be recognised that acetylene, oxygen, helium, carbon dioxide, and toxic and/or corrosive gas bottles were stored under the canopy.

In the third demonstration, the drone with the FLIR camera was utilised in pointing out the hot spots in an artificial fire (Figure 116).



Figure 116. Image outside the firehouse (upper), and FLIR image (below) showing the highest temperature of 124.8 °C near the doorway of the firehouse.

The warmest point in the image is 124.8 °C, whereas the hottest temperature inside the multipurpose firehouse, directly above the fire, was approximately 180 °C.

In the search and rescue (SAR) demonstration a missing person was detected by the FLIR camera, which senses infrared radiation emitted from a heat source (Figure 117).

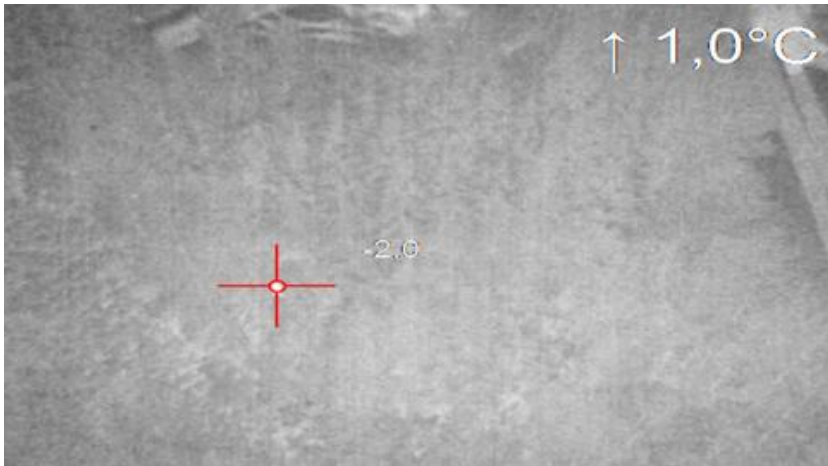


Figure 117. A missing person was detected in the forest by FLIR camera. (Image extraction from the AIF video)

During the SAR demonstration, it was noted that the target could be spotted more easily when it was moving.

During the demonstrations, the videos from the optical camera and FLIR camera could be followed from the screen of the commander van of the ESC (Figure 118).



Figure 118. Guest observers following the demonstrations from the screen of the command van. (Image: VTT/Jukka Sassi)

In addition to the abovementioned demonstrations, the magnetometer from Radai Ltd was mounted in Airborne KX8, which performed a pre-programmed test flight

(grid) above the test site. According to Pirttijärvi (Radai, 2016), the flight is controlled by an autopilot. The autopilot records flight data including GPS time and position (latitude and longitude), the orientation (roll, pitch and yaw), and barometric pressure. The real-time flight is controlled by PC software via a telemetry (radio) link. The nominal accuracy of the GPS position is about ± 10 m. However, the flight data was not recorded during the demonstration.

6.2.7 Conclusions

The Kuopio test trials with the various sensors and chemicals were performed in almost ideal conditions, since the wind conditions did not disturb the drone flights and no problems with visibility caused by environmental conditions occurred. The quality of the visible video recording was good enough for identification of the acid containers and gas bottles. The sensors were able to identify the chemicals used as targets, as expected.

The turbulence caused by the drone when approaching the target disturbs the sampling of vapours. This problem was solved by using a long suction hose with the Aeromon sensor, but with the indicator tubes the problem remained.

The applicability of the Aeromon measurement system to detect and to quantify previously known compounds was shown and this result can be extended to meet all the target gas specific sensors compatible with the BH-8 sensor module, currently 70 different target gases. (Aeromon, 2016)

The installation of indicator tubes on the drone in a way that the variation of the chemical concentration (i.e. ammonia in this case) near the target area could be observed from the video screen was considered to be an excellent option for rescue teams. One option that would extend the use of the indicator tubes would be a set-up in which several tubes with different chemical reagents are mounted in a stand. An indicator tube or set of tubes can be installed so that changes of the colour in the tubes, i.e. increases in the concentrations of the target gases, could be visually monitored from the video screen. This would assist fire and rescue experts in determining the status of the target area.

FIOH (2016b) noted that the concentrations of acids in different environmental conditions could be measured with active sampling methods in order to recognise the concentrations and dispersion of acids in prevailing environmental conditions. These results could be compared to the results of the indicator tubes mounted in RPAS in order to provide better understanding of how the tubes are suited for the detection of acid concentrations. Additionally, the data collected with the active and passive methods could be utilised together with dispersion models in such a way that the active and passive methods could be compared with each other in practice.

7. Discussion

Oil spill response (OSR) activities in arctic conditions expose remote sensing technologies and platforms to challenging operational conditions. In addition to ice and snow, rain, fog, clouds and darkness also set limitations to the sensor technology that can be typically used in moderate conditions. Weather conditions are a significant factor to be considered in sensor selection. Additionally, the location of oil, i.e. on the ice, encapsulated inside the ice, hidden under the snow or under the ice, and the ice concentration all have an important role in how effectively the oil can be detected. The most challenging environment for current remote sensors appears to be the situation in which the oil is located under the ice or snow, or captured inside the ice. Thus a combination of different sensors of which the performance has been field-tested in different arctic conditions is recommended.

The visual methods are effective during the daylight hours and in relatively calm weather. They cannot be utilised in the night time due to safety reasons and lack of visibility. The utilisation of night-vision technology may extend the operational window. The effectiveness of visible methods can be enhanced by illumination. Rough weather conditions also hinder the use of visual observation methods. Impurities inside and on the ice, dark smelt pools, sun sparkle, wind sheens and biogenic material interfere with the interpretation of the visual images, and therefore the data interpretation requires trained operators in order to avoid false alarms. Bearing in mind the limitations associated with visible methods, they cannot be relied on to provide reliable coverage in emergency situations.

Optical satellite imaging requires almost clear skies, and the irregular visiting intervals of satellites and their low spatial resolution makes this only an ancillary data source for OSR. The presence of ice and snow weaken optical signals, and characterisation of oil with them is ineffective. Furthermore, the understanding of satellite data requires specialised experts and may take too long in terms of tactical OSR. Optical satellite surveillance can be used together with radar-based oil spill monitoring such as Synthetic Aperture Radar (SAR).

Thermal infrared (TIR) sensors may offer possibilities to detect oil between floes or on ice, bearing in mind the constraints caused by fog, poor weather and rough water. TIR sensors can be used during day and night and they can provide information on relative oil slick thickness. TIR sensors can be coupled with UV sensors to detect oil slicks thicker than 20 μm . The combination of marine radar and passive or active IR has shown potential in open water conditions and could possibly be applicable in very open sea covers. Even in arctic conditions, ice is not always present.

The performance of Microwave Radiometer (MWR) is unknown in ice conditions with ice concentrations of 30% or higher. MWR appears to be effective in low visibility conditions, but false positives can be generated by waters of different temperatures, seaweed and biogenic material. MWR is not effective in cases in which oil is located under ice or snow or encapsulated.

Laser induced Fluorosensors (LFSs) can reliably detect oil on ice and among pack ice, even in dark conditions. LFSs are able to classify oil types and determine the thickness of thin slicks. LFSs are not widely used due to the requirement for dedicated aircraft, low flying altitudes and thus narrow spatial coverage. Non-UV LiDAR (Light Detection and Ranging) is a promising technology for oil detection due to lower costs and better availability compared to LFSs.

Tunable Diode Laser (TDL) systems can detect oil, but due to their long deployment time they were not considered a viable option in oil detection. The Laser-Ultrasonic Remote Sensing of Oil Thickness (LURSOT) concept has demonstrated potential in oil thickness detection, but no systems are currently in operation.

Radar systems can acquire images day and night and are available on airborne and satellite platforms. They can be utilised in general ice environment mapping and characterising, tracking ice movements and guiding the deployment of surveillance equipment. SAR satellites and airborne SAR/SLAR (Side-Looking Airborne Radar) systems may detect large spills in very open drift ice ($< 4/10$) and under moderate wind conditions in open water (approximately 3–10 m/s). The performance of radar-based systems is limited by low wind speed, biogenic slicks, presence of grease or new ice or fresh water and shear waves. The presence of ice decreases the performance due to reduced wave activity. The capability of radar to detect oil under ice is limited.

The utilisation of Ground Penetrating Radar (GPR) in detecting oil under snow and ice is a relatively new approach, and its development for oil detection is continuing. GPR may offer one solution to detect oil on the ice surface under snow and oil trapped under or within solid ice.

Acoustic sensors may be able to detect oil under ice, but only as an in-situ deployment. The inhomogeneity of ice may affect detection and logistical issues may also limit its use in oil detection.

Nuclear Magnetic Resonance (NMR) is a novel technology application in oil detection under ice. NMR requires complex data processing and the acquisition times in imaging mode are currently too long for feasible operational use.

Trained dogs can detect oil buried under snow, on melt ponds, on ice and in soil, but their performance in the case of oil embedded in or under ice is unknown. Dogs have potential in oil detection in land fast ice and large ice floes, and in the shoreline when oil is covered by sediment. Dogs trained for search and rescue emergencies could also be trained for oil detection. Dogs can contribute positively to the engagement of local stakeholders in remote communities.

Regarding the remote sensing of chemicals in field conditions, less information is available when compared to oil spill detection. Some chemicals are highly volatile, or form only a thin layer on water. This phenomenon hinders their detection with SAR imagery in microwave frequency, but SAR with X- and L-bands may have potential to detect chemicals in thin surface films. Many of the mobile methods used in chemical detection on-site require the collection of samples, which may be dangerous and laborious. Therefore there is a need for innovative sensor technologies enabling chemicals detection in challenging operational conditions and

for volatile chemicals. In addition, the utilisation of Unmanned Aerial Vehicles (UAVs) in chemical detection should also be considered in terms of weight, energy supply and mounting of the sensors.

Concerning the deployment platforms, surface vessels are widely used due to their availability, manoeuvrability and versatility in terms of equipped sensors and instrumentation, utilisation of trained observers and possibility to stay for long periods in the desired location. Heavy ice conditions and high seas restrict the effective utilisation of oil booms and arms, and smaller recovery vessels.

Manned aircrafts are the most effective platform for OSR, since they can be equipped with portable or integrated sensors of several types, are manoeuvrable, can cover large areas for the task in question in a relatively short time window and can locate spills. When using manned aircrafts, weather and safety issues in addition to flight procedures must be considered carefully.

Satellite systems can host a variety of sensors for data collection in OSR operations. They are able to cover large areas within the limitations of revisit intervals, collected data can be transmitted quickly, and they can spot large spills and anomalies. Response time to emergency calls can be from 90 minutes to 4 hours. However, the revisit intervals might not be optimal for OSR, clear skies are required for optical observations and the time required for data conversion may be considerable.

Unmanned Aerial Vehicles (UAVs), i.e. drones, have a long history in military and civilian applications but their use in oil and chemical detection is a rather new application area. UAVs have several advantages over manned aircrafts, e.g. lower flying altitude and lower costs to acquire and operate. They can also reach locations that for safety and security reasons manned aircrafts cannot, and they are less noisy and disturbing. However, UAVs have a limited payload capacity compared to manned aircrafts, environmental conditions such as darkness and wind impose limits, and local aviation regulations need to be addressed. Furthermore, many of the detection sensors were not originally designed for drone installation.

Automated Underwater Vehicle (AUV) and Remote Operated Vehicle (ROV) robots can offer long operational times underwater and they can be used for oil detection under ice. The existing user experience is gained from oil and gas exploration in the Arctic areas. In case of lost equipment or accident, no loss of life will be incurred. Regarding arctic OSR, the experiences with AUVs and ROVs are limited. They are rather expensive and require trained personnel to operate the system. Furthermore, the cables used with ROV may cause problems in rough ice conditions.

Tethered balloon systems have been used mainly for land-based observations, and thus their applications in arctic OSR are restricted. They can be equipped with various types of sensors, similar to aircrafts and UAVs, while considering the payload limits. They are quite cost effective, the primary costs being derived from selected sensors. The advantages are rather similar to those of UAVs. The operation of tethered balloon systems requires extensive training, and weather conditions (wind, visibility) must be suitable. The obtaining of an adequate amount of helium might be an issue.

Regardless of the detection technology, it is essential that the sensor operators and observers are aware of the basic operational principals and the limitations of the utilised technology in order to be able to provide reliable and accurate interpretation of the measured data. This matter is crucial in cases in which operators and/or observers are not from the companies providing the sensor technology. Additionally, the limitations of the platforms in question must be addressed during the preparation phase of the OSR operations.

In an ideal case the selected platform would be robust and agile enough to carry a set of different sensors which could be used for oil and chemical detection in different ice and weather conditions in addition to other purposes, e.g. in civil protection and coastguard missions.

Acknowledgements

The authors express their sincere acknowledgements to the sensor and platform providers for their technical support and expertise during the test trials and data analysing phase, to the Port of Kalajoki for their support during the oil detection trials, and to the Emergency Services College in Kuopio for the utilisation of their test site and for technical expertise in chemical handling and for practical arrangements during the trials.

References

- 3M. 2016. 3M™ Organic Vapor Diffusion Monitor 3500/3510 and 3520/3530.
- Aeromon. 2016. Measurements at The Emergency Services College test site in Kuopio, Finland on 29.11.2016. Matti Irjala, 29.11.2016.
- AGA. 2016. Cylinder colours - what do they mean? [Cited 14 December 2016].
- Alam, M. and Sidike, S. 2012. Trends in oil spill detection via hyperspectral imaging. 7th International Conference on Electrical and Computer Engineering, 2012. 20-22 December, 2012, Dhaka, Bangladesh.
- American Petroleum Institute (API). 2016. Canine Oil Detection (K9-SCAT) Guidelines. API Technical Report 1149-4. July 2016.
- American Petroleum Institute (API). 2013. Remote Sensing in Support of Oil Spill Response. Planning Guidance. API Technical Report 1144, September 2013.
- Angelliaume, S., Minchew, B., Chataing, S., Martineau, P. and Miegébielle, V. 2016. Multifrequency radar imagery and characterization of hazardous and noxious substances at sea. Proceedings of the 39th AMOP Technical Seminar, Environment and Climate Change Canada, Ottawa, ON, pp. 364–382. 2016.
- Argo. 2017. <http://www.euro-argo.eu/>. [Cited 2 November 2017].
- Army Technology. 2017. <http://www.army-technology.com/>. [Cited 17 November 2017].
- Arctic Monitoring and Assessment Programme (AMAP), 1998. AMAP Assessment Report: Arctic Pollution Issues. Arctic Monitoring and Assessment Programme (AMAP), Oslo, Norway. Xii + 859 pp.
- Babichenko, S., Dudelzak, A., Lapimaa, J., Lisin, A., Poryvkina, L. and Vorobiev, A. 2006. Locating water pollution and shore discharges in coastal zone and inland waters with FLS lidar. EARSeL eProceedings 5, 1/2006, 32–36.
- Baltic Operational Oceanographic System (BOOS). 2016. News from BOOS, spring 2016.
- Brandvik, P. J. and Buvik, T. 2009. Using dogs to detect oil hidden in snow and ice – Results from field training on Svalbard April 2008. SINTEF Materials and Chemistry, SINTEF, Oil in Ice – JIP, Report No. 14.

- Bruker. 2017. Technical specifications of SIGIS-2 System. <https://www.bruker.com> [Cited 15 November 2017].
- Bunker, P. 2017. Proposed certification standard for oil detection canines. Proceedings of the fortieth AMOP technical seminar, Environmental and Climate Change Canada.
- Camilli, R. 2017. HC-Sentinel: an AUV lider for high endurance subsea hydrocarbon detection. Final report submitted to Bureau of Safety and Environmental Enforcement (BSEE), Oil Spill Response Branch, January 23, 2017.
- Cardno Entrix. 2012. Surveillance Technologies for Oil Spill Response. Current Research and Emerging Trends. Centre for Remote Imaging, Sensing and Processing (CRISP). 2015. Principles of Remote Sensing.
- Chein-I, C. 2003. Hyperspectral Imaging: Techniques for Spectral Detection and Classification. Springer Science and Business Media. ISBN 978-0-306-47483-5.
- Dickins, D. (editor, DF Dickins Associates LLC). 2010. Project P5: Remote Sensing Summary Report. Oil in Ice – JIP. SINTEF Materials and Chemistry. 24.05.2010. Report no. 30.
- Dräger. 2016. Dräger tubes and accuro pump. https://www.draeger.com/en_uk/Applications/Productselector/Mobile-Gas-Detection/Draeger-Tubes-and-CMS. [Cited 14 December 2016].
- EnviroNics. 2016. ChemPro®100i Handheld Chemical Detector. <http://www.enviroNics.fi/product/chempro100i/>. [Cited 8 December 2016].
- European Gliding Observatories (EGO). 2017. <http://www.ego-network.org>. [Cited 1 November 2017].
- Fingas, M. (editor). 2015. Handbook of oil spill science and technology. John Wiley & Sons, Inc. ISBN 978-0-470-45551-7.
- Fingas, M. and Brown, C. 2014. Review of oil spill remote sensing. Marine Pollution Bulletin 83 (2014) 9–23. <http://dx.doi.org/10.1016/j.marpolbul.2014.03.059>.
- Fingas, M. and Brown, C. 2013. Detection of Oil in Ice and Snow, 2013. Journal of Marine Science and Engineering. J. Mar. Sci. Eng. 1, 10–20; doi:10.3390/jmse1010010.
- FIOH. 2016a. Onnettomuuden vaaraa aiheuttavat aineet – turvallisuusohjeet (OVA-ohjeet). In Finnish.

- FIOH. 2016b. Työterveyslaitos. RPAS avusteinen ilmanäytteenotto Kuopion Pelastusopiston harjoitusalueella 1.11.2016. Lausunto TYHYG-2016a-345929. 21.11.2016. In Finnish.
- Furuno. 2017. Oil radar FOIL-200. http://www.furuno.fi/eng/surveillance/surveillance_systems/integrated_oil_spill_detection_system/oil_radar_foil_200/. [Cited 1 June 2017].
- Grahn, H. and Geladi, P. 2007. Techniques and Applications of Hyperspectral Image Analysis. John Wiley & Sons. ISBN 978-0-470-01087-7.
- Hagen, N. and Kudenov, M. 2013. Review of snapshot spectral imaging technologies. *Opt. Eng.* 52(9), 090901 (Sep 23, 2013). doi:10.1117/1.OE.52.9.090901.
- Hall, R. 2012. "ICEMAR," presented at the 13th Meeting of the International Ice Charting Working Group (IICWG), Thirteenth IICWG Meeting, October 15-19, 2012, Tromsø, Norway.
- Harig, R., Matz, G., Rusch, P., Gerhard, H., Gerhard, J. and Schlabs, V. 2005. New Scanning Infrared Gas Imaging System (SIGIS 2) for Emergency Response Forces. Hamburg University of Technology, D-21079 Hamburg, Germany.
- Hui Y., Qun W., Zhen Z., Zhi-jie Z., Wei T., Xin T., Song, Y. and Chen-sheng W. 2017. Oil spill detection using hyperspectral infrared camera. *Proceedings Volume 10030, Infrared, Millimeter-Wave, and Terahertz Technologies IV; 100301G (2017)*; doi: 10.1117/ 12.2244924. SPIE/COS Photonics Asia, 2016, Beijing, China.
- Huppunen, J., Putula, K., Tenhu, H. and Helkala, T. 2012. Soil Investigation with a Trained Dog. Presentation at 4th Nordic Joint Meeting on Remediation of Contaminated Sites, Oslo, Norway.
- ICEYE. 2017. <https://www.iceye.com/technology>. [Cited 23 November 2017].
- International Civil Aviation Organization (ICAO). 2015. Manual on Remotely Piloted Aircraft Systems (RPAS). Doc 10019 AN/507. Approved by the Secretary General and published under his authority. First Edition - 2015.
- ICD. 2015. New laser to combat oil spill in arctic waters.
- Jha, M.N., Levy, J. and Gao, Y. 2008. Advances in Remote Sensing for Oil Spill Disaster Management: State-of-the-Art Sensors Technology for Oil Spill Surveillance. *Sensors* 2008, 8, pp. 236–255.

- Karathanassi, V. 2014. "Spectral Unmixing Evaluation for Oil Spill Characterization", *International Journal of Remote Sensing Applications* 4(1), 2014.
- Keshavarz, A., Mohammad, S. and Hashemizadeh, K. 2017. Analysis of Hyperspectral Imagery for Oil Spill Detection Using SAM Unmixing Algorithm Techniques. Article 2, Volume 6, Issue 2 – Issue Serial Number 19, 2017. DOI: 10.22050/ijogst.2017.47444.
- LOOKNorth. 2014. Oil Spill Detection and Modeling in the Hudson and Davis Straits. Final Report R-13-087-1096, Revision 2.0, 2014-05-29.
- Limnaios, G. 2014. Current Usage of Unmanned Aircraft Systems (UAS) and Future Challenges: A Mission Oriented Simulator for UAS as a Tool for Design and Performance Evaluation. *Journal of Computations & Modelling* 4 (1), 167–188. ISSN: 1792-7625 (print), 1792–8850 (online). Scienpress Ltd, 2014.
- Liu, B., Li, Y., Zhang, Q., and Han, L. 2016. Assessing Sensitivity of Hyperspectral Sensor to Detect Oils with Sea Ice. *Journal of Spectroscopy*. Volume 2016 (2016), Article ID 6584314, 9 pages. <http://dx.doi.org/10.1155/2016/6584314>
- Løge, L. 2013. Arctic communications system utilizing satellites in highly elliptical orbits. Doctoral thesis. Available: <https://brage.bibsys.no/xmlui/handle/11250/2370683>
- Najibi, N. and Jin, S. 2013. Physical Reflectivity and Polarization Characteristics for Snow and Ice-Covered Surfaces Interacting with GPS Signals. ISSN 2072-4292. *Remote Sens.* 2013, 5, 4006–4030; doi:10.3390/rs5084006.
- National Aeronautics and Space Administration (NASA). 2017. Introduction to the Electromagnetic Spectrum. https://science.nasa.gov/ems/01_intro. [Cited 27 November 2017].
- NHL University of Applied Sciences (NHL). 2017. Spill response manuals. <http://www.spillresponse.nl/>. [Cited 27 November 2017].
- NOAA. 2016. National Oceanic and Atmospheric Administration (NOAA). Database of Hazardous Materials. <http://response.restoration.noaa.gov/oil-and-chemical-spills/chemical-spills/resources/acute-exposure-guideline-levels-aegls.html>. [Cited 2 December 2016].
- Nuka Research and Planning Group, LLC (Nuka Research). 2007. Oil Spill Response Challenges in Arctic Waters. ISBN: 978-2-88085-283-2. Published in October 2007 by WWF International Arctic Programme, Oslo, Norway.

- Optris. 2016. Optris infrared thermometers. <http://www.optris.com/infrared-cameras>. [Cited 29 November 2016].
- Partington, K. 2014. An Assessment of Surface Surveillance Capabilities for Oil Spill Response using Airborne Remote Sensing. Polar Imaging Limited. 21 May 2014. PIL-4000-38-TR-1.0.
- Polak, A., Marshall, S., Ren, J., R., Hwang, B., Hagan, B. and Stothard, D. 2016. Remote oil spill detection and monitoring beneath sea ice. The 2016 European Space Agency Living Planet Symposium, 2016-05-09–2016-05-13.
- Puestow, T., Parsons, L., Zakharov, I., Cater, N., Bobby, P., Fuglem, M., Parr, G., Jayasiri, A. and Warren, S. (C-CORE), Warbanski, G. (Emergency Spill and Consulting Inc.). 2013. Oil Spill Detection and Mapping in Low Visibility and Ice: Surface Remote Sensing. Final Report 5.1, 15 October 2013. Arctic Oil Spill Response Technology Joint Industry Programme (JIP).
- Radai. 2015. Ryssänlampi magnetic survey using Radai UAV system and its comparison to airborne and ground magnetic data of GTK. Detailed Survey Report. 21.9.2015. Markku Pirttijärvi, Radai Oy.
- Salem, F. 2002. Hyperspectral remote sensing: A new approach for oil spill detection and analysis. George Mason University. Publication Number: AAI3079345; ISBN: 9780496272235.
- Senop. 2017. <http://senop.fi/optronics-hyperspectral#hyperspectralCamera>. [Cited 28 September 2017].
- Sony. 2017. Sony HDR-CX410VE specifications. <http://www.sony.co.uk/support/en/content/cnt-specs/HDR-CX410VE/list>. [Cited 29 June 2017].
- Specim. 2017. <http://www.specim.fi/>. [Cited 28 September 2017].
- Suomen ympäristökeskus (SYKE). 2015. Työsuojelu avoimilla vesialueilla tapahtuvien öljyvahinkojen torjunnassa. Helsinki, 2015. Suomen ympäristökeskus. (In Finnish).
- Svejkovsky, J., Lehr, W., Muskat, J., Graettinger, G. and Mullin, J. 2012. Operational Utilization of Aerial Multispectral Remote Sensing during Oil Spill Response: Lessons Learned During the Deepwater Horizon (MC-252) Spill. Photogrammetric Engineering and Remote Sensing 78(10), pp. 1089–1102.

- Svejkovsky, J. and Muskat, J. 2009. Real-time Detection of Oil Slick Thickness Patterns with a Portable Multispectral Sensor. Final Report for U.S. Minerals Management Service Contract 0105CT39144, 37 P.
- Telops. 2017. Hyper-Cam Hyperspectral Imaging Systems.
- Trafi. 2015. TRAFI/4482/03.04.00.00/2015, OPS M1-32OPS. Kauko-ohjatun ilma-aluksen ja lennokin lennättäminen (In Finnish).
- University of Manitoba, Centre of Earth Observation Science (CEOS). 2014. Research Gaps in Scientific Understanding of Oil in Sea Ice. Submission to the Tanker Safety Expert Panel – Phase 2. May 16, 2014.
- VTT. 2017. VTT's miniature hyperspectral camera launched to space in Aalto-1 satellite. VTT News, 26 June 2017.
- VTT. 2015. Kuljetuskonttikaasujen mittausmenetelmät. Kajolinna, T. and Pellikka T. Tutkimusraportti VTT-R-01420-15. (In Finnish).
- Wikipedia. 2017. Hyperspectral imaging.
https://en.wikipedia.org/wiki/Hyperspectral_imaging. [Cited 27 November 2017].
- Widdowson, C. 2012. Chemicals in containers – problems and risks. Port Technology International 56:46–48.
- Yarovenko, N., Cruz, M. and Vilas, L. 2011. Oil pollution using shipborne LIF/LIDAR. 5thEARSel Workshop on Remote Sensing of the Coastal Zone. Prague, Czech Republic, 1st–3rd June, 2011.

Appendix A: Properties of the test oil HFO180 in the Kalajoki trials

NESTE

TUOTETIEDOTE
TUNGASPOLTTOÖLJY 180
VAHARIKKIENEN

PRODUCT DATA SHEET
HEAVY FUEL OIL 180
LOW SULPHUR

ABBREVIATION: PORL180

L'YHENNE: PORL180
FORKORTNING: PORL180

1.1.2017

	Yksikö Unit	Laturaja Specification	Tyypillinen arvo Typical analysis	Muuttyminenä Terminä Test method ¹⁾
Riikki ²⁾ Sulfur content ²⁾	P-% mass-% % m/m	max.	0,87	EN ISO 8754 NM 389
Leimainpääte ³⁾ Flash point ³⁾	°C	66	96	EN ISO 2719
Tiheys ⁴⁾ Density at 15 °C	kg/m ³	910	1020	690
Viskoositeetti ⁵⁾ Viscosity at 80 °C	mm ² /s	36	43	EN ISO 3104
Viskoositeetti ⁵⁾ Viscosity at 100 °C	mm ² /s	140	180	EN ISO 3104
Viskoositeetti ⁵⁾ Viscosity at 150 °C	mm ² /s	15	10	EN ISO 10370
Hiloksisuus, MCR Krause, MCR Carbon residue, MCR	P-% mass-% % m/m	15	3	DN 51666
Ash content ⁶⁾ Ash content	P-% mass-% % m/m	15	6	ISO 3016 ASTM D 5650
Ilmestyspiste Ligula fyysinen Four point	°C	0,7	0,1	ISO 3733 ASTM D 4552 ASTM D 6304 C
Viskoositeetti Sediment	P-% mass-% % m/m	0,15	0,06	ISO 10307-1
Tuhas Total ash	P-% mass-% % m/m	0,1	0,08	EN ISO 6246
Tuhas Ash content	MU/kg	40,2	41	ASTM D 240
Tuhas Net heat of combustion, reported	wt-%	Imotoitaan reported		D 5291
Tuhas Carbon content	wt-%	Imotoitaan reported		D 5291
Tuhas Carbon content	wt-%	Imotoitaan reported		D 5291

PORL180	Yksikö Unit	Laturaja Specification	Tyypillinen arvo Typical analysis	Muuttyminenä Terminä Test method ¹⁾
Vanadiini Vanadium	mg/kg	max. 100	38	ISO 10478 M NM 122
Nikkeli Nickel	mg/kg	50	18	ISO 10478 M NM 122
Palautuskatalyytti Förbränningskatalysator Burning catalyst		+ 4)	+	

¹⁾ NM-numero viittaa Neste Öljin sisällyseen menetelmään

²⁾ Perustuu Vaharikkienasetukseen 689/2006

³⁾ 50 °C:een viskoositeetti lasketaan 80 °C:ssa mitatun arvon perusteella

⁴⁾ Lidiainetta ei lisätä, mikäli hillojäljänä on alle 5 p-%

⁵⁾ Asetus 655/2012

⁶⁾ Voidaan valmistaa sekoittamalla tuotteesta PORL420 ja keskeisistä osista viskoositeettiä. Sekoitustuote analysoidaan vain mitalarjon.

Spezifikation lukimassa käytetään ISO 4259:n mukaisella menetelmällä.

Käyttöturvallisuuden osalta viittaamme Neste Öljin julkaisemiin käyttövaikalisuus- ja turvallisuusohjeisiin sekä tuotteiden käyttöä koskeviin oppaasi.

TUOTETIEDOT
Neste Öljä
Neste Markkinointi
PL 95
00095 Neste Öj
Puhelin 0200 80100

Yksikö
Unit

Laturaja
Specification

Tyypillinen arvo
Typical analysis

Muuttyminenä
Terminä
Test method¹⁾

max.

100

38

50

18

+

mg/kg

mg/kg

+

ISO 10478 M
NM 122

ISO 10478 M
NM 122

+

¹⁾ NM-nummer refererar till respektive Neste Öj -metod

²⁾ Baserar på förordning 689/2006

³⁾ Viskositeten vid 50 °C är beräknad på basen av värdet mätt vid 80 °C

⁴⁾ Tillätsämnen skall inte tilläggas om kokstäm är under 5 mass-%

⁵⁾ Föreskrift 655/2012

Produkten kan tillverkas genom blandning av PORL420 och mellanslag till önskad viskoositet. Blandningsprovet analyseras endast produktet.

Produktspecifikationen tolkas i enlighet med proceduren beskriven i ISO 4259.

Angående skyddsinformation hänvisar vi till skyddsinformationsblad publicerade av Neste Öj samt till produktens bruksanvisningar.

INQUIRIES
Neste Öj
Neste Retail
POB 95
FIN-00095 Neste Öj, Finland
Telephone +358 20 80100

Title	Utilisation of RPAS in oil and chemicals detection
Author(s)	Jukka Sassi, Sami Siikanen & Marko Höyhtyä
Abstract	<p>This report provides an overview of various sensor technologies and deployment platform options utilised in the remote sensing of oil and chemicals in field conditions. The data is based on published information, whereas the reported field experiments were performed by VTT Technical Research Centre of Finland and Finnish Environmental Institute (SYKE) with their partners.</p> <p>The sensors with field-tested validation for oil detection include optical, infrared and hyperspectral sensors in addition to fluorosensors which were provided by AIF, LDI Innovations OÜ, NLS and Rikola Ltd for field testing. Additionally, some experimental options such as trained dogs are discussed in the report based on information from literature sources.</p> <p>Chemical detection focuses on the options demonstrated in field conditions by VTT and SYKE with their partners or other stakeholders which have provided documented information. These options include products provided by e.g. Aeromon Ltd, Bruker Ltd, Dräger, Environics Ltd, and Telops Ltd.</p> <p>The deployment platforms include surface vessels, manned aircrafts, satellites, aerostats, autonomous underwater vehicles (AUVs), remote operated vehicles (ROVs) and unmanned aerial systems (UASs). UASs have also shown great potential in environmental monitoring as a novel, agile and cost-effective option. ROVs and AUVs also offer potential for underwater detection of oil.</p> <p>The detection of oils and chemicals exposes numerous challenges related to the prevailing environmental conditions (e.g. visibility, presence of ice or snow), limitations of the platform performance (e.g. payload, wind conditions, operational time) and sensors available for the mission. Consequently, different sensors are needed for different target substances and for different weather conditions.</p>
ISBN, ISSN, URN	ISBN 978-951-38-8640-0 (Soft back ed.) ISBN 978-951-38-8639-4 (URL: http://www.vttresearch.com/impact/publications) ISSN-L 2242-1211 ISSN 2242-1211 (Print) ISSN 2242-122X (Online) http://urn.fi/URN:ISBN:978-951-38-8639-4
Date	9 May 2018
Language	English
Pages	166 p. + app. 1 p.
Name of the project	
Commissioned by	Finnish Environmental Institute (SYKE)
Keywords	Arctic, chemical, HNS, oil, platform, RPAS, sensor
Publisher	VTT Technical Research Centre of Finland Ltd P.O. Box 1000, FI-02044 VTT, Finland, Tel. 020 722 111

Utilisation of RPAS in oil and chemicals detection

ISBN 978-951-38-8640-0 (Soft back ed.)
ISBN 978-951-38-8639-4 (URL: <http://www.vttresearch.com/impact/publications>)
ISSN-L 2242-1211
ISSN 2242-1211 (Print)
ISSN 2242-122X (Online)
<http://urn.fi/URN:ISBN:978-951-38-8639-4>

